Spatial and Temporal Dynamics of Dissolved Oxygen and Nitrous Oxide

Concentrations in the Hyporheic Zone

A Dissertation

Presented in Partial Fulfillment of the Requirements for the

Degree of Doctor of Philosophy

with a

Major in Civil Engineering

in the

College of Graduate Studies

University of Idaho

by

William Jeffery Reeder

Major Professor: Daniele Tonina, Ph.D.

Committee Members: Shawn G. Benner, Ph.D.; Ralph Budwig, Ph.D.; Kevin P. Feris, Ph.D.; Peter Goodwin, Ph.D.; Alessandra Marzadri, Ph.D.

Department Administrator: Patricia J. S. Colberg, Ph.D.

August 2017

Authorization to Submit Dissertation

This dissertation of William Jeffery Reeder, submitted for the degree of Doctor of Philosophy with a major in Civil Engineering and titled "Spatial and Temporal Dynamics of Dissolved Oxygen and Nitrous Oxide Concentrations in the Hyporheic Zone," has been reviewed in final form. Permission as indicated by the signatures below is granted to submit final copies to the College of Graduate Studies for approval.

Major Professor: _____ Date _____
                 Daniele Tonina Ph.D.

Committee Members: _____ Date _____
                   Shawn G. Benner Ph.D.

                   _____ Date _____
                   Ralph Budwig Ph.D.

                   _____ Date _____
                   Kevin P. Feris Ph.D.

                   _____ Date _____
                   Peter Goodwin Ph.D.

                   _____ Date _____
                   Alessandra Marzadri Ph.D.

Department
Administrator: _____ Date _____
               Patricia J. S. Colberg Ph.D.

Abstract

The majority of chemical reactions in rivers and streams occur within the hyporheic zone (HZ), the saturated sediments directly beneath and adjacent to the stream flow. Hyporheic exchange, flow into and out of the hyporheic zone, represents a primary control over those reactions because the flow rate will determine the residence time and amount of chemical constituents in the HZ. Thus, activity within the HZ is of major importance to the biochemical state and habitat quality of riverine systems. Yet, due to the inherent difficulties associated with obtaining non-invasive chemical measurements in the HZ and the complexity of flow in the HZ as well as interactions between hyporheic hydraulics and the biogeochemical processes, a detailed, mechanistic and predictive understanding of the biogeochemical activity in the HZ has not been developed. To date, the details and complexities of reactive solute transport in the HZ have been described mainly through numerical simulations.

Previous research has demonstrated that an estimated 10% of nitrous oxide (N_2O), a potent greenhouse gas, which is released to the atmosphere, comes from rivers and streams. The controls over these emissions are not well understood and a fine-scale predictive model has not been developed. This research focuses on two primary aspects of chemical activity in the HZ, both of which are key elements of the processes that lead to N_2O emissions; the metabolic consumption of dissolved oxygen (DO) and the microbially mediated denitrification reaction sequence.

To overcome the difficulties associated with obtaining non-invasive DO measurements in the HZ we developed a new multi-point, *in situ*, multiplexed fiber optic measurement system. With this system, we were able to profile DO concentrations in the HZ at spatial and temporal resolutions that had not been previously achieved. These high-density measurements allowed us to uncover a significant shortcoming in the current conceptualization of reactive solute transport in the HZ. Previous studies of microbial activity in the HZ have treated the metabolic DO consumption rate (K_{DO}) as a fixed and homogeneous property of the hyporheic environment that is primarily controlled by the availability of labile organic carbon. Our findings demonstrate that aerobic respiration rates are substantially controlled by stream hydraulics. K_{DO} is a distributed property whose values are log-normally

distributed and can vary by an order of magnitude across the span of a single bedform. These studies have also perceived the HZ as temporally steady state. This perspective yields a static view of the biogeochemical activity and redox state of the HZ and fails to capture the temporal dynamics of a changeable system. Our results demonstrate that for a system in which nutrient replenishment is largely episodic, for instance annual leaf fall, DO concentration profiles and DO consumption rates will vary with time.

The denitrification reaction sequence that is the direct source for N2O emissions is a kinetic process that takes a period of time to proceed from beginning to end. The time it takes for a parcel of water to travel along a flowline is termed residence time (τ). However, because of the variable dynamics of reactive processes in the HZ, residence time, by itself, is not an adequate predictor of N_2O emissions. We present a predictive model based on a Damköhler-type transform ($\tilde{\tau}$) of the residence times (τ) along a flowline multiplied by the dissolved oxygen consumption rate. This model can identify which bedforms have the potential to produce and emit N2O as well as the portion and location from which those emissions may occur. Our results indicate that that flowlines that that have $\tilde{\tau}_{up}$, the $\tilde{\tau}$ value at which a flowline exits back into the surface water, between 0.54 and 4.4 are likely to produce and emit N_2O. N_2O production peaks approximately at $\tilde{\tau} = 1.8$ along a flow line.

Acknowledgements

A multitude of people contributed to this project. Without their help, it would not have been possible. I want to thank them all.

I especially want to express my sincere gratitude it Daniele Tonina. Thank you for including me in this project. Thank you for your kindness, enthusiasm, insights and encouragement. Thank you for encouraging me to go forward during those times that I was absolutely convinced that I could not.

In addition, a special thanks to my student co-researchers, Annika Quick and Tiffany Farrell. Group projects can be a bit chancy. You were both more than wonderful to work with.

I would like to acknowledge my committee members, Shawn Benner, Ralph Budwig, Kevin Feris, Peter Goodwin and Alessandra Marzadri. Your support and guidance is deeply appreciated.

Special thanks goes to Bob Basham, Eric Schlueter and Christina Beeson for contributions above and beyond. It is a true delight to work with you.

Dedication

This work and my life are dedicated to my loving wife, Deborah. Thank you for supporting this.

Table of Contents

List of Figures

List of Tables

Chapter 1

Reactive solute transport in the hyporheic zone

The hyporheic zone is the volume of porous sediments adjacent to and below the stream water where saturated surface water exchanges with subsurface flows. These saturated sediments include the stream bed, stream banks, particularly in outcroppings and meander bends, and abandoned channels (paleo channels) that maintain hydraulic connectivity with the stream waters [*Elliott and Brooks*, 1997b; *Findlay*, 1995; *A L Packman et al.*, 2004; *Tonina and Buffington*, 2007; *Triska et al.*, 1993]. Hyporheic exchange, the flow of water into and out of the HZ, is driven by pressure gradients that exist at the interface between the surface waters and the streambed. At local, bedform scales these pressure gradients are primarily caused by flow obstructions from bedform features (e.g. dunes, riffles and woody debris) protruding into the stream flow.

As surface-water, flow lines impinge upon an obstructing feature a high-pressure zone is formed on the upstream (stoss) side of the feature due to an increase in the dynamic pressure component of the total bed pressure. The surface flow lines continue over and around the feature detaching from the feature on the downstream (lee) side of the feature causing a depression in the dynamic pressure. The net effect is a gradient in the total pressure across the feature. If the feature is porous, such as in a dune, water will flow through the feature, downwelling into the stoss face (high pressure) and upwelling from the lee face (low pressure), rejoining the main stream flow. This pressure gradient driven flow is termed "hydraulic pumping" and was originally introduced by Elliot and Brooks in 1997 [*Elliott*, 1990; *Elliott and Brooks*, 1997b] and the concept has since been expanded by a variety of

researchers [*Cardenas and Wilson*, 2007; *Jin et al.*, 2010; *A I Packman et al.*, 2000; *Tonina and Buffington*, 2007]. The rate (velocity and mass flux) at which water and solutes flow through the feature will be determined by the size of the pressure gradient and the hydraulic conductivity of the sediments within the feature. Because the total pressure at the bed/surface water interface is prohibitively difficult to measure or model, most of the models employed in the aforementioned research use a simplified representation of the surface pressure distribution. Typically, the pressure distribution is represented as a sinusoid whose amplitude is determined from the ratio of the height of the feature to the depth of the fully submerging flow. The wavelength of the sinusoid is matched to the wavelength of the feature, typically a dune. This simplification has been shown to work well for determining the bulk or mean characteristics (upwelling and downwelling fluxes as well as mean residence times)[*Elliott and Brooks*, 1997a; b; *Fox et al.*, 2014], but it is still a bit of an open question as to how the simplified pressure gradient describes the behavior of individual flow lines.

The chemical activity in the HZ has direct influence over the stream water chemistry and temperature. At reach and regional scales, the HZ provides an interface to aquifer groundwater flows that allows groundwater, with its own unique chemistry and temperature, to mix with surface waters. At the bedform scale, downwelling fluxes carry oxygen, chemicals and nutrients into the HZ while, at the same time, upwelling fluxes carry metabolic waste products and chemically transformed species back to the surface flow, altering the stream chemistry. Thus hyporheic flow provides a variety of services to the benthic creatures, macrophytes and bacterium (as biofilm attached to sediment surfaces) living there. Additionally, hyporheic flow provides oxygen and nutrients to redds, supporting incubation and growth of hatchling. As such, hyporheic flow supports a rich ecotone that facilitates a wide variety of biochemical activities including, among others, aerobic respiration (oxidation of DOC), nitrification (oxidation of ammonium) and denitrification (reduction of nitrate). Taken together, these reactions define the microbially mediated nitrification/denitrification cycle. DO enters the HZ at downwelling sites and is initially consumed by bacteria (carbon and ammonium oxidation) for metabolic activities. As water moves deeper into the HZ, oxygen continues to be consumed until the concentration reaches a threshold level (~2ppm) at which aerobic (oxidative) metabolic activity is no longer the most feasible energy providing process [*Chapelle et al.*, 1995; *Harvey et al.*, 2013]. As the oxygen depleted water continues

to move through the HZ the metabolic activities of the bacterial communities is supported (in part) by denitrification (the sequential reduction of $NO_3^- \rightarrow NO_2^- \rightarrow NO \rightarrow N_2O \rightarrow N_2$) [*Chapelle*, 1993; *Tiedje*, 1988]. In streams that are in a natural equilibrium with the local environment (e.g. mountain headwater stream), the vast majority of the reactive nitrogen (Nr) that enters the stream is processed through nitrification and denitrification to N_2 [*Beaulieu et al.*, 2008; *Beaulieu et al.*, 2011]. However, the character of urban and rural streams has been altered due to anthropogenic activities [*Anderson et al.*, 2010; *Galloway et al.*, 2004; *Wuebbles*, 2009]. Agricultural activities have resulted in an overload of Nr, primarily form fertilizer runoff, in many urban and rural streams while channelization has altered stream hydraulics, potentially reducing hyporheic flow and thus the Nr processing capacity of the stream. One net result of these anthropogenic alterations is that some impacted streams emit substantial quantities of N_2O as part of their effluent stream.

The interesting part of the previous statement is that "some impacted streams emit." Clearly, streams have some control over the chemical processing that occurs between the banks. In an overarching sense, this is what is not well understood. What are the specific control mechanisms that determine whether a particular stream, a particular reach, a particular bedform or a particular flow line will or will not emit N_2O? To shine some light on this question we will focus on reaction mechanics at the bedform and flow line scale with the hope that the results can expanded to larger scales.

This dissertation is composed of five chapters.

- Chapter 1 presents a brief overview of hyporheic flow and reactive solute dynamics in the HZ.
- Chapter 2 presents a new technique and apparatus for measuring DO in the HZ. This technique offers an unprecedented view of DO concentration profiles and dynamics in the HZ.
- Chapter 3 presents of the high-density DO data from the measurement technique detailed in Chapter 2. DO consumption rates are resolved to the individual flowline level. A predictive model for DO consumption, based upon bed morphology and stream hydraulics is presented.

- Chapter 4 presents the temporal dynamics of DO consumption in the HZ for streams for streams that experience episodic nutrient (carbon) replenishment.
- Chapter 5 presents a generalized, predictive model for N_2O emissions from the HZ. We show that N_2O emissions are bracketed between two values of flowline residence times that have been transformed, at the flowline level, by a characteristic reaction rate along that flowline (i.e., K_{DO}).

References

Anderson, B., K. Bartlett, S. Frolking, K. Hayhoe, J. Jenkins, and W. Salas (2010), Methane and Nitrous Oxide Emissions From Natural Sources*Rep.* EPA-430-R-10-001, EPA, Washington, DC.

Beaulieu, J. J., C. P. Arango, S. K. Hamilton, and J. L. Tank (2008), The production and emission of nitrous oxide from headwater streams in the Midwestern United States, *Global Change Biology*, *14*(4), 878-894, doi:10.1111/j.1365-2486.2007.01485.x.

Beaulieu, J. J., et al. (2011), Nitrous oxide emission from denitrification in stream and river networks, *Proceedings of the National Academy of Sciences*, *108*(1), 214-219, doi:10.1073/pnas.1011464108.

Cardenas, M. B., and J. L. Wilson (2007), Dunes, turbulent eddies, and interfacial exchange with permeable sediments, *Water Resources Research*, *43*(8), W08412, doi:10.1029/2006wr005787.

Chapelle, F. H. (1993), *Ground-Water Microbiology and Geochemistry*, John Wiley & Sons, New York.

Chapelle, F. H., P. B. McMahon, N. M. Dubrovsky, R. F. Fujii, E. T. Oaksford, and D. A. Vroblesky (1995), Deducing the Distribution of Terminal Electron-Accepting Processes in Hydrologically Diverse Groundwater Systems, *Water Resources Research*, *31*(2), 359-371, doi:10.1029/94WR02525.

Elliott, A. H. (1990), Transfer of solutes into and out of streambeds, edited, California Institute of Technology, Pasadena, CA.

Elliott, A. H., and N. H. Brooks (1997a), Transfer of nonsorbing solutes to a streambed with bed forms: Laboratory experiments, *Water Resources Research*, *33*(1), 137-151, doi:10.1029/96WR02783.

Elliott, A. H., and N. H. Brooks (1997b), Transfer of nonsorbing solutes to a streambed with bed forms: Theory, *Water Resources Research*, *33*(1), 123-136, doi:10.1029/96WR02784.

Findlay, S. (1995), Importance of surface-subsurface exchange in stream ecosystems: The hyporheic zone, *Limnology and Oceanography*, *40*(1), 159-164, doi:10.4319/lo.1995.40.1.0159.

Fox, A., F. Boano, and S. Arnon (2014), Impact of losing and gaining streamflow conditions on hyporheic exchange fluxes induced by dune-shaped bed forms, *Water Resources Research*, *50*(3), 1895-1907, doi:10.1002/2013WR014668.

Galloway, J. N., et al. (2004), Nitrogen Cycles: Past, Present, and Future, *Biogeochemistry*, *70*(2), 153-226.

Harvey, J. W., J. K. Böhlke, M. A. Voytek, D. Scott, and C. R. Tobias (2013), Hyporheic zone denitrification: Controls on effective reaction depth and contribution to whole-stream mass balance, *Water Resources Research*, *49*(10), 6298-6316, doi:10.1002/wrcr.20492.

Jin, G., H. Tang, B. Gibbes, L. Li, and D. A. Barry (2010), Transport of nonsorbing solutes in a streambed with periodic bedforms, *Advances in Water Resources*, *33*(11), 1402-1416, doi:http://dx.doi.org/10.1016/j.advwatres.2010.09.003.

Packman, A. I., N. H. Brooks, and J. J. Morgan (2000), A physicochemical model for colloid exchange between a stream and a sand streambed with bed forms, *Water Resources Research*, *36*(8), 2351-2361, doi:10.1029/2000WR900059.

Packman, A. L., M. Salehin, and M. Zaramealla (2004), Hyporheic Exchange with Gravel Beds: Basic Hydrodynamic Interactions and Bedform-Induced Advective Flows, *Journal of Hydraulic Engineering*, *130*(7), 647-656, doi:doi:10.1061/(ASCE)0733-9429(2004)130:7(647).

Tiedje, J. M. (1988), Ecology of denitrification and dissimilatory nitrate reduction to ammonium, John Wiley and Sons, New York.

Tonina, D., and J. M. Buffington (2007), Hyporheic exchange in gravel bed rivers with pool-riffle morphology: Laboratory experiments and three dimensional modeling, *Water Resources Research*, *43*, W01421, doi:1029/2005WR004328.

Triska, F. J., J. H. Duff, and R. J. Avanzino (1993), The role of water exchange between a stream channel and its hyporheic zone in nitrogen cycling at the terrestrial-aquatic interface, *Hydrobiologia*, *251*(1-3), 167-184, doi:10.1007/BF00007177.

Wuebbles, D. J. (2009), Nitrous Oxide: No Laughing Matter, *Science*, *326*(5949), 56-57, doi:10.1126/science.1179571.

Chapter 2

Dissolved oxygen concentration profiles in the hyporheic zone through the use of

a high-density fiber optic measurement system[1]

Dissolved oxygen (DO) concentration is a primary indicator of redox and biogeochemical activity in the hyporheic zone (HZ) of fluvial systems. Due to the inherent difficulty of measuring chemical concentrations in hyporheic sediments, field measurements are typically spatially sparse and of limited temporal resolution. As such, most conceptualizations of biogeochemical processes are based upon numerical simulations. To overcome this limitation, we developed a new multi-point, in situ method based on a multiplexed optical network coupled with a precision robotic surface probe system, which measured DO at unprecedented spatial and temporal resolution. This method allowed us to measure HZ DO concentrations in a large-scale flume experiment almost continuously for five months. Our findings demonstrate the partitioning of the HZ from oxic to anoxic

resulting from microbial respiration but also illuminate some shortcomings in the current conceptualization of reactive solute transport in the HZ.

2.1 Introduction

The majority of chemical reactions in streams occur within the hyporheic zone (HZ) [*Fischer et al.*, 2005; *Alessandra Marzadri et al.*, 2017; *Master et al.*, 2005; *Wuhrmann*, 1972], the saturated sediments directly beneath and adjacent to stream flow [*Findlay*, 1995; *Tonina and Buffington*, 2007]. Redox processes are an important class of reactions occurring in the HZ, particularly for microbial respiration, nutrient uptake and reactive solute processing [*Appelo and Postma*, 2010; *Chapelle*, 1993; *Chapelle et al.*, 1995]. The general trends of DO consumption in the HZ have been described through relatively sparse point measurements in field studies [*Harvey et al.*, 2013; *Triska and Oremland*, 1981; *Triska et al.*, 2007; *Zarnetske et al.*, 2011a; b]. However, these sparse measurements have insufficient resolution to capture the details of individual flowlines, micro sites of metabolic activity or irregularities in flow. Due to these complexities, studies based upon field measurements have been unable to define a fully developed and well-validated, detailed, mechanistic and predictive understanding of reactive solute transport and biogeochemical activity in the HZ.

Current theory describing these activities is expressed primarily as numerical simulations [*Bardini et al.*, 2012; *Cardenas and Wilson*, 2007; *Gualtieri*, 2011; *Hunter et al.*, 1998; *Jin et al.*, 2010; *Alessandra Marzadri et al.*, 2010; *A. Marzadri et al.*, 2012]. It proposes that pressure gradients along the bed surface cause solute-laden water to flow into the HZ in downwelling areas and return to the surface flow in upwelling areas [*Elliott and Brooks*, 1997; *Alessandra Marzadri et al.*, 2010]. Hyporheic flow can be conceptualized as discreet, quasi-parallel flowlines, each with its own flux and residence time (Figure 2-1). A variety of chemical transformations may take place along these flowlines. The extent to which a reaction sequence may proceed will be determined by the magnitude of the flux, the residence time and the biogeochemical state of the HZ. If the reaction rates are slow or the residence times are short, intermediate products of a reaction sequence (e.g., N_2O from the denitrification sequence) may be released into the stream flow [*Alessandra Marzadri et al.*, 2010; *Quick et al.*, 2016]. As such, hyporheic flow exerts primary control over those reactions [*Findlay*, 1995; *Master et al.*, 2005]. While this conceptualization seems intuitively

correct, due to the inherent complexity of obtaining detailed, non-invasive chemical measurements in the HZ, the details and complexities of reactive solute transport through the HZ have not yet been well described and validated through direct physical measurements.
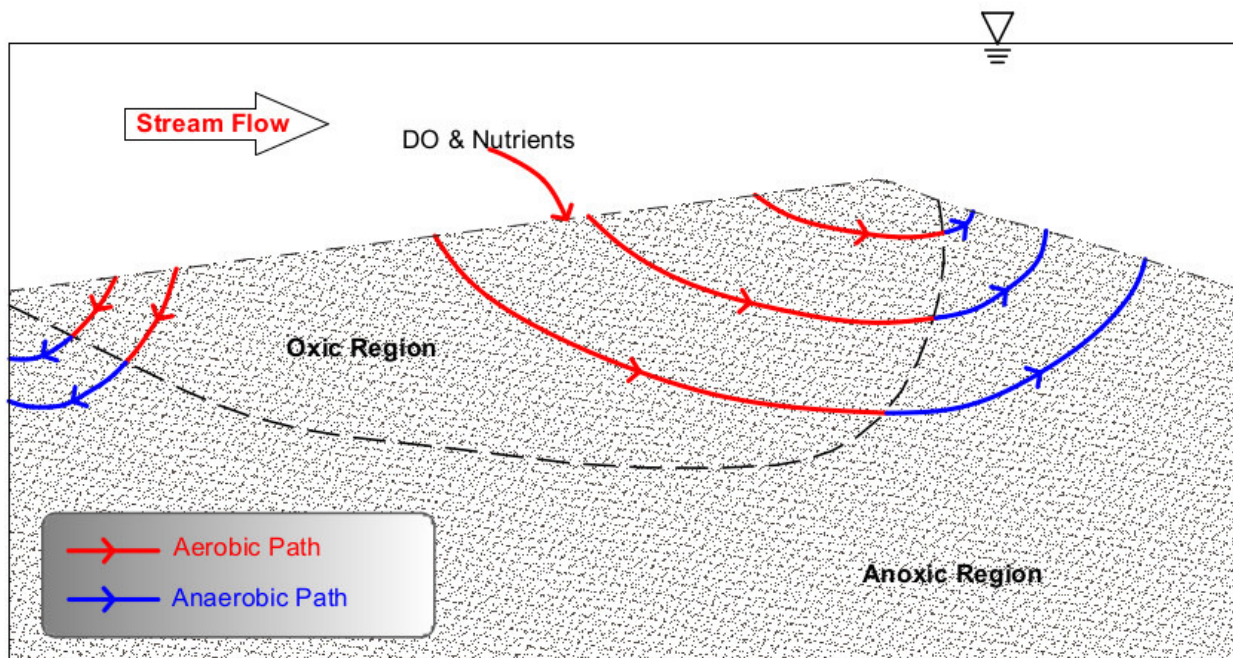
Figure 2-1. Conceptual representation of hyporheic flow through a dune. Porewater transport is represented as discreet, quasi-parallel flowlines. As porewater moves through the HZ, a variety of chemical transformations will occur including metabolic oxygen consumption and other biologic and non-biologic redox reactions.

To address this limitation, we developed and deployed a new methodology and apparatus for measuring pore water DO concentrations at a spatial and temporal scale and resolution never before achieved within sediments. Its application is demonstrated by mapping DO concentrations in the HZ, below dune-like bedforms, but it can be used in any three dimensional setting. We focus on DO because it is a primary indicator of the redox state of the HZ [*Chapelle*, 1993; *Greig et al.*, 2007; *Tonina and Buffington*, 2009] and because the DO consumption rate is a measure of metabolic activity and may serve as a predictor of potential anaerobic activity in the HZ [*Kessler et al.*, 2012; *A. Marzadri et al.*, 2012; *Alessandra Marzadri et al.*, 2016; *A. Marzadri et al.*, 2010; *Stonedahl et al.*, 2010]. Our direct physical measurements elucidate transport and reaction processes in the HZ and reveal

a significant misconception in existing theory related to reactive solute transport and transformation in the HZ.

2.2 Materials and Methods

2.2.1 Flume Experiment

We conducted controlled and replicated experiments at flows and physical scales that are directly representative of conditions in natural settings in the large-scale flume (approximately 20 m x 2 m) at the Center for Ecohydraulics Research Stream Laboratory [*Budwig and Goodwin*, 2012] (CERSL) at the University of Idaho, Boise (Figure 2-2). Two experiments, conducted in 2013 (Flume 1) and 2015 (Flume 2), divided the flume into three 30 cm-wide channels, which were separated by service corridors. Both experiments ran continuously for approximately 15 weeks. Each channel contained a series of triangular sand dunes that were 70 cm and 100 cm in length and of varying height (3 cm, 6 cm and 9 cm). Ports in the sidewalls of the channels allowed for *in situ* measurements of DO. The sand used to form the dunes was a mixture of 90% quarry sand (sieved to <2.4 mm and washed to remove fines) and 10% Boise River (Idaho, USA) sand that served as microbial inoculum. Shredded cottonwood leaves (0.15% dry weight) were added to the sand mix as an organic carbon substrate to support the metabolic activities of the microbes. The hydraulic conductivity of the sand/leaf mix was 0.002 m/s. Recirculating flow through the channels (2.1 L/s/channel) was supplied by a submersible pump in the flume's 50,000-gallon catch basin. We measured total carbon concentration of the streambed sediments at the beginning and end of the experiments (see supplemental materials). Hyporheic fluxes, residence times and bed-surface pressure amplitudes were calculated using the methodology defined by Elliot and Brooks [1997]. The following nomenclature will be used to reference the various dune configurations. From Flume 1, we have 3 cm tall, 6 cm tall and 9 cm tall by 1 m long dunes, hereafter referred to as "3 cm dune", "6 cm dune and "9 cm dune", respectively. From Flume 2, we will consider a 9 cm tall by 100 cm long dune and a 9 cm tall by 70 cm long dune, hereafter referenced as "100 cm dune" and "70 cm dune", respectively. The energy slopes for Flume 1 and Flume 2 were 0.002 and 0.003.
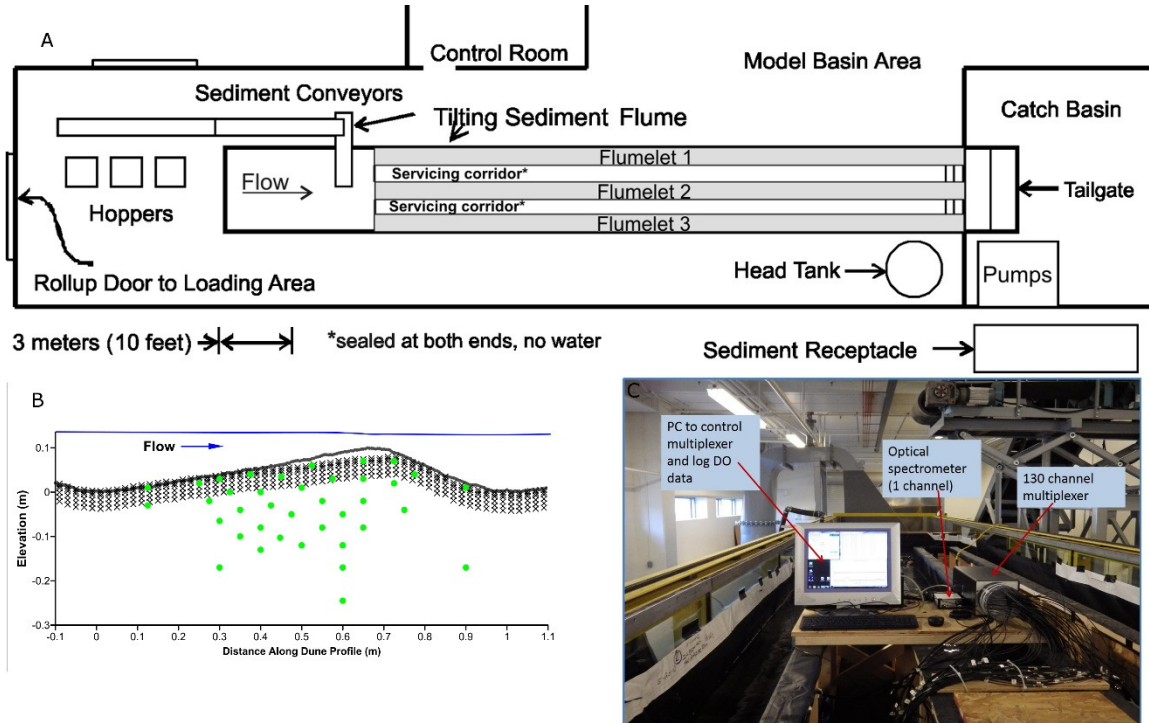
Figure 2-2. Elements of the experimental setup and the dissolved oxygen measurement system: A) an aerial diagram of the flume setup with the flume divided into three stream channels and two service corridors, B) cross-sectional view of measurement positions for the fiber optic system (green dots – *in situ* probe positions) and the surface probes (black Xs) and C) the fiber optic measurement system with the controlling computer, the optical spectrometer and the 130-channel multiplexer.

2.2.2 Dissolved Oxygen Measurement

The heart of the DO measurement system is the optical spectrometer and sensor spots developed and marketed by PreSens Precision Sensing GmbH, Regensburg, Germany. The sensor spots are saturated with a dye that fluoresces when light (505 nm wavelength) [*PreSens*, 2016] shines upon them. That fluorescence is quenched in the presence of DO. The degree of quenching is proportional to the concentration of the DO [*Gatti et al.*, 2002; *Klimant et al.*, 1995]. In a "normal" application of this technology, a sensor spot is glued to the inside of a beaker. A fiber optic cable connected to the spectrometer is touched to the outside of the beaker at the backside of the sensor spot. The spectrometer shines the excitation wavelength of light down the fiber optic cable fluorescing the sensor spot. The

measurement signal, which occurs at a different wavelength, travels up the fiber optic cable to the spectrometer where it is separated, interpreted and stored.

We modified the typical application of this technology by inserting a custom-built optical multiplexer (Agiltron Inc., Woburn MA, USA) into the optical path between the spectrometer and the point of measurement. Additionally, we sheathed the distal ends of multiple fiber optic cables with stainless steel tubing (4 mm diameter by 15 cm length) and glued sensor spots directly onto those ends and imbedded them, through the ports in the service corridors, into the dunes. The small diameter of the *in situ* probes made them minimally disruptive to the hyporheic flow hydraulics. The green dots in Figure 2-2B indicate the probe locations for the 100 cm dunes. The pattern for the 70 cm dunes was similar. In the 2013 experiment, the sensors were located on a regular grid pattern. The irregular arrangement used in Flume 2 was designed to align the sensors more closely to oxic area and with the hyporheic flowlines. The optical sensor spots are ideal for *in situ* measurements due to their long-term stability and lack of drift [*Jørgensen and Elberling*, 2017; *Kohfahl et al.*, 2010; *Tengberg et al.*, 2003; *Tengberg et al.*, 2006]. Any potential drift was monitored by probes that were constantly immersed in the surface flow. The DO values for those sensors were compared to values obtained from Clark-type, ion selective sensors and Henry's Law calculations for the solubility of oxygen in water. No divergence between the three methods was observed. A Windows® automation script (AutoHotKey v1.1.12.00) was used to control which multiplexer channels were activated, activation order, measurement duration and the number of passes through a measurement cycle. These adaptations allow us to automate a large number of *in situ* DO measurements. We deployed 120 and 240 measurement channels in Flume 1 and Flume 2, respectively. Cycle time for one complete set of measurements was approximately one hour.

The flume has a programmable instrument cart that runs its length. A robotic arm that can traverse the width of the flume and travel about 30 cm vertically is attached to the instrument cart. We attached Clark-type micro sensors, manufactured by Unisense A/S (Aarhus, Denmark), to the robotic arm to measure DO concentrations at depths of 0, 5, 10, 20, 30 and 40 mm along the top of the bed profile (black Xs, Figure 2-2B). The Unisense sensors are a consumable product whose response shifts progressively with time. To compensate, we

calibrated the Unisense sensors before every run using a two-point calibration profile (0% and 100% oxygen saturation). Because of the lack of drift, the PreSens® sensors do not need routine calibration. However, to be conservative we recalibrated the PreSens® sensors every time there was a major change in atmospheric pressure using the same two-point methodology as with the Unisense® sensors. We never observed a significant shift in the PreSens® calibration parameters. DO concentration profiles (Figure 2-3) were created for each dune on each evaluation date by kriging and gridding all the measured surface and *in situ* DO data for that dune and date, using the mapping software Surfer® Version 10 (Golden Software, Inc., Golden CO). These profiles allowed us to accurately track the DO concentrations in the bulk of the HZ and define the concentration gradients in the sediments.
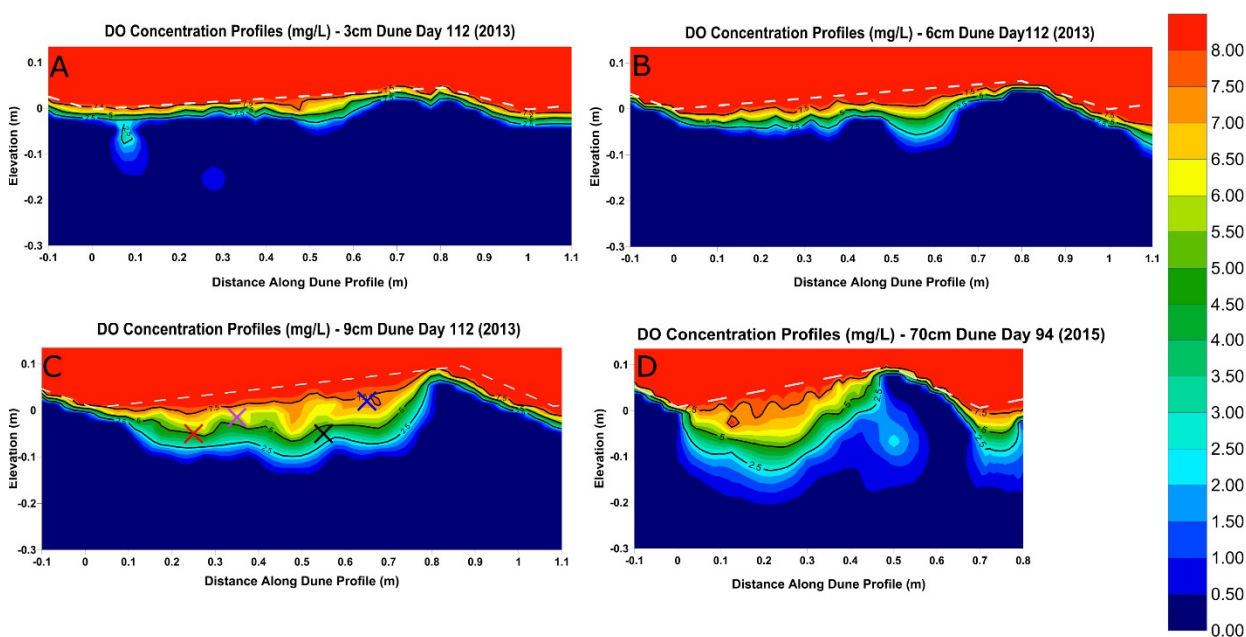
Figure 2-3. Measured DO concentration profiles for the two experimental runs and different dune configurations. Panel A: DO for a 3 cm-tall by 1 m long dune (2013 run, day 112). Panel B: DO for a 6 cm-tall by 1 m-long dune (2013 run, day 112). Panel C: DO for a 9 cm-tall by 1 m-long dune (2013 run, day 112). Panel D: DO for a 9 cm-tall by 0.7 m-long dune (2015 run, day 94). DO concentration profiles were created by kriging the measured values. X-marks (**X X X X**) indicate the measurement positions for Figure 4. The dashed white line indicates the dune surface.

2.3 Results and Discussion

2.3.1 Results

The net result of these spatially and temporally dense measurements is illustrated in Figure 2-3, Figure 2-4 and Figure 2-5. Figure 2-3 illustrates the detailed DO concentration profiles that are possible from spatially dense measurements. The presented profiles are from the endpoints of the respective experiments. Similar profiles were produced at several points along the span of the experimental runs. It should be noted that these profiles are generated entirely from physical measurements - aside from data kriging, no modeling is involved in these concentration profiles. Figure 2-4 shows the continuous temporal record of DO concentration from four selected sensors. The sensor locations are indicated by the colored Xs in Figure 2-3C. The colors of the Xs correspond to the colors of the traces in Figure 2-4. Figure 2-5 shows the measured DO profile for the 70 cm dune near the midpoint of the Flume 2 experiment (panel A). Panels B and D show modeled profiles for the same dune. These models were created in the same sense as Bardini et al. [2012], Jin et al. [2010], Kessler et al. [2012], Marzadri et al. [2010] and others. Panels 5C and 5E show the difference between the two models from the measured values.
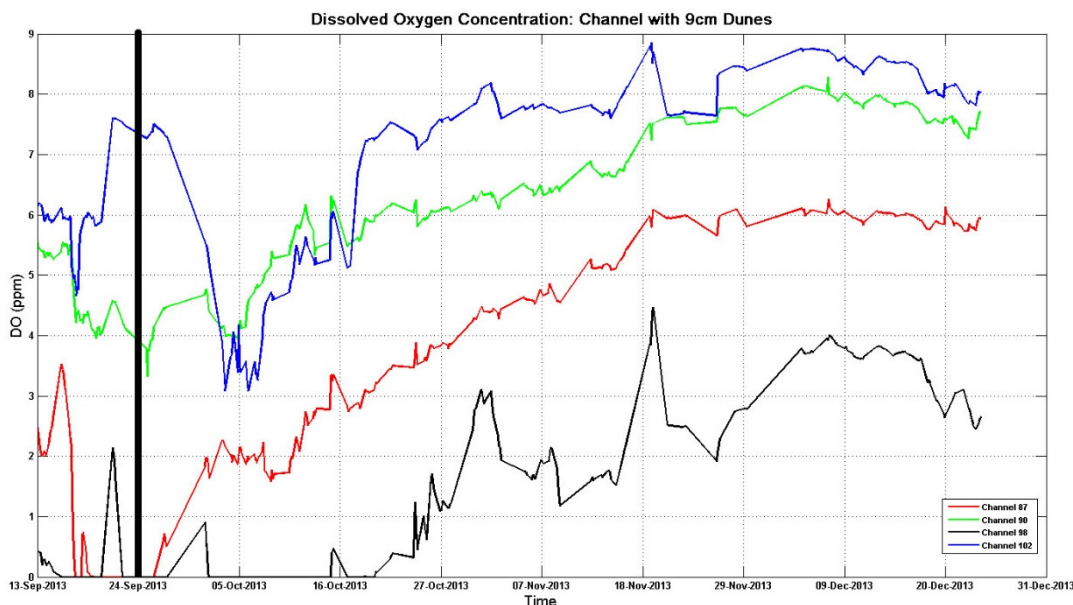
Figure 2-4. DO concentration at four locations within the body of a 9 cm tall dune from the 2013 experiment. Dissolved oxygen concentrations change over time as the labile organic carbon is consumed and respiration (and oxygen consumption) slow. The dark black line marks a pump failure that essential reset the system.
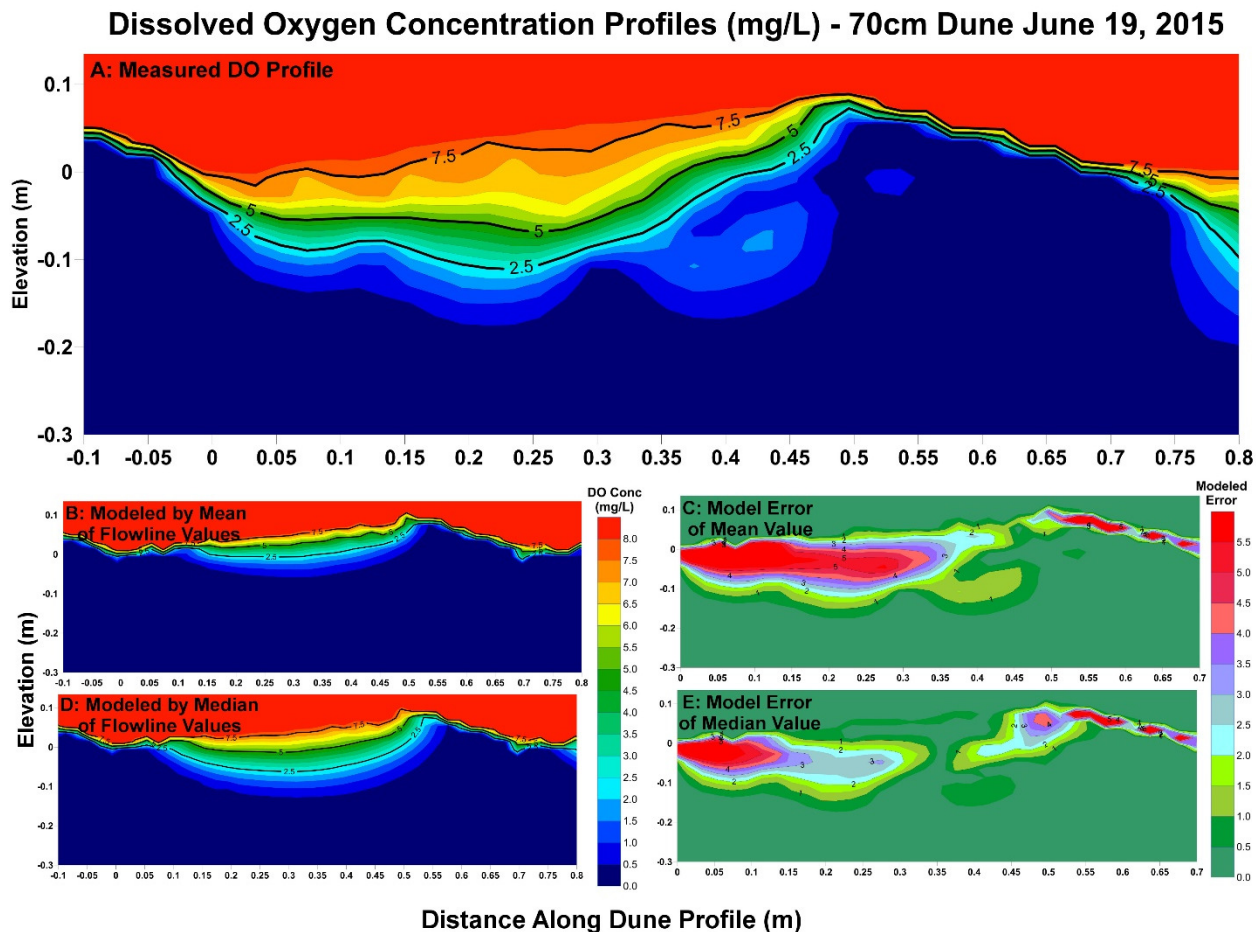
Figure 2-5. Measured and modeled DO concentration profiles for the 70 cm dune on June 19, 2015 (day 91). Panel A: DO profile generated from physical measurements. Panes B and D show the DO profiles for two different models that both employed, as is common practice, a single value of K_{DO}. The model in Panel B used the mean ($K_{DO} = 10.9 \times 10^{-5}$ s^{-1}) of all of the values calculated for the individual flowlines. The median ($K_{DO} = 4.5 \times 10^{-5}$ s^{-1}) value was used for the model in Panel D. The error (absolute value of modeled minus measured) is shown in Panels C and E.

2.3.2 Discussion

This is as far as we know, aside from planar optode measurements [*Kessler et al.*, 2012; *Larsen et al.*, 2011; *Precht et al.*, 2004; *Vieweg et al.*, 2013], the first time that DO or any chemical constituent has been recorded in the HZ with this kind of resolution. These high-resolution DO profiles give an unprecedented view of the DO dynamics in the HZ. It is

true that planar optodes can yield finer resolution than is achievable using our approach. It is worth noting, though, that planar optodes are generally not deployed with the duration and spatial scale as was employed in these experiments. Further, in our view, the question of preferential flow paths that are likely to be associated with large-scale planar optodes has not been well addressed. Additionally, due to the invasive process that would be involved in their deployment and the precise optical requirements needed for these devices, large-scale planar optodes are best suited for laboratory deployment and less so for natural settings. Small-scale planar optodes have been effectively deployed in field settings [*Vieweg et al.*, 2013]. In cases where millimeter-scale resolution is of real benefit, the added complexity of this type of deployment is worth the effort. For most efforts, centimeter-scale measurements are sufficient and, as will be discussed later, we have deployed our technique, to good effect, in a difficult field setting.

The visual aspect of the measured DO profiles presented in Figure 2-3 is remarkably similar to DO profiles generated by numerical models that compute DO consumption by first-order reaction kinetics (see, for example, Bardini et al. [2012] or Kessler et al. [2012]). Those models typically use a single value of the DO consumption rate (K_{DO}) to represent the reaction kinetics for the entire domain. From a visual aspect, it is tempting to conclude that our measurements validate those models. However, direct comparison of measured DO concentrations (Figure 2-5A) to two different DO consumption models, both using single-valued, first-order reaction kinetics (Figure 2-5B and Figure 2-5D), show substantial discrepancy between the measured and modeled values (Figure 2-5C and Figure 2-5E). The K_{DO} values used in the two models are the mean and median of DO consumption rates calculated individually for approximately thirty different flowlines and are likely to be typical of values obtained in the literature or from field studies. The main take away here is that while the single-valued, first-order model seems to capture the character of DO consumption dynamics it potentially misrepresents the morphology and extent of the DO plume. The causes for this discrepancy and a proposed refinement of existing theory will be discussed fully in a subsequent publication.

In keeping with current theory, we note that bed morphology (size and shape of the dunes) exhibits primary control over the DO profiles. The four panels in Figure 3 represent

different dune configurations, while the overlying flow (discharge and chemistry) is approximately identical for all four cases. The difference in the depth of the oxic/anoxic front is a direct effect of the different dune configuration. All other factors held equal, taller dunes induce larger pressure gradients across the bed profile. The stronger pressure gradients cause larger fluxes, greater flow velocities and deeper flow penetration into the HZ (see supplemental material). As a result, bed morphology directly influences the distribution of chemical compounds in the HZ.

Finally, we note that for measurements at fixed locations, the DO concentrations change over time (Figure 4). At fixed locations, the DO concentrations rise over time indicating the oxic/anoxic front is moving deeper into the HZ. We hypothesize that this is driven by the reduction of total carbon within the HZ (see supplemental material). For a system that has a relatively fixed carbon supply (e.g., a stream whose main carbon supply is from seasonal leaf litter), once a microbial community becomes well established, the rate of aerobic respiration will be regulated by the concentration and the availability of DO and labile organic carbon. Early in a carbon replenishment cycle, there is presumably an abundance of dissolved organic carbon. Thus, the respiration rate will be relatively high and DO will be consumed quickly, constraining the oxic/anoxic front to near the bed surface. As the most readily available organic carbon is consumed, (first near the bed surface) respiration rates, in that area will drop and DO will be transported deeper into the HZ [*Quick et al.*, 2016]. Over time, and lacking either an external source of bioavailable carbon or an alternate electron donor substrate, microbial metabolic activity will slow substantially and the majority of the HZ will be rendered oxic.

For a measurement technique to be broadly accepted it must be deployable in field settings. Our initial installation in the CER flume is among the most user-friendly setting for deployment that one might imagine. To test the field readiness of the system, we installed the fiber optic DO measurement system in the headwater stream of Watershed 1 in the H. J. Andrews Experimental Forest, Oregon, USA. This extensively studied field site already had multiple piezometers in place to track groundwater and hyporheic flows. We installed individual, fiber optic DO sensors in fourteen of those wells. Additionally, we installed nine new wells that were vertically stratified; each of which contained six DO sensors (Figure

2-6A). The installation supported a project whose objective was to track the evolution of organic carbon to inorganic carbon (CO_2) and quantify CO_2 outputs at watershed scales. DO measurements were scheduled to align with specific experimental events and a continuous record of DO concentrations was not desired or obtained. Within the constraints of those objectives, the fiber optic DO measurement system performed well. The automation enabled us to schedule measurements when no one was present and to take more measurements at higher frequency than is possible using conventional water extraction techniques. Time series measurements from two of the existing wells are shown in Figure 2-6B. The fiber optic (triangles) and conventional (circles) DO measurements track well but the fiber optic measurements offer a much more detailed record. The time series for one of the new, multi-level piezometers is shown in Figure 2-6C. The multi-level sensors reveal a distinct stratification of the DO concentrations, suggesting significant microbial activity in the HZ, which varies.
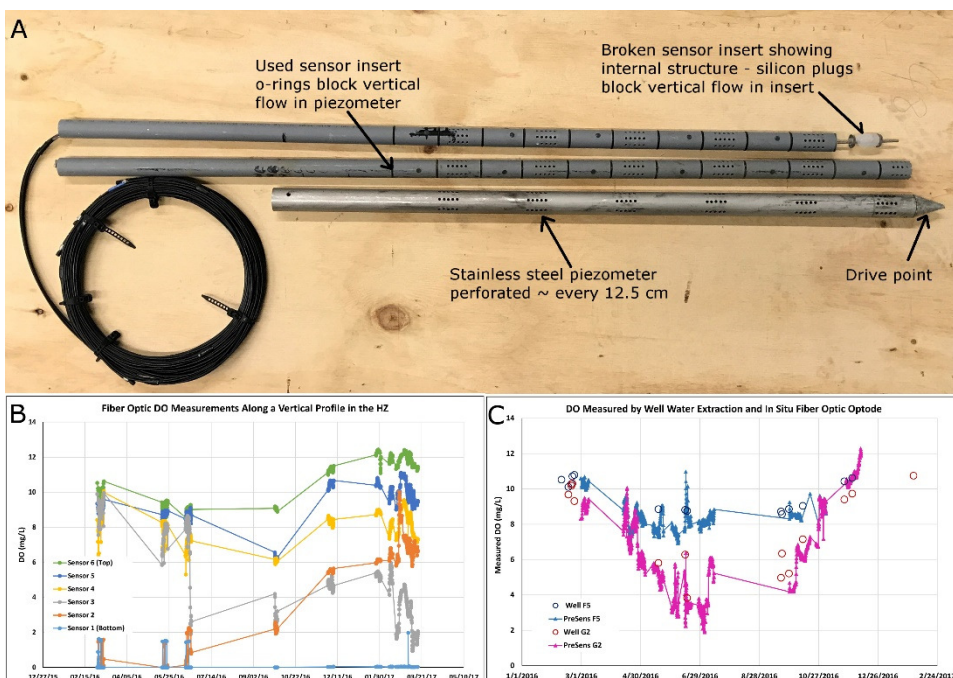
Figure 2-6. To install the sensors in the boulder/cobble bed of Watershed 1 of the H. J. Andrews Experimental Forest we used two-part sensor wells (Panel A). The outer, stainless steel piezometer was driven into the streambed in the conventional manner and a removable sensor insert was installed into the piezometer. Each insert had six sensors. O-rings prevent vertical flow between the two tubes. Silicone plugs prevent vertical flow in the sensor insert. Panel B shows the time series for each of the six-sensor in one of the multi-level piezometers. Stratification of DO is clearly present. The straight lines that connect the measurement clusters are only there to group visually the measurements for an individual sensor. Additionally, we installed individual sensors in fourteen existing wells. Panel C shows the DO concentrations for two of those wells measured by well water extraction (open circles ○) and the *in situ* fiber optic sensors (solid triangles ▲).

2.4 Conclusions

High-resolution mapping of DO concentrations offers a much more detailed picture of the biochemical state of the HZ than has been previously available. It reveals the complexity of biogeochemical activity in the HZ and enables us to map heterogeneity and identify micro sites of enhanced or diminished activity. Additionally, it allows us to track DO concentrations over time and, coupled with measured or modeled residence times, calculate the rate of DO consumption (K_{DO}) as a function of time and location. Defining the redox character of the HZ, which is complex and dynamic in both space and time, through the use of sparse measurements risks misidentifying its actual distribution. This research has clearly

demonstrated the utility of chemical measurements taken at high spatial and temporal density. Further, we have shown through the use of detailed DO measurements that the current application of single-valued, first order reaction mechanics will likely significantly misrepresent the extent and the morphology of the DO plume. Further, our measurements have demonstrated the strong control that stream morphology exerts over transport and consumption dynamics. While this study focuses on the dynamics of dissolved oxygen, other chemical constituents, particularly redox products, will be expected to respond in the same manner and the same approach could be used.

2.5 Acknowledgements

2.6 Supporting Information.

A more detailed description of the fiber optic DO measurement system is presented in the supplemental material, including sourcing information.

2.7 Funding Sources

2.8 Notes

Dr. Christian Huber is employed by PreSens and provided essential advice and guidance for the selection, use and implementation of the DO measurement equipment. He did not participate in the running of the experiments, the data analysis or the conclusions drawn from those data. He declares no competing interests. The other authors also declare no competing financial interests.

2.9 References

Appelo, C. A. J., and D. Postma (2010), *Geochemistry, groundwater and pollution*, 2 ed., CDC Press, Boca Raton.

Bardini, L., F. Boano, M. B. Cardenas, R. Revelli, and L. Ridolfi (2012), Nutrient cycling in bedform induced hyporheic zones, *Geochimica et Cosmochimica Acta*, *84*, 47-61.

Budwig, R., and P. Goodwin (2012), The Center for Ecohydraulics Research Mountain StreamLab - a facility for collaborative research and education, in *Innovations 2012: world innovations in engineering education and research*, edited, iNeer, Potomac, Maryland, USA.

Cardenas, M. B., and J. L. Wilson (2007), Dunes, turbulent eddies, and interfacial exchange with permeable sediments, *Water Resources Research*, *43*(8), W08412.

Chapelle, F. H. (1993), *Ground-Water Microbiology and Geochemistry*, John Wiley & Sons, New York.

Chapelle, F. H., P. B. McMahon, N. M. Dubrovsky, R. F. Fujii, E. T. Oaksford, and D. A. Vroblesky (1995), Deducing the Distribution of Terminal Electron-Accepting Processes in Hydrologically Diverse Groundwater Systems, *Water Resources Research*, *31*(2), 359-371.

Elliott, A. H., and N. H. Brooks (1997), Transfer of nonsorbing solutes to a streambed with bed forms: Theory, *Water Resources Research*, *33*(1), 123-136.

Findlay, S. (1995), Importance of surface-subsurface exchange in stream ecosystems: The hyporheic zone, *Limnology and Oceanography*, *40*(1), 159-164.

Fischer, H., F. Kloep, S. Wilzcek, and M. T. Pusch (2005), A River's Liver: Microbial Processes within the Hyporheic Zone of a Large Lowland River, *Biogeochemistry*, *76*(2), 349-371.

Gatti, S., T. Brey, W. Müller, O. Heilmayer, and G. Holst (2002), Oxygen microoptodes: a new tool for oxygen measurements in aquatic animal ecology, *Marine Biology*, *140*(6), 1075-1085.

Greig, S. M., D. A. Sear, and P. A. Carling (2007), A review of factors influencing the availability of dissolved oxygen to incubating salmonid embryos, *Hydrological Processes*, *21*(3), 323-334.

Gualtieri, C. (2011), *Essays on Fundamental and Applied Environmental Topics*, 1st ed., Nova Science, New York, USA.

Harvey, J. W., J. K. Böhlke, M. A. Voytek, D. Scott, and C. R. Tobias (2013), Hyporheic zone denitrification: Controls on effective reaction depth and contribution to whole-stream mass balance, *Water Resources Research*, *49*(10), 6298-6316.

Hunter, K. S., Y. Wang, and P. Van Cappellen (1998), Kinetic modeling of microbially-driven redox chemistry of subsurface environments: coupling transport, microbial metabolism and geochemistry, *Journal of Hydrology*, *209*(1–4), 53-80.

Jin, G., H. Tang, B. Gibbes, L. Li, and D. A. Barry (2010), Transport of nonsorbing solutes in a streambed with periodic bedforms, *Advances in Water Resources*, *33*(11), 1402-1416.

Jørgensen, C. J., and B. Elberling (2017), Subsurface Oxygen Availability Controls Greenhouse Gas Emission From Wetland Ecosystems, edited by P. P. Sensing, PreSens Precision Sensing.

Kessler, A. J., R. N. Glud, M. B. Cardenas, M. Larsen, M. F. Bourke, and P. L. M. Cook (2012), Quantifying denitrification in rippled permeable sands through combined flume experiments and modeling, *Limnology and Oceanography*, *57*(4), 1217-1232.

Klimant, I., V. Meyer, and M. Kuhl (1995), Fiber-Optic Oxygen Microsensors, a New Tool in Aquatic Biology, *Limnology and Oceanography*, *40*(6), 1159-1165.

Kohfahl, C., T. Graupner, C. Fetzer, and A. Pekdeger (2010), The impact of cemented layers and hardpans on oxygen diffusivity in mining waste heaps A field study of the Halsbrücke lead–zinc mine tailings (Germany), *Science of The Total Environment*, *408*(23), 5932-5939.

Larsen, M., S. M. Borisov, B. Grunwald, I. Klimant, and R. N. Glud (2011), A simple and inexpensive high resolution color ratiometric planar optode imaging approach: application to oxygen and pH sensing, *Limnology and Oceanography: Methods*, *9*(9), 348-360.

Marzadri, A., D. Tonina, and A. Bellin (2010), A semianalytical three-dimensional process-based model for hyporheic nitrogen dynamics in gravel bed rivers, *Water Resources Research*, *47*(11).

Marzadri, A., D. Tonina, and A. Bellin (2012), Morphodynamic controls on redox conditions and on nitrogen dynamics within the hyporheic zone: Application to gravel bed rivers with alternate-bar morphology, *Journal of Geophysical Research: Biogeosciences*, *117*(G3).

Marzadri, A., D. Tonina, A. Bellin, and A. Valli (2016), Mixing interfaces, fluxes, residence times and redox conditions of the hyporheic zones induced by dune-like bedforms and ambient groundwater flow, *Advances in Water Resources*, *88*, 139-151.

Marzadri, A., D. Tonina, A. Bellin, G. Vignoli, and M. Tubino (2010), Semianalytical analysis of hyporheic flow induced by alternate bars, *Water Resources Research*, *46*(7), n/a-n/a.

Marzadri, A., M. M. Dee, D. Tonina, A. Bellin, and J. L. Tank (2017), Role of surface and subsurface processes in scaling N2O emissions along riverine networks, *Proceedings of the National Academy of Sciences*.

Master, Y., U. Shavit, and A. Shaviv (2005), Modified Isotope Pairing Technique to Study N Transformations in Polluted Aquatic Systems: Theory, *Environmental Science & Technology*, *39*(6), 1749-1756.

Precht, E., U. Franke, L. Polerecky, and M. Huettel (2004), Oxygen Dynamics in Permeable Sediments with Wave-Driven Pore Water Exchange, *Limnology and Oceanography*, *49*(3), 693-705.

PreSens (2016), IM_FB4-FB4trace_dv3.pdf, edited, p. Fibox 4 Instruction Manual, PreSens Precision Sensing.

Quick, A. M., W. J. Reeder, T. B. Farrell, D. Tonina, K. P. Feris, and S. G. Benner (2016), Controls on Nitrous Oxide Emissions from the Hyporheic Zones of Streams, *Environmental Science & Technology*, *50*(21), 11491-11500.

Stonedahl, S. H., J. W. Harvey, A. Wörman, M. Salehin, and A. I. Packman (2010), A multiscale model for integrating hyporheic exchange from ripples to meanders, *Water Resources Research*, *46*(12).

Tengberg, A., J. Hovdenes, and D. Barranger (2003), Optodes to Measure Oxygen in the Aquatic Environment, *Sea Technology*, *44*(2), 10-15.

Tengberg, A., et al. (2006), Evaluation of a lifetime-based optode to measure oxygen in aquatic systems, *Limnology and Oceanography: Methods*, *4*(2), 7-17.

Tonina, D., and J. M. Buffington (2007), Hyporheic exchange in gravel bed rivers with pool-riffle morphology: Laboratory experiments and three dimensional modeling, *Water Resources Research*, *43*, W01421.

Tonina, D., and J. M. Buffington (2009), A three-dimensional model for analyzing the effects of salmon redds on hyporheic exchange and egg pocket habitat, *Canadian Journal of Fisheries and Aquatic Sciences*, *66*(12), 2157-2173.

Triska, F. J., and R. S. Oremland (1981), Denitrification Associated with Periphyton Communities, *Applied and Environmental Microbiology*, *42*(4), 745-748.

Triska, F. J., J. H. Duff, R. W. Sheibley, A. P. Jackman, and R. J. Avanzino (2007), DIN Retention-Transport Through Four Hydrologically Connected Zones in a Headwater Catchment of the Upper Mississippi River1, *JAWRA Journal of the American Water Resources Association*, *43*(1), 60-71.

Vieweg, M., N. Trauth, J. H. Fleckenstein, and C. Schmidt (2013), Robust Optode-Based Method for Measuring in Situ Oxygen Profiles in Gravelly Streambeds, *Environmental Science & Technology*, *47*(17), 9858-9865.

Wuhrmann, K. (1972), Stream Purification, in *Water pollution microbiology*, edited by R. Mitchell, pp. 119-151, Wiley-Interscience, New York, NY.

Zarnetske, J. P., R. Haggerty, S. M. Wondzell, and M. A. Baker (2011a), Labile dissolved organic carbon supply limits hyporheic denitrification, *Journal of Geophysical Research: Biogeosciences*, *116*(G4).

Zarnetske, J. P., R. Haggerty, S. M. Wondzell, and M. A. Baker (2011b), Dynamics of nitrate production and removal as a function of residence time in the hyporheic zone, *Journal of Geophysical Research: Biogeosciences*, *116*(G1), G01025.

Chapter 3

Spatial dynamics of dissolved oxygen concentrations and bioactivity in the

hyporheic zone[2]

The majority of chemical reactions in streams occur within the hyporheic zone (HZ). Hyporheic exchange, flow into and out of the hyporheic zone, exerts primary control over those reactions because flow rate determines the residence time and delivery of chemical constituents to the HZ. Dissolved oxygen (DO) concentrations and consumption rates are primary indicators of heterotrophic respiration and redox conditions. Due to the complexity of hyporheic flow and interactions between hyporheic hydraulics and the biogeochemical processes, a detailed, mechanistic and predictive understanding of the biogeochemical activity in the HZ has not yet been developed. Previous studies of microbial activity in the HZ have treated the metabolic DO consumption rate (K_{DO}) as a fixed and homogeneous property that is determined primarily by the concentration of bioavailable carbon. Here we demonstrate that, aerobic respiration is limited largely by the availability of DO as opposed to the availability of

nutrients (carbon). We show that, in a hyporheic system that is characterized by typical and relatively abundant bioavailable carbon, K_{DO} is a linear function of the local downwelling flux (velocity) within a bedform and, by extension, throughout a stream reach. We further demonstrate that, at least for triangular dunes, the downwelling velocities are lognormally distributed and as a result so too are the distribution of K_{DO} values. We compare a measured DO profile to modeled profiles and demonstrate that treating K_{DO} as a function of the downwelling flux yields a significant improvement in the accuracy of predicted DO profiles.

3.1 Introduction

Dissolved oxygen (DO) is the primary oxidizing agent in most riverine systems and their associated hyporheic zones (HZ). Dissolved oxygen promotes the respiration of organic carbon. DO concentrations strongly regulate a suite of processes including nitrogen and carbon cycling, anaerobic respiration [*Cooper*, 1965; *Ocampo et al.*, 2006; *J Rutherford et al.*, 1995] and the processing of metabolic waste and environmental pollutants [*Master et al.*, 2005]. Collectively, these chemical processes have a profound effect upon benthic habitat, surface water quality and the capacity of streams to process biological and environmental compounds [*Greig et al.*, 2007; *Tonina and Buffington*, 2009]. Most of these processes occur in the hyporheic zone (HZ), where pore water exchange and mixing support active biogeochemical processing. Thus DO concentration within the HZ, along with the associated gradients and consumption rates, are primary indicators of the redox and biochemical state of the HZ [*Appelo and Postma*, 2010; *Cardenas et al.*, 2008; *Chapelle*, 1993; *Chapelle et al.*, 1995].

With surface waters often near saturation with respect to oxygen, and the subsurface often oxygen limited, the flux of oxygen from the surface to the hyporheic zone dictates the magnitude of oxidative processes. The rate of DO consumption (K_{DO}) is determined by the hyporheic exchange rate (the rate at which surface water enters the HZ and is eventually returned to the surface) and the activity level of the microbial communities in the HZ [*Beaulieu et al.*, 2011; *Chapelle*, 1993; *Henry et al.*, 2006; *Moreno-Vivián et al.*, 1999; *Richardson et al.*, 2009; *Wrage et al.*, 2001].   However, not all environmentally important processes in the HZ are aerobic [*Pinay et al.*, 2009; *Zarnetske et al.*, 2011a]. The DO consumption rate defines the extent of the oxic zone and, thus, the extent of the anoxic zone.

The extent of the anoxic zone defines the necessity for and/or feasibility of anaerobic metabolic processes and places limits on the potential for multi-step, anaerobic processes to be carried to completion.

Common perception holds that the redox and metabolic activity rates of microbial communities are primarily a function of the availability of labile carbon [*Harvey et al.*, 2013; *Hunter et al.*, 1998; *Sobczak and Findlay*, 2002; *Zarnetske et al.*, 2011a; b], an assumption that is often appropriate when oxygen concentrations are constant. During hyporheic influx, DO concentrations decline with respiration and therefore are typically variable. Further, even at the scale of individual bedforms, hyporheic flux rates are also variable. Thus, DO concentrations and flux rates have the potential to influence respiration rate. Current practice, in numerical studies of microbially mediated redox dynamics, is to treat the reaction rates of the constituent species (e.g. DO (K_{DO}), carbon (K_C) and nitrogen compounds (K_{NOX})) as bulk and relatively fixed material properties that are applied homogeneously over the entire domain; see for example: [*Bardini et al.*, 2012; *Kessler et al.*, 2012; *Alessandra Marzadri et al.*, 2010; *A. Marzadri et al.*, 2012; *J C Rutherford et al.*, 1995; *Wriedt and Rode*, 2006; *Zarnetske et al.*, 2012]. Yet, empirical studies have reported local zones of increased biologic activity (hot spots). "Hot spot" variations in activity been attributed to local and random surpluses in high quality, bioavailable carbon [*Cleveland et al.*, 2007; *Curiel Yuste et al.*, 2007; *Kayser et al.*, 2005; *Zarnetske et al.*, 2011c]. However, another cause may exist. To the best of our knowledge, no one has attempted to associate variations in hyporheic metabolic activity with a more systemic and ordered cause, such as stream hydraulics. Within the stream ecology community, the notion that microbial aerobic respiration or other redox rates may be a function of the hyporheic flux rate would seem to be a new idea, but within the microbiology-community, it has been, at least by analogy, relatively widely reported. Microbiological reaction and growth rates are commonly studied in chemostatic experiments. A chemostat is a reaction vessel in which the biochemical state of a process can be held in relative stasis. This is accomplished by adding and removing media (nutrients, oxygen and bio reactive species) to and from the reaction vessel at the same rate. This keeps the reactive constituents in a steady balance and the reaction rate constant. The flux rate through the

chemostat is termed the dilution rate. In chemostatic, microbial growth experiments, it has been shown that growth rates, respiration rates, nutrient uptake rates and carbon dioxide release rates all increase linearly with dilution rate [*Furukawa et al.*, 1983; *Harrison*, 1972; *Kayser et al.*, 2005; *Laanbroek et al.*, 1994; *Nobre et al.*, 2002; *PIRT*, 1957; *Ramirez and Mutharasan*, 1990; *Rosenberger and Kogut*, 1958; *Sinclair and Ryder*, 1975]. In the context of hyporheic flow systems, the chemostatic dilution rate can be seen to be analogous to the downwelling flux along a particular flow line.

If we are to understand properly the dynamics of aerobic respiration and the synergy between aerobic and anaerobic processes that enables them to efficiently process nutrients and pollutants, we need to have a clear and detailed understanding of the controlling dynamics. In general, previous field studies have not taken sufficiently detailed and replicated measurements to parse DO consumption to the individual flowline level [*Harvey et al.*, 2013; *Naranjo et al.*, 2015; *Nogaro et al.*, 2013; *Pretty et al.*, 2006]. When modeling reactive processes in the HZ, researchers have made the explicit assumption that the rate of DO consumption, K_{DO}, is constant within a homogeneous domain [*Bardini et al.*, 2012; *Kessler et al.*, 2012; *Alessandra Marzadri et al.*, 2010; *J Rutherford et al.*, 1995]. Similarly, most work has not attempted to make a strong link between flow hydraulics and DO consumption rates [*Boano et al.*, 2014]. In the present study, we address these limitations by taking high-resolution DO measurements, both temporally and spatially, over two long-duration, large-scale flume experiments. Our aims are to (1) elucidate the role of stream hydraulics in DO consumption dynamics and, by extension, hyporheic redox dynamics and (2) separate the roles of mass transfer (hydraulics) and the reaction rates of chemical constituents.

3.2 Methods and Materials

3.2.1 Experimental setup

The experimental setup has been described in detail in other publications [*Quick et al.*, 2016; *Reeder et al.*, 2017b]. In summary, we conducted two sets of experiments, in the large-scale flume (approximately 20 m x 2 m) at the Center for Ecohydraulics Research Stream Laboratory [*Budwig and Goodwin*, 2012] at the University of Idaho, Boise, to test the impact

of bed morphology, stream hydraulics and surface water chemistry (reactive nitrogen loading) on DO and nitrogen consumption dynamics and the impact of those processes on N_2O emissions from streams. The first flume experiment (Flume 1) ran continuously from August 2013 through December 2013 and the second (Flume 2) ran from February 2015 through June 2015. In both sets of experiments, the flume was divided into three stream channels (30 cm wide x 60 cm deep x 15 m long) which were separated by two access corridors. Dunes of various sizes were constructed from 90% quarry sand (D_{50} ~1.5 mm) and 10% natural sand collected from the Boise River (Boise, ID, USA). The natural sand provided an inoculum to initiate bacterial communities, which were representative of those that typically reside in streambed sediments. To provide an organic carbon nutrient source, 0.15% by dry weight of finely divided (< 5 mm) cottonwood leaves were added to the sand mix. *In-situ* DO sensors embedded in the bulk of the dunes and surface probes attached to the flume's robotic instrument cart allowed us to obtain high-density DO measurements throughout the duration of the experimental runs. A typical placement of the *in situ* DO probes is illustrated by the blue stars in Figure 3-1. Surface probe measurements were taken at 2 cm longitudinal intervals along the bed surface profiles at depths of 0, 5, 10, 20, 30 and 40 millimeters. For the present discussion, we will consider three different dune variants. From Flume 1, we will evaluate the response of a 9 cm tall by 1 m long dune, hereafter referred to as the "9 cm dune." The energy slope for the 9 cm dune was 0.002. From Flume 2, we will consider a 9 cm tall by 100 cm long dune and a 9 cm tall by 70 cm long dune, hereafter referenced as "100 cm dune" and "70 cm dune", respectively. The energy slope for the Flume 2 experiments was 0.003.
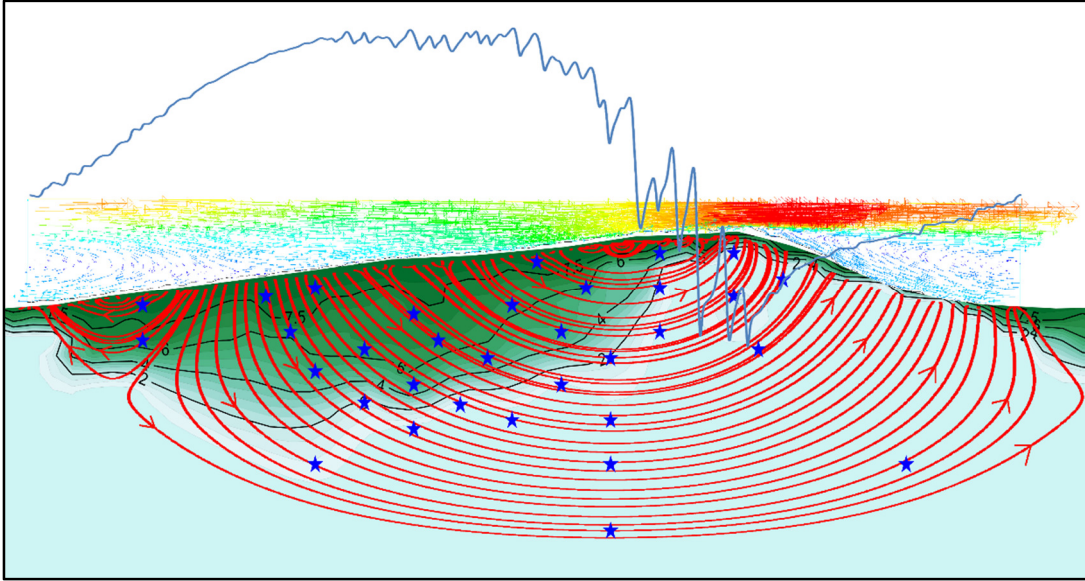
Figure 3-1 A cross-section of a typical dune profile is shown at the bottom of the figure. The bed surface profile was measured by laser scan. The water surface elevation was measured by ultrasonic scan. These measurements along with the measured discharge were used to model surface flow velocity (multi-colored vectors) and the bed-surface pressure profile (blue trace at the top of the figure). Hyporheic flowines (red traces overlain on the dune and measured DO profile) were modeled using GMS ModFlow [Aquaveo, 2015] and the model of Marzadri [Alessandra Marzadri et al., 2010]. Surface flow is from left to right.

3.2.2 Bed-surface pressure profiles and hyporheic flowlines

At the bedform scale, hyporheic flow is driven by local pressure gradients along the bed surface. As illustrated in Figure 3-1, flow generally enters the dune on the upstream face and exists on the downstream face. This results in a series of quasi-discreet and arched flowlines, with the shortest near the dune peak and the longest entering more proximal to the upstream dune trough and exiting near the downstream trough (red lines, Figure 3-1). In order to calculate residence times at specific locations within the bed and the flow paths to those locations the total pressure (static plus dynamic pressure) must be known along the entire profile of the bedform. Unfortunately, we did not have the physical capability to measure the bed surface pressure with sufficient accuracy. Instead, following the approach described by Cardenas and Wilson [2007], we modeled the pressure profiles using ANSYS Fluent CFD (ANSYS Inc., Canonsburg, PA, USA). ANSYS CFD provides a numerical solution to the Reynolds-Averaged, Navier Stokes surface flow equations. Our models, which

were constructed from between 65,000 to 95,000 triangular elements, used a k-ω turbulence closure with a Low-Reynolds-Number correction. Physical inputs into the models included measured bed surface a water surface profiles and surface flow velocity. The bed surface profiles were measured by laser scanning as a single trace along the centerline of each dune. Longitudinal spacing of the bed surface elevation measurements was 2 cm with a vertical resolution of less than 1 mm. Similarly, water surface elevation measurements were obtained using an ultrasonic sensor (Omega Engineering, Inc., CT, USA; Model LVU30). The inlets and outlets of the surface flow models were treated as periodic boundaries with the periodic pressure gradient defined by the energy slope of the water surface. The water surface was modeled as a symmetry boundary and the bed surface as a no-slip wall boundary. Residual error for continuity, x-velocity, y-velocity, k and ω was set to less than $1x10^{-6}$ for convergence. Figure 3-1 shows, without scaling, a typical bed-surface pressure profile (jagged blue line at the top of the figure) and surface water velocity vectors (multicolored vectors in the center of the figure) of a typical modeled surface flow. The overall CFD modeling approach was validated against the pressure measurements provided by Fehlman [1985] (Figure 3-2A). The excellent agreement of the simulated bed-pressures to the measured values, over a broad range of discharges and energy head, gave us a high degree of confidence that our modeling approach was robust, accurate and not overly sensitive to the applied boundary conditions.

Hyporheic flowlines and the associated residence times (τ) were calculated using the model of Marzadri [2010] and GMS ModFlow. The red lines overlain on the dune cross-section and DO concentration profile in Figure 3-1 are typical of flowline profiles used for analysis in this experiment. The data stream, for each flowline, is a series of X, Y positions coupled with a calculated residence time, τ, for a parcel of water to reach those positions. To validate the calculated residence times, at the end of Flume 2, we removed the instrument clusters from several of the *in situ* measurement locations (green dots on the inset of Figure 3-5) and replaced them with electrical conductivity (EC) sensors. We then injected a concentrated salt solution into the head box of the flume as a continuous stream for approximately 30 minutes. Residence times were measured with EC sensors at 9 locations in

a 70 cm dune and 20 locations in a 100 cm dune. The correlation of measured to modeled

residence times is shown in Figure 3-2B.
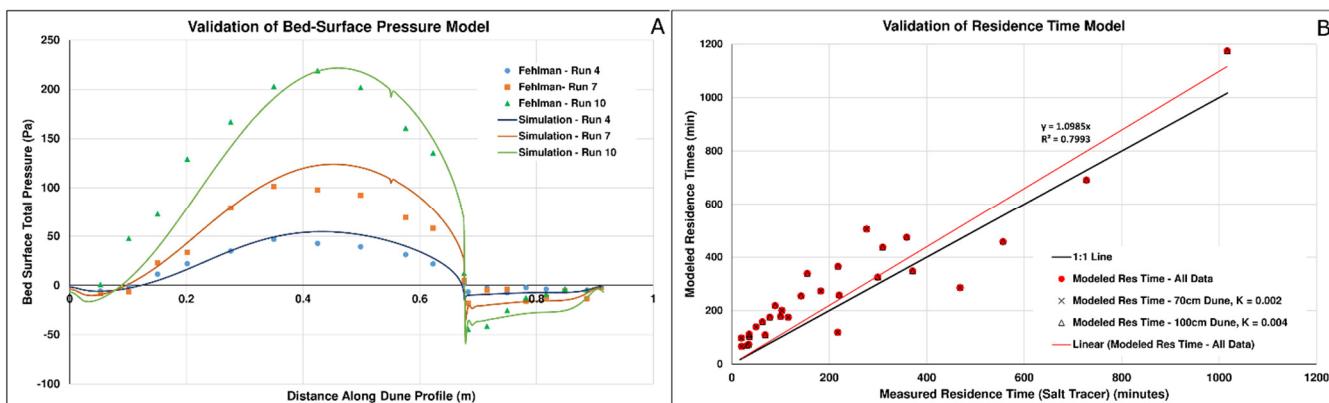
Figure 3-2 The modeled quantities used in these experiments were validated against physical measurements. A)
The modeling technique used to create the bed-surface pressure profiles was validated against the data of Fehlman
[1985]. The discreet points represent the measured values provided by Fehlman. The continuous lines are the
modeled simulations. The same mesh and geometry was used for all three simulations. The ∆P for Run 4 was
23Pa/m, 54Pa/m for Run 7 and 98Pa/m for Run10. Discharges for the same runs were 65 kg/s/m, 98 kg/s/m and
130 kg/s/m, respectively. Flow depth at the dune crest was 0.15m for all runs. B) The residence times derived
from the calculated flowlines were validated with physical measurements using salt tracer tests.

3.2.3 DO consumption rate calculation

We used two separate methods to calculate DO consumption rates (K_{DO}) at the

resolution of individual flowlines. In the primary methodology, we first created DO

concentration profiles for each dune on each evaluation date using all the surface and *in situ*

DO probe data for that dune and date. Using the mapping software Surfer® Version 10

(Golden Software, Inc., Golden CO) the measured DO data were krigged and gridded to

create DO concentration maps (see the green shaded concentration profiles in Figure 3-1 and

Figure 3-6). These DO concentration profiles are comprised of a regular array of X-Y

locations and a DO concentration at each location. We then mapped the appropriate flowlines

(red lines, Figure 3-1) onto all the DO concentration profiles. The flowline traces are

comprised of a series of X-Y locations and a residence time at each location. From the two

overlain data sets, we extracted, for each flowline, a data stream that is the mated pair of

residence time and the DO concentration (τ, [DO]). In this approach, the residence time for

any position along a particular flowline is a function of all of the prior positions along that flowline. The DO concentrations, at any given point, are interpolated from nearby measured values.

The second method was use to insure that the form of the K_{DO} response was not simply an artifact of the data structure in the krigged DO profiles and also to isolate the activity of the sediments along the surface profile. In that approach, K_{DO} values for the sediments along the surface profile were calculated using only the surface probe data. Residence times to each of the measurement positions along the surface profile were calculated individually by back-particle tracking. That is, for the purpose of determining residence time, each of the surface-profile measurement positions, was considered to be the terminus point for its own individual flowline. All of the DO concentrations used in the surface profile calculations are from direct measurement (no interpolation). Each set of six vertically aligned measurement points was treated as a functional flowline and an exponential fit was calculated for each of those vertically aligned sets.

For both methods, we considered that the reaction mechanics of DO consumption were either zero-order or first-order. For zero-order consumption the form of the reaction equation is:

$$[DO]_\tau = -K_{DO}\tau + DO_0 \qquad\qquad (3.1)$$

Where $[DO]_\tau$ is the DO concentration at residence time τ along a flowline, K_{DO} is the zero-order reaction rate, τ is the residence time of a parcel of water traveling along a flowline and DO_0 is the surface water DO concentration. For first-order reactions, the decay is exponential and the reaction equation takes the form:

$$[DO]_\tau = DO_0\, e^{-K_{DO}\tau} \qquad\qquad (3.2)$$

The quantities are the same as for Equation 1, with the exception that the values and the units for the rate constant, K_{DO}, will be different for the two models. To test which of the reaction models best describe the physical reaction processes, we calculated linear (zero-order) and exponential (first-order) fits to all (n = 2008) of the flowline (τ, DO) data streams.

While both models provided useful descriptions of the DO consumption dynamics, the first-order model was visually and in terms of R^2 values clearly better. Figure 3-3A shows the R^2 values of the exponential fits for all of the flowlines evaluated for this paper. The mean and median R^2 values were 0.92 and 0.94, respectively. Approximately 95% of the flowlines had an R^2 of 0.8 of higher. Considering only flowlines whose R^2 values were greater than 0.8, Figure 3-3B and Figure 3-3C show examples of "best" and "worst" exponential fits to individual flowlines. In cases where the exponential fit matches the measured data to a very high degree of determination ($R^2 > 0.95$) (Figure 3-3B), it would seem that the modeled flowlines are tracking the physical and related chemical processes with a high degree of objective accuracy. On the other hand, cases that do not fit as neatly to the measured data (Figure 3-3C) suggest two possibilities: 1) the idealized flowlines are not, in these cases, matching perfectly the actual flow path and, in essence, the idealized flowlines are "cutting across" physical flowlines or, 2) the idealized flowlines are, in fact, generally correct, but the transitions in the measured data are indications of physical or biologic heterogeneity, i.e. "hot" or "cold" spots due to variations in nutrient density or hydraulic conductivity.
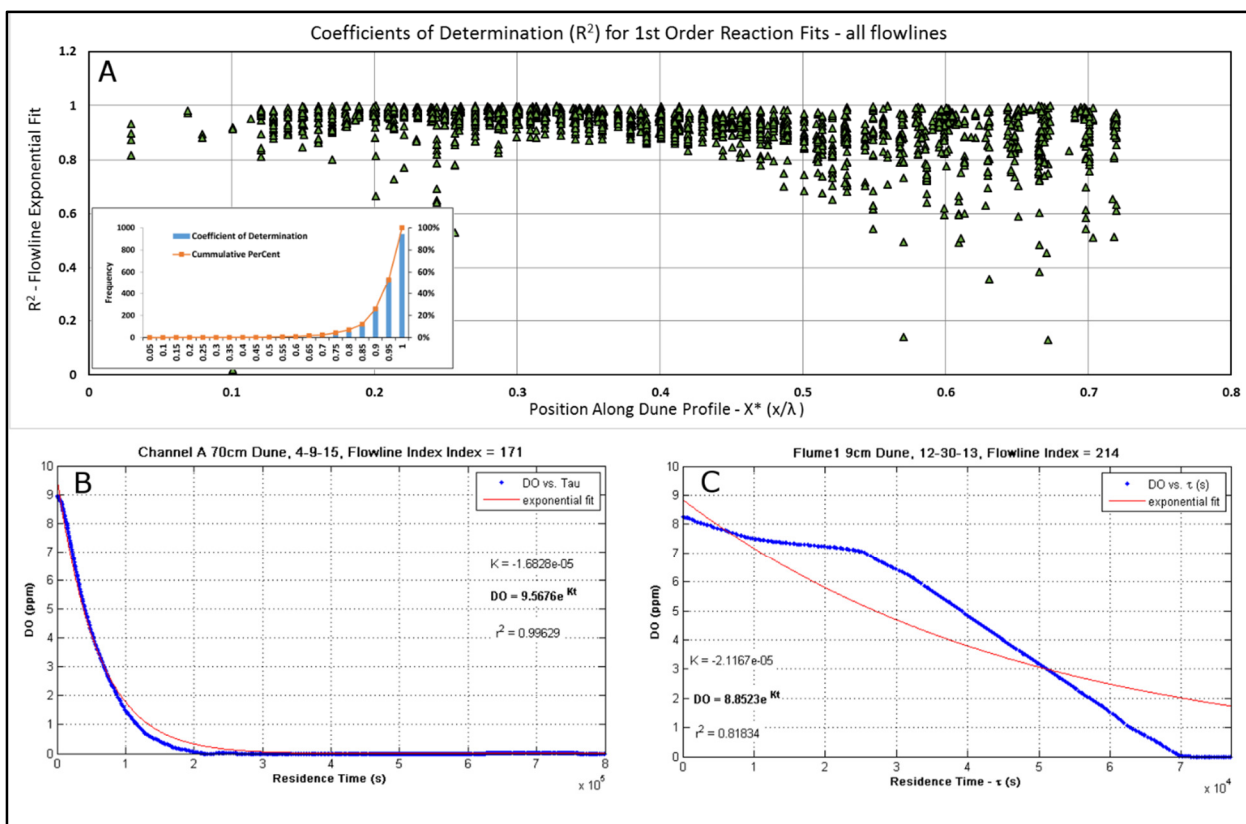
Figure 3-3 1st-order reaction kinetics, in the case of DO consumption through microbial metabolic processes, are described by an exponetial decay in the DO concentration. The governing equation takes the form: $[DO] = DO_0e^{-K\tau}$, where K (K_{DO}) is the reaction rate constant for the consumption of DO, τ is the residence time along a flowline and DO_0 is the DO concentration in the surface water. The top plot show the R^2 values for the exponetial (1st-order reaction) fits for all of the flowlines used in this experiment. Approximately 93% of the flowlines had an R^2 value of 0.80 or higher (see inset), indicating that 1st-order reaction kinetics are a strong descriptor of the true behavior of the system. The two bottom plots are examples of exponetial fits for individual flowlines. They represent the "best" and the "worst" of the majority of the flowlines evaluated.

3.2.4 Data presentation

Using the procedure previously described we calculated the DO consumption rates (K_{DO}) for all of the modeled flowlines for the 9 cm, 70 cm and 100 cm dunes at several dates through the two experimental runs. Longitudinal spacing of the modeled flowlines, along the bed surface, was roughly 2 cm. To describe the spatial distribution of K_{DO} values, the locations of the calculated values are assigned to the x-locations of the entry points of the flowlines into the HZ. To represent different bed geometries on the same scale, we plot the

K_{DO} as a function of X^*, which is the downwelling location (x) normalized by the length (λ') of the downwelling area ($X^* = x/\lambda'$). Note that for all of the graphs that employ calculated K_{DO} values or calculated downwelling fluxes (q_{dw}) values, the presented values have been multiplied by a factor of 1×10^5. That is to say, if a value of K_{DO} or q_{dw} of 2.5 is read from a graph, the associated physical value is 2.5×10^{-5}.

3.3 Results and Discussion

This paper focuses primarily on K_{DO} as it is impacted by spatial dynamics. K_{DO} also varies temporally; therefore, a companion paper will focus on the temporal dynamics [*Reeder et al.*, 2017a]. As outlined in the methods, we tracked changes in dissolved oxygen along flowpaths of known velocity to calculate K_{DO}. Figure 3-4 shows the calculated K_{DO} values for the individual replicates (Channels A, B and C) of the 70 cm and 100 cm dunes near the end of the experiment. It is important to note the form of the K_{DO} profile. For all of the traces, the K_{DO} values are quite low near the trough of the dune and rise gently moving towards the crest. In the middle of the downwelling area, the K_{DO} values are relatively constant and then rise sharply at the crest of the dune. The general observation is that K_{DO} values are low where the downwelling flux (velocity) is low and high in areas of high downwelling velocity. Importantly, K_{DO} values are calculated and expressed as a function of residence time (τ). The DO consumption rates are not based upon mass or the size of a control volume. Therefore, the variation in the reported K_{DO} values is, in fact, an indication that the activity levels of the microbial community are differentiated across the flowlines and not a simple linear scaling of the mass flux. The form and magnitude of the DO consumption profiles is consistent across the replicate dunes. It is also generally consistent in form across time but shows a distinct temporal trend that will be described fully in the companion publication [*Reeder et al.*, 2017a]. Finally, we note that the rising arm of the Channel C, 100 cm dune is shifted upstream relative to the other profiles. This is most likely due to upstream migration of the dune crest. Dune crest migration was visually observed but not measured during the run of the experiment. It was not specifically recorded for this or any other dune. Earlier profiles have the rising limb of the K_{DO} profile for this dune at the downstream location. For the three dune configurations, the shapes of the K_{DO} profiles generated by the surface profile method and the bulk flowline methods are completely consistent indicating that the form of the K_{DO}

profile is not a function of the data structure but, rather, due to variations in biological activity levels (Figure 3-5). This consistent behavior also shows that aerobic respiration starts at the bed-surface/water interface and continues consistently along the flowlines until DO is depleted below the aerobic threshold. It is interesting to note, though, that near the crest (X^* > 0.6) the bulk flowlines exhibit consistently higher values of K_{DO} than the surface profile sediments. This may be an indication of decreased bioactivity in the surface sediments, possibly due to carbon depletion relative to the bulk sediments.
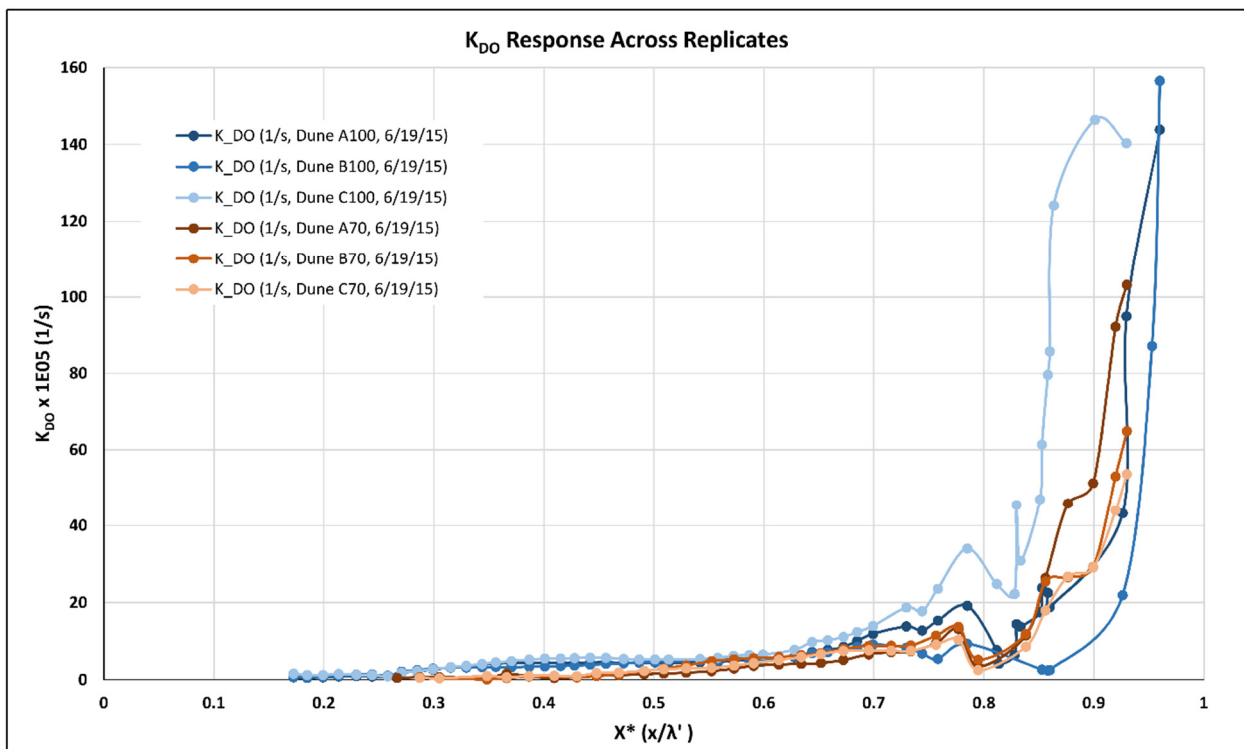
Figure 3-4 In Flume 2, we ran replicates of the two dune configurations evaluated during that experiment. The replicates were designated as Channels A, B and C. These K_{DO} profiles, from the end of the Flume 2 experiment, demonstrate the repeatability across replicates and the consistency between dune geometries of the of the response of the system.
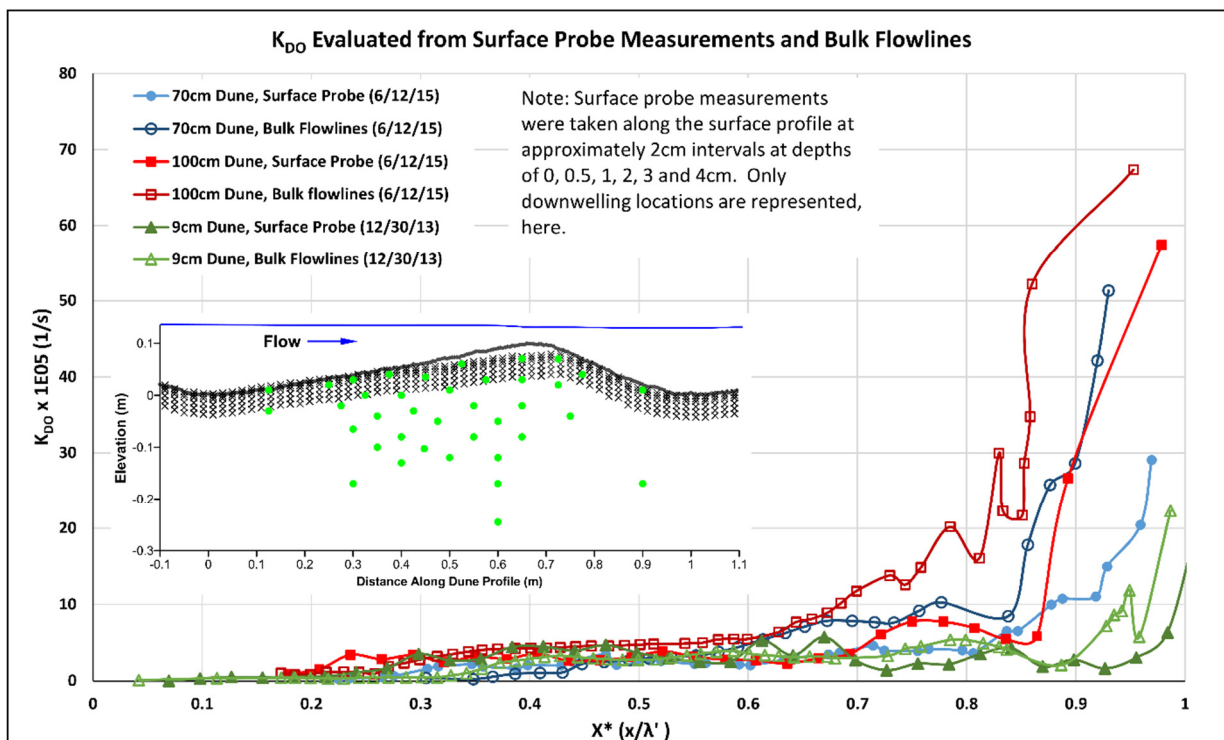
Figure 3-5 In both flume experiments, DO concentration was measured using two independent techniques. DO concentrations along the dune surface profile were taken using surface probes (Unisense, Aarhus, Denmark). DO measurements in the bulk of the dune were obtained using in-situ optical sensors (PreSens, Regensburg, Germany). K_{DO} values for the bulk flowlines (open markers) were calculated by mapping the flowlines onto DO profiles that were krigged from the collective surface and bulk measurements. An exponential fit was calculated for each of flowlines that were mapped onto the krigged DO profiles. K_{DO} values for the surface measurements (filled markers) were calculated by calculating a residence time for each suface measurement position, by back-particle tracking, and treating each measurement set as a flow line. That is, at each measurement position (X^*) along the dune surface profile, DO concentration and residence time (τ) values were defined at depths of 0, 5, 10 ,20, 30 and 40 millimeters. An exponential fit was calculated for these six measured points at each position (X^*).

The consistent and persistent form of the K_{DO} profiles suggests that an overarching and steady process is driving the response. This would suggest that the observed values for the downwelling flux and aerobic respiration rate (q_{dw} and/or K_{DO}) would adhere to a recognizable probability distribution; for example, they might be normally distributed. The model of Marzadri [2010] provides a value of the downwelling flux ($q_{dw} = V_{dw} \times \rho$) at each flowline entry point. We tested the downwelling fluxes against a variety of distributions and found that, for all of the bedform configurations investigated, the calculated q_{dw} values

conform to a lognormal distribution (Figure 3-6A). The quality of fit for the flux data, to a lognormal distribution, was evaluated using the Kolmogorov-Smirnoff test. All data sets passed the acceptance criteria. Figure 3-6B show the quality of fit for the 9 cm, 70 cm and 100 cm dunes at the end of the experiments. We similarly tested the K_{DO} data sets and found that for all configurations and on all evaluation dates, the K_{DO} values also conform to a lognormal distribution (Figure 3-6C). The quality of fit for the K_{DO} distribution is shown in Figure 3-6D. All data sets passed the Kolmogorov-Smirnoff acceptance criteria.
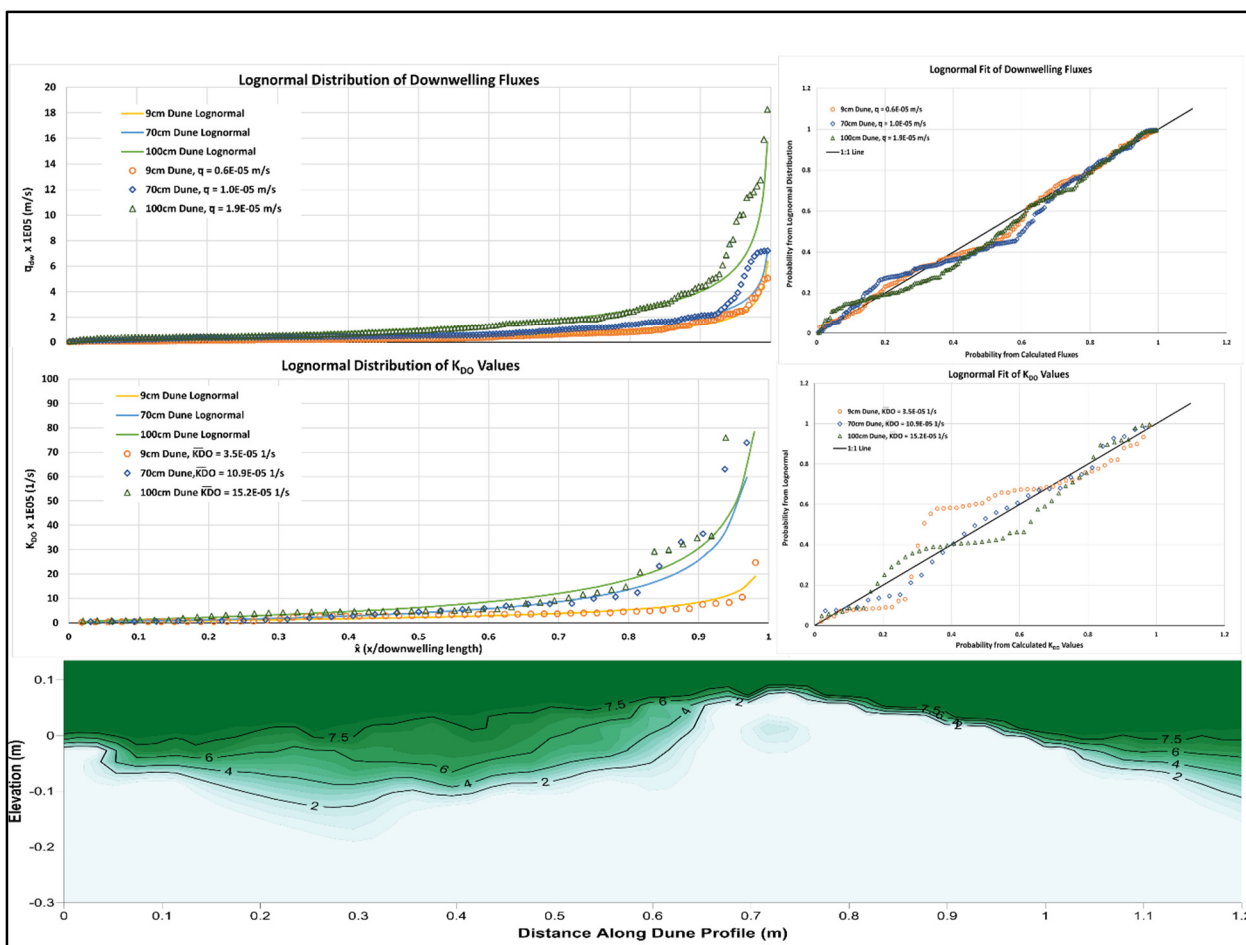
Figure 3-6 The values of the downwelling flux (V_{dw} x ρ) and K_{DO}, for individual flowlines, are lognormally distrubuted across stoss face (downwelling area) of the dunes. The two top graphs demonstrate the lognormal distribution of the downwelling fluxes. The chart on the upper left is the lognaormally distributed downwelling fluxes for the 9cm, 100cm and 70cm dunes. The open markers are the calculated q_{dw} values for the individual flow lines and the solid lines are the lognormal profile calculated from the mean and standard deviations of the log-transformed data. The chart on the upper right demonstrates the quality of the lognormal fit with calculated q_{dw} versus modeled values tightly grouped around the 1:1 line. Similarly the calculated and lognormal modeled values of K_{DO} are shown in the center plots. For spatial context, the lognormal profiles (charts on the left) are spatially aligned with downwelling area of a representative dune, shown by the DO profile at the bottom of the figure.

The lognormal distribution of downwelling velocities, for triangular dunes is a natural property of the interaction between the stream hydraulics and the bed morphology [*Wörman et al.*, 2002]. The lognormal distribution of K_{DO} values is a result of the fact that biological activity levels are linearly proportional to the flux (Figure 3-7). This relationship may be

modulated to some degree by the transitory nature of carbon supplies and adaptation of the microbial communities to changes in nutrient availability. Previous studies have noted, without causal explanation, that hyporheic residence time values are log-normally distributed [*Alessandra Marzadri et al.*, 2010; *Wörman et al.*, 2002]. We can now propose that, at least for dune-type bedforms, the reason for the lognormal distribution of hyporheic residence times is that downwelling velocities are log-normally distributed. Whether or not the downwelling velocities of other bedforms will adhere to a lognormal distribution is unknown (expect for pool-riffle which seems to be also log-normal) [*Tonina and Buffington*, 2011]. Nonetheless, we can propose with some confidence that, regardless of the bed morphology and given a relative abundance of bioavailable carbon, downwelling flux rates will have strong influence over the levels of biological activity. At some lower limit of carbon availability, it is expected that the variability in K_{DO} in response to downwelling flux distribution would be diminished or eliminated because of extremely low levels of bioactivity in a truly carbon limited system (Figure 3-8). Stated another way, if a constant value of K_{DO} is observed across a system, this implies that the system is substantially carbon deficient. For high-mountain, headwater streams where organic carbon supplies are relatively scarce, the value of K_{DO} should be relatively constant. Streams below the tree line and in agricultural and urban environs are not likely to be carbon limited and thus, in these streams, the value of K_{DO} should be a function of the downwelling velocity. This may result in log-normally distributed reaction rates, assuming the lognormal distribution of downwelling flux rates applies generally.
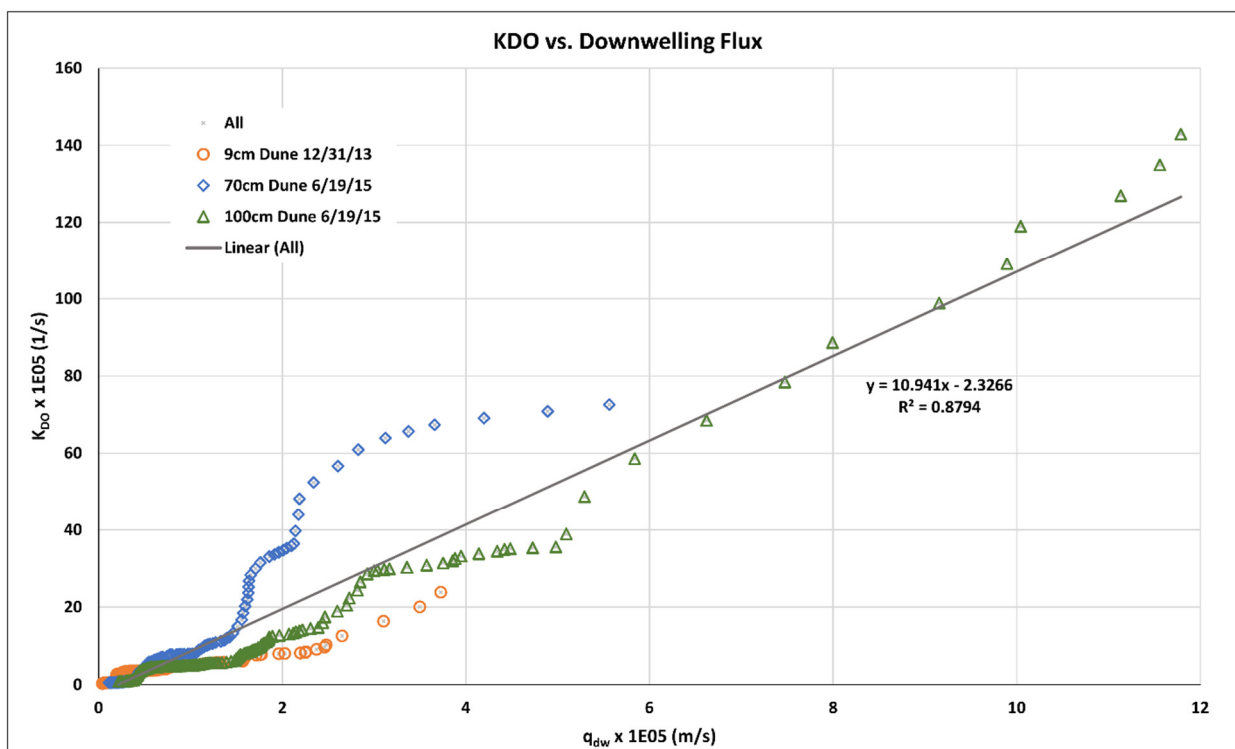
Figure 3-7 In steady-state (continuous) chemostat experiments, biologic activity, i.e. aerobioc respiration rate, has been shown to be linearly proportional to the dilution rate (media exchange rate) through the experimental vessel. For the case of the dune bedforms, the downwelling flux, q_{dw}, can be seen as analogous to the dilution rate in a chemostatic experiment. Here, K_{DO} values are plotted against the associated q_{dw}. The relationship is linear with an r^2 of 88%.

Most reactive solute transport models use a procedure similar to the one that we described to generate bed-surface pressure profiles and, as a result, apply hyporheic fluxes that correctly represent those in the associated physical system. However, applying a single value of K_{DO} to describe the reaction dynamics for the entire volume of the modeled bedform may result in a misrepresentation of the morphology and extent of the DO plume. More importantly, it is likely to result in a misrepresentation of the functionality of the microbial communities. The lognormally derived K_{DO} values more accurately reproduces the true shape and extent of the DO plume.
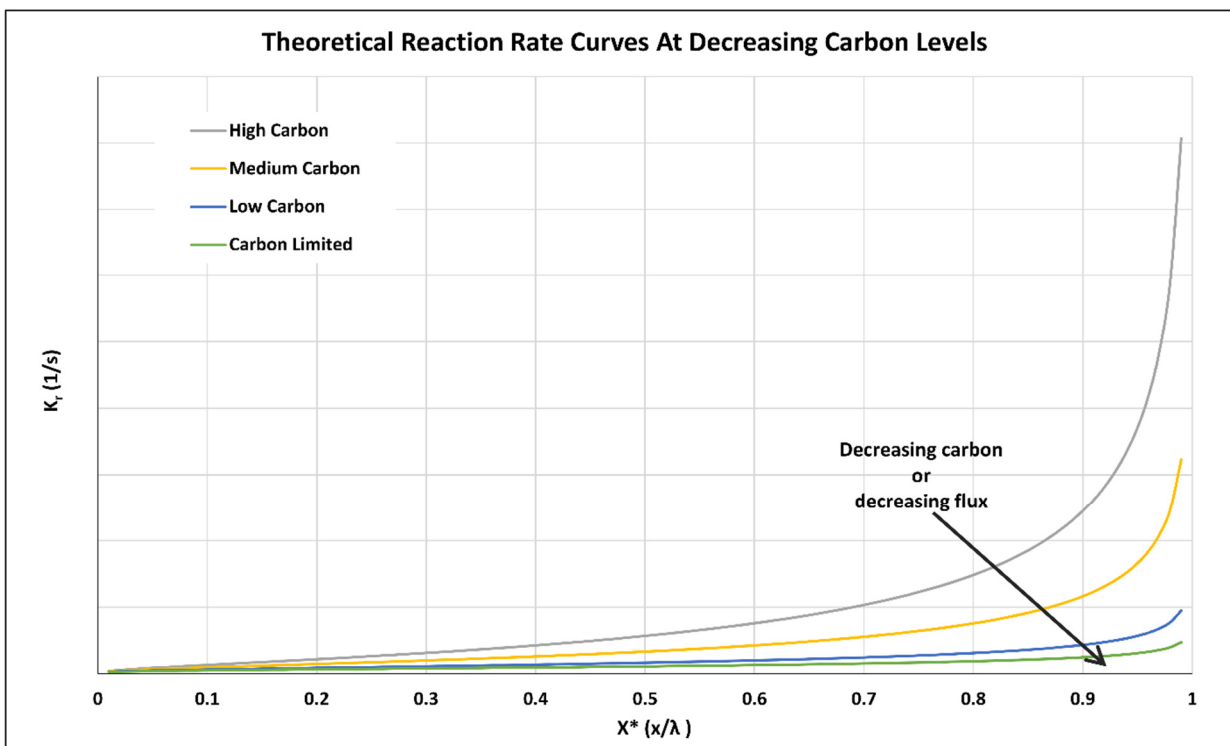
Figure 3-8 As cabon is depleted from a system, the overall biological reaction rate is expected to decrease and at some limiting carbon concentration the impact of the downwelling flux rate will be minimized. Similarly, for any given bedform morphology and carbon concentration, the strength of the lognormal relationship will decrease as the flux decreases.

The measured DO concentration profile for the 100 cm dune on 6/19/2015 is shown in Figure 3-9A. A DO profile generated using a single value of K_{DO} for all flowlines is presented in Figure 3-9B. The K_{DO} value used in this model was the mean of the DO consumption rates for all of the flowlines for that dune on that date. Other values are certainly possible but the mean of the flowline values is likely to be representative of what might be determined from point measurements in a field study. Figure 3-9C shows the modeled DO profile generated using K_{DO} values from the lognormal distribution. Visually, the difference between the two models is quite striking. The extent and morphology of the DO plume in the model that uses the log-normally distributed K_{DO} values matches the measured profile much more closely than the single-valued model. More quantitatively, the difference (error) between the measured profile and the modeled profiles is shown in Figure 3-9D and E. The model using a single value for K_{DO} (Figure 3-9D) has significantly higher

errors than the distributed model and, importantly, the largest errors are in the heart of the oxic zone.
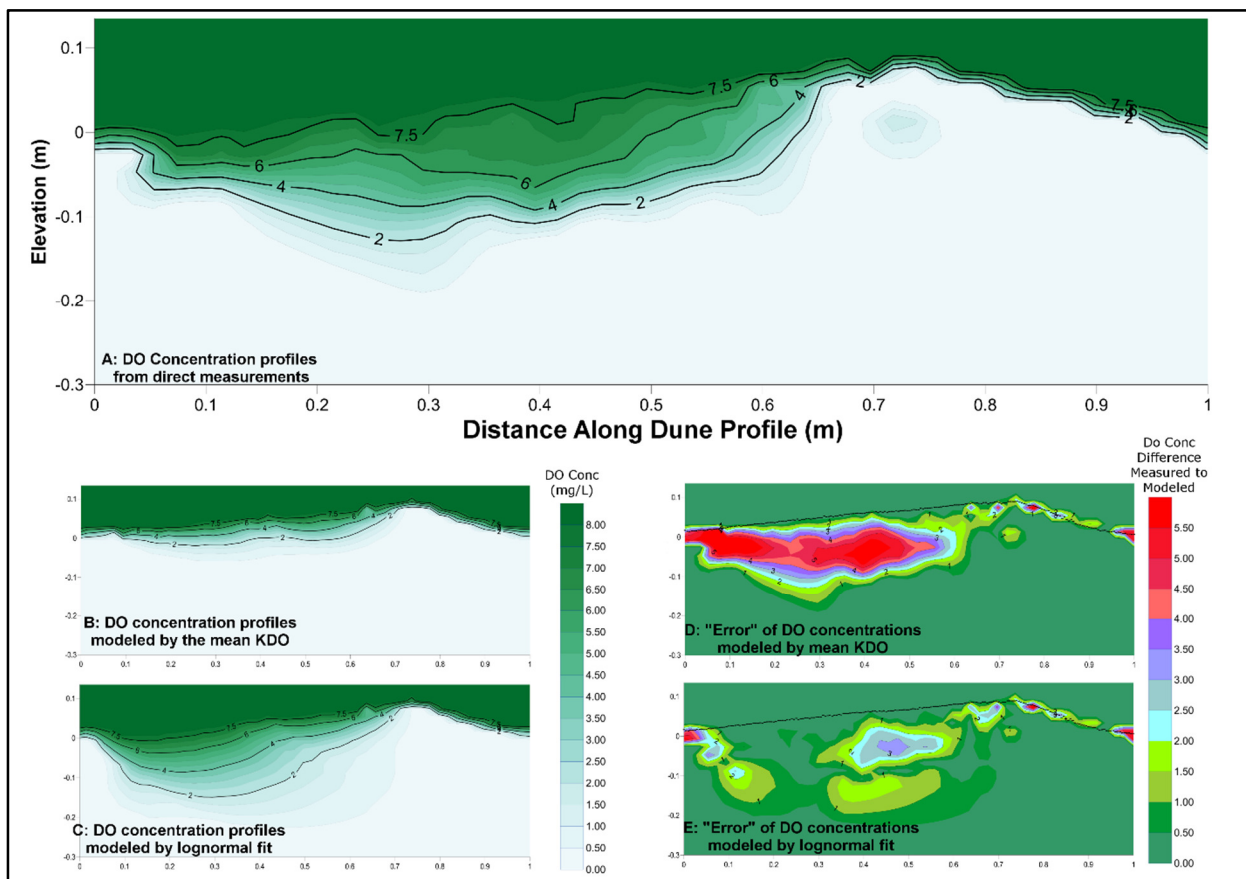
Figure 3-9 The top chart (A) is the measured DO profile for the 100cm dune on 6/19/15. To model such systems, researchers typically solve the groundwater flow equations coupled with 1st-order reaction rate equations. A single value for K_{DO}, gleaned from the literature or field measurements, is assigned to the entire system, i.e. all flowlines. The two charts on the lower left are modeled estimations of the DO profile in Chart A. Chart B was generated using a single value of K_{DO} (the mean of all of the calculated flowline K_{DO} values). DO profile (C) was generated by assigning unique K_{DO} values to the individual flowlines per the lognormal distribution. The charts to the right of the modeled DO profiles are the calculated difference (error) between the measured and modeled profiles.

If the only point of interest were the DO consumption capacity of this bedform, the net result difference between the two approaches would be small; in this physical context DO is completely consumed along the substantial majority of the flowlines before they exit the HZ. If, however, downstream, anaerobic processes are of interest, the constant K_{DO} model will likely allocate an incorrect amount of residence time to those processes, significantly

misrepresenting the capacity for those processes and the potential for them to be carried to completion. In this particular case, the constant K_{DO} model allocates significantly more time for anaerobic processes than is actually available in the physical system. Further, as time goes forward and carbon is consumed there will come a point at which a significant portion of the flowlines will not consume all of the dissolved oxygen that is being transported. That is, some of the flowlines will exit the HZ still in a semi-oxic state. The single-value model will likely do a poor job of representing this scenario.

All of this raises a problem for simulations that are based upon field-gathered data, how to define properly the lognormal distribution of K_{DO} values. Fortunately, the lognormal distribution is fully defined by the log-mean and log-standard deviation and is expressed as:

$$f(X^*|\mu, \sigma) \; \frac{1}{X^* \sigma \sqrt{2\pi}} e^{\left\{ \frac{-(\ln x - \mu)^2}{2\sigma^2} \right\}}; \; X^* > 0 \qquad (3.3)$$

Where μ is the log-mean and σ is the log-standard deviation. Thus, if enough measurements are taken to make a reasonable estimate of the mean and standard deviation (K_{DO} or q_{dw}), then the lognormal distribution can be constructed from those values. Alternatively, at least within the constraints of our experimental system we found some relationships that might be useful in estimating the parameters needed to construct the lognormal distribution. There is a modest linear relationship between the mean downwelling flux of a bedform and the mean K_{DO} and, also, the standard deviation (Figure 3-10). In addition, the mean and standard deviation of the (untransformed) K_{DO} values appear to be linearly related i.e., the standard deviation is proportional to the mean (Figure 3-11). Whether or not these relationships hold in a more general sense is unknown but, at a minimum, the trends are instructive of the basic relationships.
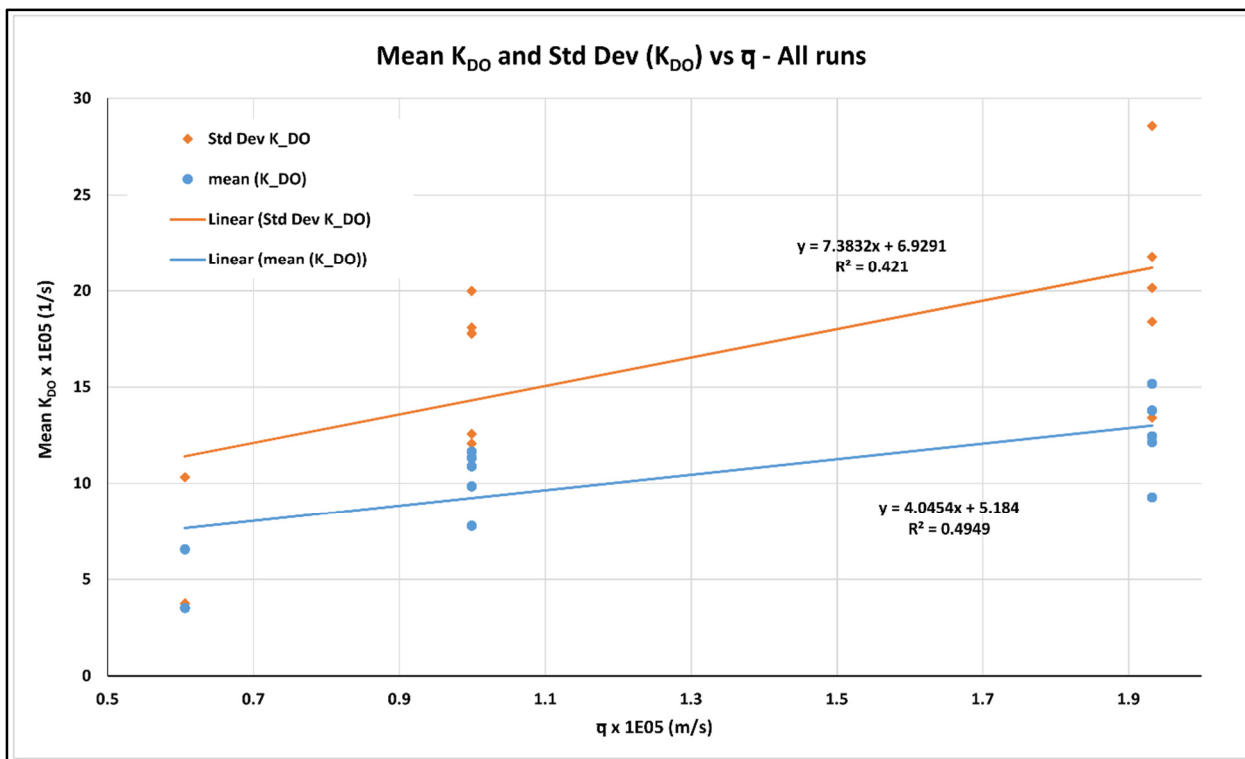
Figure 3-10 Plotting the mean value of K_{DO} for all of the individual experimental runs (9cm, 100cm and 70cm dunes over approximately 2 months run time) versus $\bar{q}_{dw}$ yields a linear relationship.

Our data and numerical models suggest that there are two mechanisms that exert primary control over biochemical activity in the HZ: the magnitude of the downwelling flux (downwelling velocity) and the concentration of bioavailable carbon. The distribution of the downwelling fluxes is the primary driver of the spatial distribution of K_{DO} values and carbon concentrations are the primary driver of temporal distribution of K_{DO} values. The effect of carbon consumption will be discussed more fully in the companion paper [ref]. The proportionality of K_{DO} to the downwelling velocity suggests that the crest of a dune and, indeed, any area of relatively high downwelling flux will be a "hotspot" of biochemical activity. These hotspots are zones of high consumption/production capacity and are, on a volume basis, likely to contribute disproportionally to the process capacity of the streambed. We expect that the dependency of K_{DO} values on flux rates can be scaled from the flowline regime to the bedform or reach scale. It seems certain that, within a given reach, features such as step-pools, pool-riffle sequences and woody debris obstructions that cause large pressure gradients and high downwelling fluxes will have significantly higher redox rates, i.e.

aerobic respiration, than features such as small dunes and ripples. Extending this idea further, we fully expect that other respiratory and biologically mediated redox processes in the HZ to follow the same pattern as DO consumption. That is, we expect the rate constants for the chemical transformations in processes such as the nitrification/denitrification sequence to be linearly proportional to the local flux and, thus, lognormally distributed over the extent of the downwelling area, or areas, in the case of dune-like bedforms.
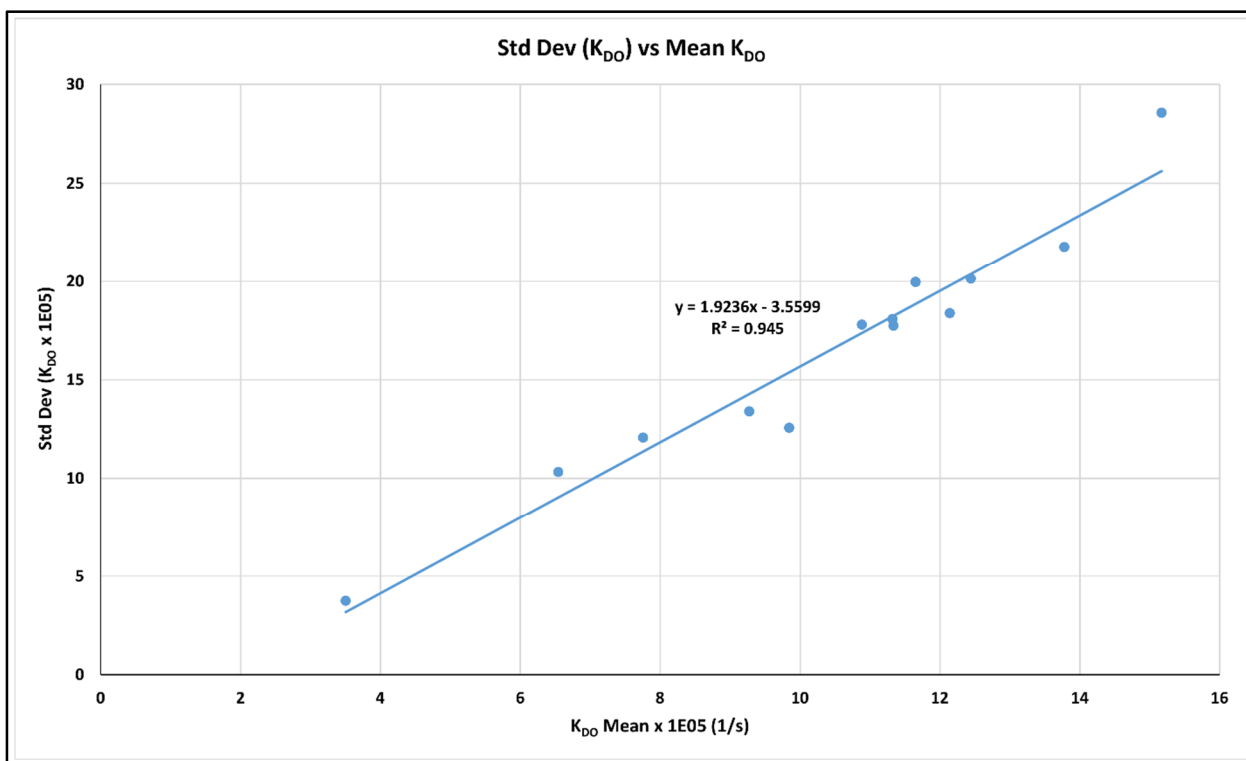
Figure 3-11 Over the range of values described by the present experiment, the standard deviations of the various KDO distributions have a linear relationship with the means of those distributions. If this relationshipcan be show to be general, it could be used to generate a lognormal K_{DO} profile from relatively few field measurements.

The temporal and spatial trends in DO consumption rates suggests that researchers engaged in field studies need to be cognizant of the temporal and spatial nutrient regime of the study area as well as the hydraulic context and complexity of that area. These trends in bioactivity also add a new dimension to how we interpret field data. For instance, it has been observed that hyporheic activity decreases as the size of rivers increases [Marzadri et al.

2017]. This has been previously attributed, at least partially, to decreased hyporheic flux in large rivers, which is due to low hydraulic conductivity of the streambeds and the relatively flat bed morphology of those rivers. Now we can demonstrate that, in addition to these factors, the lower hyporheic activity in large, flatbed streams are also due to lower specific reaction rates in the HZ because of the lower downwelling velocities.

3.4 Conclusions

All other factors being held equal, bed morphology and its interaction with stream hydraulics exerts primary control over the functionality of the microbial communities that reside within the hyporheic zone. In a system in which carbon availability is above a minimum sufficiency level, biologic activity is limited largely by the availability of DO as opposed to the availability of nutrients (carbon). In this scenario, the biochemical respiration rate, for microbial communities residing in the HZ, is a linear function of the local velocity of the downwelling flux that feeds nutrients and dissolved oxygen to those communities. Due to the complex pressure gradients that exist within even a simple bedform, there is a broad range of downwelling velocities present within bedforms and, by extension, across the extent of stream reaches. At least within the context of triangular dune morphologies examined in this study, downwelling velocities are log-normally distributed and, because the aerobic respiration rate, K_{DO}, is a linear function of downwelling velocity, the values of K_{DO} are also log-normally distributed. The full distribution of KDO can be described by knowing the mean K_{DO} value, which is a function of mean downwelling velocity and carbon availability, and the K_{DO} variance, which we found linearly related to the mean. The range of the K_{DO} values exhibited by a single bedform at a given point in time can be substantial and in our experiments spanned significantly more than an order of magnitude. This range of KDO values has significant implications for how and where we measure biochemical activity in the HZ and also how we interpret those measurements. Observed biochemical hotspots may be more a function of the local downwelling velocity rather than a function of the local nutrient supply. Further, the relationship between downwelling velocity and K_{DO} suggests that we need to consider how we evaluate the biogeochemical processing capacity of individual bedforms and stream reaches. Applying K_{DO}, or other chemical species rate constants, as a

monolithic, constant value risks misrepresenting the processing capacity of the area of interest and will almost certainly distort the perceived reactive volume of sediment in the hyporheic zone.

3.5 Acknowledgements

3.6 Funding Sources

3.7 Data

The data that was used in support of these findings will be made available at the time of publication through an open-access data repository.

3.8 References

Appelo, C. A. J., and D. Postma (2010), Geochemistry, groundwater and pollution, 2 ed., CDC Press, Boca Raton.

Aquaveo (2015), GMS ModFlow, edited by G. M. System, Aquaveo LLC.

Bardini, L., F. Boano, M. B. Cardenas, R. Revelli, and L. Ridolfi (2012), Nutrient cycling in bedform induced hyporheic zones, Geochimica et Cosmochimica Acta, 84, 47-61.

Beaulieu, J. J., et al. (2011), Nitrous oxide emission from denitrification in stream and river networks, Proceedings of the National Academy of Sciences, 108(1), 214-219.

Boano, F., J. W. Harvey, A. Marion, A. I. Packman, R. Revelli, L. Ridolfi, and A. Wörman (2014), Hyporheic flow and transport processes: Mechanisms, models, and biogeochemical implications, Reviews of Geophysics, 52(4), 603-679.

Budwig, R., and P. Goodwin (2012), The Center for Ecohydraulics Research Mountain StreamLab - a facility for collaborative research and education, in Innovations 2012: world innovations in engineering education and research, edited, iNeer, Potomac, Maryland, USA.

Cardenas, M. B., and J. L. Wilson (2007), Exchange across a sediment–water interface with ambient groundwater discharge, Journal of Hydrology, 346(3–4), 69-80.

Cardenas, M. B., P. L. M. Cook, H. Jiang, and P. Traykovski (2008), Constraining denitrification in permeable wave-influenced marine sediment using linked hydrodynamic and biogeochemical modeling, Earth and Planetary Science Letters, 275(1–2), 127-137.

Chapelle, F. H. (1993), Ground-Water Microbiology and Geochemistry, John Wiley & Sons, New York.

Chapelle, F. H., P. B. McMahon, N. M. Dubrovsky, R. F. Fujii, E. T. Oaksford, and D. A. Vroblesky (1995), Deducing the Distribution of Terminal Electron-Accepting Processes in Hydrologically Diverse Groundwater Systems, Water Resources Research, 31(2), 359-371.

Cleveland, C. C., D. R. Nemergut, S. K. Schmidt, and A. R. Townsend (2007), Increases in soil respiration following labile carbon additions linked to rapid shifts in soil microbial community composition, Biogeochemistry, 82(3), 229-240.

Cooper, A. C. (1965), The effect of transported stream sediments on the survival of sockeye and pink salmon eggs and alevin.

Curiel Yuste, J., D. D. Baldocchi, A. Gershenson, A. Goldstein, L. Misson, and S. Wong (2007), Microbial soil respiration and its dependency on carbon inputs, soil temperature and moisture, Global Change Biology, 13(9), 2018-2035.

Fehlman, H. M. (1985), Resistance components and velocity distributions of open channel flows over bedforms, 169 pp, Colorado State University, Fort Collins, CO.

Furukawa, K., E. Heinzle, and I. J. Dunn (1983), Influence of oxygen on the growth of Saccharomyces cerevisiae in continuous culture, Biotechnology and Bioengineering, 25(10), 2293-2317.

Greig, S. M., D. A. Sear, and P. A. Carling (2007), A review of factors influencing the availability of dissolved oxygen to incubating salmonid embryos, Hydrological Processes, 21(3), 323-334.

Harrison, D. E. F. (1972), Physiological effects of dissolved oxygen tension and redox potential on growing populations of micro-organisms, Journal of Applied Chemistry and Biotechnology, 22(3), 417-440.

Harvey, J. W., J. K. Böhlke, M. A. Voytek, D. Scott, and C. R. Tobias (2013), Hyporheic zone denitrification: Controls on effective reaction depth and contribution to whole-stream mass balance, Water Resources Research, 49(10), 6298-6316.

Henry, S., D. Bru, B. Stres, S. Hallet, and L. Philippot (2006), Quantitative Detection of the nosZ Gene, Encoding Nitrous Oxide Reductase, and Comparison of the Abundances of 16S rRNA, narG, nirK, and nosZ Genes in Soils, Applied and Environmental Microbiology, 72(8), 5181-5189.

Hunter, K. S., Y. Wang, and P. Van Cappellen (1998), Kinetic modeling of microbially-driven redox chemistry of subsurface environments: coupling transport, microbial metabolism and geochemistry, Journal of Hydrology, 209(1–4), 53-80.

Kayser, A., J. Weber, V. Hecht, and U. Rinas (2005), Metabolic flux analysis of Escherichia coli in glucose-limited continuous culture. I. Growth-rate-dependent metabolic efficiency at steady state, Microbiology, 151(3), 693-706.

Kessler, A. J., R. N. Glud, M. B. Cardenas, M. Larsen, M. F. Bourke, and P. L. M. Cook (2012), Quantifying denitrification in rippled permeable sands through combined flume experiments and modeling, Limnology and Oceanography, 57(4), 1217-1232.

Laanbroek, H. J., P. L. E. Bodelier, and S. Gerards (1994), Oxygen consumption kinetics of Nitrosomonas europaea and Nitrobacter hamburgensis grown in mixed continuous cultures at different oxygen concentrations, Archives of Microbiology, 161(2), 156-162.

Marzadri, A., D. Tonina, and A. Bellin (2010), A semianalytical three-dimensional process-based model for hyporheic nitrogen dynamics in gravel bed rivers, Water Resources Research, 47(11).

Marzadri, A., D. Tonina, and A. Bellin (2012), Morphodynamic controls on redox conditions and on nitrogen dynamics within the hyporheic zone: Application to gravel bed rivers with alternate-bar morphology, Journal of Geophysical Research: Biogeosciences, 117(G3).

Master, Y., U. Shavit, and A. Shaviv (2005), Modified Isotope Pairing Technique to Study N Transformations in Polluted Aquatic Systems: Theory, Environmental Science & Technology, 39(6), 1749-1756.

Moreno-Vivián, C., P. Cabello, M. Martínez-Luque, R. Blasco, and F. Castillo (1999), Prokaryotic Nitrate Reduction: Molecular Properties and Functional Distinction among Bacterial Nitrate Reductases, Journal of Bacteriology, 181(21), 6573-6584.

Naranjo, R. C., R. G. Niswonger, and C. J. Davis (2015), Mixing effects on nitrogen and oxygen concentrations and the relationship to mean residence time in a hyporheic zone of a riffle-pool sequence, Water Resources Research, 51(9), 7202-7217.

Nobre, A., L. Duarte, J. Roseiro, and F. Gírio (2002), A physiological and enzymatic study of Debaryomyces hansenii growth on xylose- and oxygen-limited chemostats, Applied Microbiology and Biotechnology, 59(4), 509-516.

Nogaro, G., T. Datry, F. Mermillod-Blondin, A. Foulquier, and B. Montuelle (2013), Influence of hyporheic zone characteristics on the structure and activity of microbial assemblages, Freshwater Biology, 58(12), 2567-2583.

Ocampo, C. J., C. E. Oldham, and M. Sivapalan (2006), Nitrate attenuation in agricultural catchments: Shifting balances between transport and reaction, Water Resources Research, 42(1), n/a-n/a.

Pinay, G., T. C. O'Keefe, R. T. Edwards, and R. J. Naiman (2009), Nitrate removal in the hyporheic zone of a salmon river in Alaska, River Research and Applications, 25(4), 367-375.

PIRT, S. J. (1957), The Oxygen Requirement of Growing Cultures of an Aerobacter Species Determined by means of the Continuous Culture Technique, Microbiology, 16(1), 59-75.

Pretty, J. L., A. G. Hildrew, and M. Trimmer (2006), Nutrient dynamics in relation to surface–subsurface hydrological exchange in a groundwater fed chalk stream, Journal of Hydrology, 330(1–2), 84-100.

Quick, A. M., W. J. Reeder, T. B. Farrell, D. Tonina, K. P. Feris, and S. G. Benner (2016), Controls on Nitrous Oxide Emissions from the Hyporheic Zones of Streams, Environmental Science & Technology, 50(21), 11491-11500.

Ramirez, O. T., and R. Mutharasan (1990), Cell cycle- and growth phase-dependent variations in size distribution, antibody productivity, and oxygen demand in hybridoma cultures, Biotechnology and Bioengineering, 36(8), 839-848.

Reeder, W. J., A. M. Quick, T. B. Farrell, S. G. Benner, K. P. Feris, and D. Tonina (2017a), Temporal dynamics of dissolved oxygen concentrations and bioactivity in the hyporheic zone, in review with Water Resources Research.

Reeder, W. J., A. M. Quick, T. B. Farrell, S. G. Benner, K. P. Feris, D. Tonina, W. J. R. Basham, and C. Huber (2017b), Dissolved oxygen concentration profiles in the hyporheic zone through the use of a high-density fiber optic measurement system, In revision.

Richardson, D., H. Felgate, N. Watmough, A. Thomson, and E. Baggs (2009), Mitigating release of the potent greenhouse gas N2O from the nitrogen cycle – could enzymic regulation hold the key?, Trends in Biotechnology, 27(7), 388-397.

Rosenberger, R. F., and M. Kogut (1958), The Influence of Growth Rate and Aeration on the Respiratory and Cytochrome System of a Fluorescent Pseudomonad Grown in Continuous Culture, Microbiology, 19(2), 228-243.

Rutherford, J., J. Boyle, A. Elliott, T. Hatherell, and T. Chiu (1995), Modeling Benthic Oxygen Uptake by Pumping, Journal of Environmental Engineering, 121(1), 84-95.

Rutherford, J. C., J. D. Boyle, A. H. Elliot, T. V. J. Hatherell, and T. W. Chiu (1995), Modeling Benthic Oxygen Uptake by Pumping, Journal of Environmental Engineering, 121(1), 84-95.

Sinclair, C. G., and D. N. Ryder (1975), Models for the continuous culture of microorganisms under both oxygen and carbon limiting conditions, Biotechnology and Bioengineering, 17(3), 375-398.

Sobczak, W. V., and S. Findlay (2002), VARIATION IN BIOAVAILABILITY OF DISSOLVED ORGANIC CARBON AMONG STREAM HYPORHEIC FLOWPATHS, Ecology, 83(11), 3194-3209.

Tonina, D., and J. M. Buffington (2009), A three-dimensional model for analyzing the effects of salmon redds on hyporheic exchange and egg pocket habitat, Canadian Journal of Fisheries and Aquatic Sciences, 66(12), 2157-2173.

Tonina, D., and J. M. Buffington (2011), Effects of stream discharge, alluvial depth and bar amplitude on hyporheic flow in pool-riffle channels, Water Resources Research, 47(8), n/a-n/a.

Wörman, A., A. I. Packman, H. Johansson, and K. Jonsson (2002), Effect of flow-induced exchange in hyporheic zones on longitudinal transport of solutes in streams and rivers, Water Resources Research, 38(1), 2-1-2-15.

Wrage, N., G. L. Velthof, M. L. van Beusichem, and O. Oenema (2001), Role of nitrifier denitrification in the production of nitrous oxide, Soil Biology and Biochemistry, 33(12–13), 1723-1732.

Wriedt, G., and M. Rode (2006), Modelling nitrate transport and turnover in a lowland catchment system, Journal of Hydrology, 328(1–2), 157-176.

Zarnetske, J. P., R. Haggerty, S. M. Wondzell, and M. A. Baker (2011a), Dynamics of nitrate production and removal as a function of residence time in the hyporheic zone, Journal of Geophysical Research: Biogeosciences, 116(G1), G01025.

Zarnetske, J. P., R. Haggerty, S. M. Wondzell, and M. A. Baker (2011b), Labile dissolved organic carbon supply limits hyporheic denitrification, Journal of Geophysical Research: Biogeosciences, 116(G4), n/a-n/a.

Zarnetske, J. P., R. Haggerty, S. M. Wondzell, and M. A. Baker (2011c), Labile dissolved organic carbon supply limits hyporheic denitrification, Journal of Geophysical Research: Biogeosciences, 116(G4).

Zarnetske, J. P., R. Haggerty, S. M. Wondzell, V. A. Bokil, and R. González-Pinzón (2012), Coupled transport and reaction kinetics control the nitrate source-sink function of hyporheic zones, Water Resources Research, 48(11).

Chapter 4

Temporal dynamics of dissolved oxygen concentrations and bioactivity in the

hyporheic zone[3]

Dissolved oxygen (DO) concentration profiles and DO consumption rates are primary indicators of the redox state of porewaters in the hyporheic zone (HZ). Previous studies of reactive solute transport in the HZ have perceived the hyporheic zone as spatially homogenous and temporally steady state. This perspective yields a static view of the biogeochemical activity and redox state of the HZ and fails to capture the temporal dynamics of a changeable system. Through the use of a novel, multichannel fiber optic DO measurement system and a robotic surface probe system in a large flume experiment, we have been able to track DO concentration, in the HZ, over time and at unprecedented high spatial and temporal resolutions. Our research shows that in hyporheic systems, which are relatively abundant in bioavailable carbon but in which carbon replenishment is largely episodic, DO concentration profiles and DO consumption rates will vary as a function of time. As the most

readily available organic carbon is consumed, first near the bed surface/water interface, respiration rates in that area will drop and DO will be transported deeper into the HZ. Over time, and lacking either an external source of bioavailable carbon or an alternate electron donor substrate, microbial metabolic activity will slow substantially and the majority of the HZ will be rendered oxic. Hyporheic fluxes affect the time scale of biological reactions resulting in faster growth of the aerobic zone in high-flux systems.

4.1 Introduction

While a variety of biochemical reactions can and do occur in the water column of streams, the bulk of the chemical activity in riverine environments occurs in the sediments directly adjacent to the surface flow [*Fischer et al.*, 2005; *Krause et al.*, 2011; *Alessandra Marzadri et al.*, 2017; *Master et al.*, 2005; *Wuhrmann*, 1972]. This region of enhanced biochemical activity and active exchange of surface waters and groundwater is termed the hyporheic zone (HZ) [Findlay, 1995]. Hyporheic exchange, the flow of surface water into and out of the HZ, transports nutrients, pollutants and dissolved oxygen (DO) into the HZ and transformed products back in the surface flow [*Elliott and Brooks*, 1997; *Krause et al.*, 2011; *Packman et al.*, 2004; *Tonina and Buffington*, 2007; *Triska et al.*, 1993]. Because of the high level of chemical activity in the HZ, hyporheic exchange has a strong impact on both aquatic [Cardenas et al., 2008] and terrestrial environments [Greig et al., 2007; Tonina and Buffington, 2009]. It is useful to conceptualize hyporheic flow, which is driven by pressure gradients at the bed surface/surface water interface [*Elliott and Brooks*, 1997], as a series of quasi-discreet and arched flowlines (red lines, Figure 4-1) each of which is characterized by a residence time (τ), the time it takes a packet of water to travel along the flowline before it reenters the surface flow. The interaction between stream bed morphology and surface flow hydraulics influences hyporheic flow velocity and residence times by modulating the pressure gradients at the bed surface [*Elliott and Brooks*, 1997]. Of the chemical transformations that occur in the HZ, microbially mediated redox reactions are drivers of the biogeochemical state of the HZ. Primary among those reactions is the metabolic consumption of DO. The rate at which oxygen is consumed is controlled by the population density and types of organisms living in the HZ, the rate at which DO is supplied to the organisms and the reactive concentration of bioavailable nutrients (most generally, organic carbon) [Beaulieu et al.,

2011; Chapelle, 1993; Moreno-Vivián et al., 1999]. If the rate of consumption along a particular flowline is high enough, all of the DO on that flowline will be consumed before it rejoins the surface flow [*Rutherford et al.*, 1995; *Tonina et al.*, 2015]. The specific rate of DO consumption coupled with travel times (τ) along those flowlines will determine the apportionment of the HZ into oxic and anoxic domains [Bardini et al., 2012; Alessandra Marzadri et al., 2010]. In the physical sense, this partitioning of the HZ into oxic and anoxic domains becomes important when coupled aerobic and anaerobic processes are active.

The first step in understanding temporal and spatial dynamics of coupled aerobic/anaerobic redox processes is to have a clear view of reactive solute transport and redox dynamics in the HZ, particularly the dynamics of metabolic DO consumption. Our present understanding of these dynamics comes primarily from numerical studies [*Bardini et al.*, 2012; *Kessler et al.*, 2012; *A Marzadri et al.*, 2011; *A. Marzadri et al.*, 2012; *Rutherford et al.*, 1995; *Wriedt and Rode*, 2006; *Zarnetske et al.*, 2012] These studies have typically made the explicit assumption that the rate of DO consumption, K_{DO}, is constant within a homogeneous domain and that rate is usually tied to the reactive concentration of bioavailable organic carbon [*Judson W. Harvey et al.*, 2013; *Hunter et al.*, 1998; *Sobczak and Findlay*, 2002; *Zarnetske et al.*, 2011a; b]. Further, these studies have made the implicit assumption that K_{DO} is constant over time yielding a steady state, fixed-in-time view of the biogeochemical activity and redox state of the HZ, thus ignoring the potential temporal aspects of DO consumption. In general, these studies have been limited by the fact that they did not have access to sufficiently detailed and replicated measurements that would have enabled them to resolve DO consumption at the individual flowline level. Additionally, they have not attempted to make a strong link between flow hydraulics and redox dynamics, particularly at scales smaller that stream reaches.

In the companion paper [*Reeder et al.*, 2017a], we address the spatial aspect of DO consumption and demonstrate that, in a system that has a relatively normal abundance of bioavailable carbon, the rate of DO consumption is a function of the local downwelling velocity. That is, K_{DO} is spatially variable across the span of the downwelling area and is tied to the local flux velocity. That spatial variability persists across a significant range of organic carbon concentrations [*Reeder et al.*, 2017a]. In this context, stream hydraulics exert

substantial control of over the bioactivity in the HZ that, at some level, overshadows the influence of nutrient supplies.   In the present contribution, we address the temporal aspect of DO consumption. Our goal is to demonstrate that, as carbon is consumed, the magnitude of K_{DO} will decrease and, to some degree, the form of the K_{DO} profile will change over time. We posit that as carbon concentrations decrease, the influence of steam hydraulics and DO flux will decrease and, at some low carbon threshold, bioactivity will be truly carbon limited and K_{DO} will exhibit a relatively constant value across the hyporheic domain.

4.2 Methods and Materials

The experimental setups, measurement methodologies and analysis procedures are described in detail in other publications [*Quick et al.*, 2016; *Reeder et al.*, 2017b] and those details will not be represented here. The general features of the experimental design are outlined in Table 4-1. For the present discussion it is useful to note that we ran two large-scale flume experiments at the Center for Ecohydraulics Research Stream Laboratory [*Budwig and Goodwin*, 2012] located at the University of Idaho, Boise. The overarching objective of those experiments was to investigate the impact of bed morphology, stream hydraulics and surface water chemistry (reactive nitrogen loading) leading to and controlling N_2O emissions from rivers and streams. A key component of those investigations was the dynamics of DO consumption. This discussion will focus on that aspect of our investigations. The first flume experiment (Flume 1) ran continuously from August 2013 through December 2013 and the second (Flume 2) ran from February 2015 through June 2015. In both experiments, triangular dunes of various sizes were constructed from 90% quarry sand (D_{50} ~1.5 mm) and 10% natural sand collected from the Boise River (Boise, ID, USA). The natural sand provided an inoculum to initiate bacterial communities, which were representative of those that typically reside in streambed sediments. From Flume 1, we will evaluate the response of a 9 cm tall by 1 m long dune, hereafter referred to as the "9 cm dune." From Flume 2, we will consider a 9 cm tall by 100 cm long dune and a 9 cm tall by 70 cm long dune, hereafter referenced as "100 cm dune" and "70 cm dune", respectively. In the Flume 2 experiment, there were three replicates of each dune geometry, identified by the flume channel in which the individual dune was located (Channel A, B or C). As such, a 70 cm dune in Channel A is designated as

"A70." In both experiments, we measured DO (and other chemical constituents) at a spatial resolution that allowed us to calculate reaction rates at the scale of individual flowlines. For our calculations, we assumed first-order reaction mechanics. The governing equation for first-order DO consumption takes the form:

$$[DO]_\tau = DO_0 e^{-K_{DO}\tau} \qquad\qquad (4.1)$$

where $[DO]_\tau$ is the DO concentration at residence time τ and K_{DO} is the first-order reaction rate. To calculate K_{DO} at the individual flowline scale, we calculated an exponential fit to individual [DO] vs. τ data strings that were resolved to the individual flowline. The exponential fit yields two parameters: the intercept and the exponential decay rate which for our data are DO_0 and K_{DO}, respectively.

A representative longitudinal dune cross-section and DO profile is shown in Figure 4-1. Superimposed on the cross-section are the DO measurement positions (blue triangles and black dots) and a representative set of calculated flowlines (red lines). In both experiments, DO measurements were taken at several points in time over a period spanning two to three months of continuous run time. The only bioavailable carbon present in the system, to support the metabolic activities of the microbes living in the sand dunes, was particulate organic matter (POM) in the form of chopped cottonwood leaves (0.015% by dry weight). There was no carbon replenishment during the run of the experiment. This carbon amendment can be seen to be analogous to a natural system in which the main source of bioavailable organic carbon is leaf-fall that is turned into the bed during episodic scour events.

Table 4-1. Experimental Setup

Experiment				
Geometry	**Sediment**	**Initial POM**	**Energy Slope**	**Measurements**
2013 Flume Experiment – Flume 1 (duration 16 weeks)				
1 m dune x 9 cm height (9 cm dune)	90% quarry sand (D50 ~ 1.5 mm) 10% inoculum sand	0.015% by dry weight	0.002	DO Dissolved N_2O NO_3^- NO_2^- NH_4^+ Microbial population densities
2015 Flume Experiment – Flume 2 (duration 13 weeks)				
70 cm long x 9 cm height (70 cm dune) **100 cm long x 9 cm height (100 cm dune)**	90% quarry sand (D_{50} ~ 1.5 mm) 10% inoculum sand	0.015% by dry weight	0.003	DO Dissolved N_2O NO_3^- NO_2^- NH_4^+ Microbial population densities
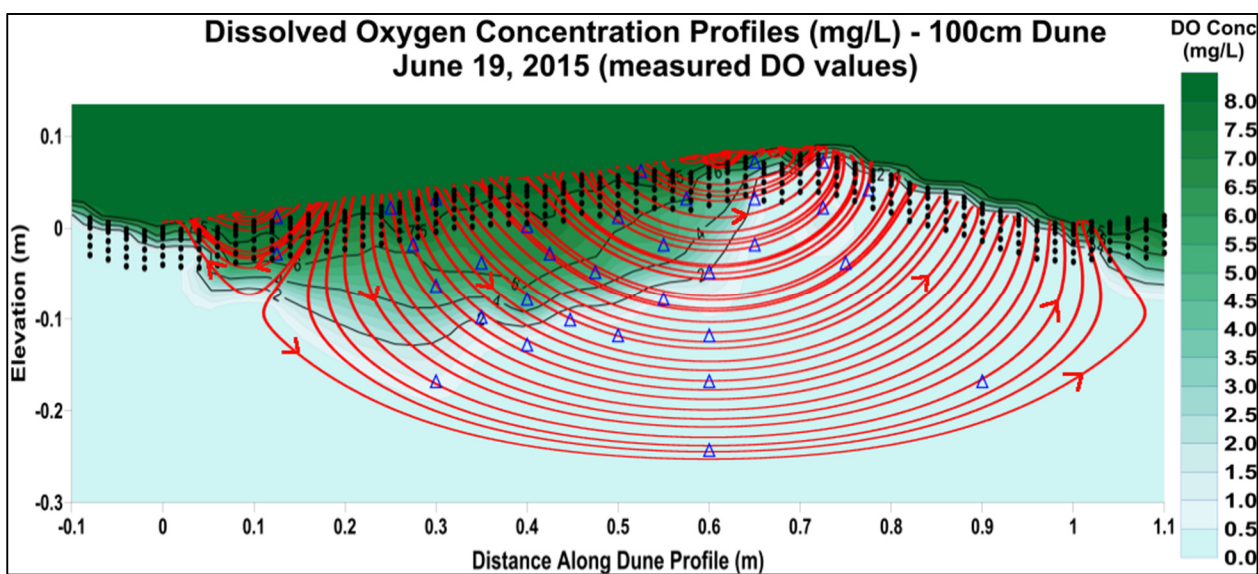
Figure 4-1. A longitudinal, cross-sectional view of a 100cm dune from Flume 2. The green shading represents the DO concentration profiles calculated from DO measurements. The blue traingles show the locations of *in situ* DO sensors that were embedded in the HZ for the duration of the experiment. The black dots show the measurement positions of the robotic surface probe. The red lines represent a typical set of calculated flowlines. The DO concentration and residence time at the points along these flowines were used to calculate K_{DO} for each of the flowlines. Surface flow is from left to right.

4.2.1 Notes on data presentation

To describe the spatial distribution of K_{DO} values, the locations of the calculated values are assigned to the x-locations of the entry points of the flowlines into the HZ. To represent different bed geometries on the same scale, we plot the K_{DO} as a function of X^*, which is the downwelling location (x) normalized by the length (λ') of the downwelling area ($X^* = x/\lambda'$). Note that for all of the graphs that employ calculated K_{DO} values or calculated downwelling fluxes (q_{dw}), the presented values have been multiplied by a factor of 1×10^5. That is to say, if a value of K_{DO} or q_{dw} of 2.5 is read from a graph, the associated physical value is 2.5×10^{-5}.

4.3 Results and Discussion

At the beginning of the project and in agreement with current understanding of reactive solute transport dynamics, our expectation was that all of the flowlines would exhibit essentially the same rate of DO consumption – that is, K_{DO} (the rate of DO consumption by the microbial communities) at any particular point in time would be a constant. If this were the case, when DO consumption rates were evaluated at the scale of individual flowlines, all of the DO consumption profiles (τ vs. [DO]) would map onto a single, common profile. Short flowlines would occupy a relatively short segment of that profile with the longest flowlines defining the full extent of the consumption profile. Further, we expected that over time the consumption profile would shift to the right (longer residence times) and flatten (lower consumption rate). Our results indicate that our assumptions were only partially correct. When evaluated at the scale of individual flowlines, microbial respiration exhibits a broad range of consumption profiles (blue traces, Figure 4-2) and, thus, a broad range of DO consumption rates (K_{DO}). The profiles presented in Figure 4-2 are for a single dune at one point in time (Channel A, 70 cm dune, 6/19/15) but this behavior is characteristic of all of the dunes at all measurement points over the durations of both of the experiments (Figure 4-3). At any one point in time, the multiplicity of DO consumption profiles and the resulting range of K_{DO} values is driven primarily by the flow hydraulics. There are two reasons that these profiles would exhibit this unexpected behavior; 1) there are different processes active along

the various flowlines causing them to exhibit different outcomes or 2) the same processes are active but operating at different rates. A single profile response can be produced by multiplying the residence times (τ) for each of the individual flowlines by the individual K_{DO} values for each of the flowlines (red lines, Figure 4-2), suggesting that the same processes are active in all of the flowlines, however, they are proceeding at different rates along the various flowlines. Overlying this spatial variability, however, is a steady and consistent temporal trend that is driven by an apparent change in nutrient availability.
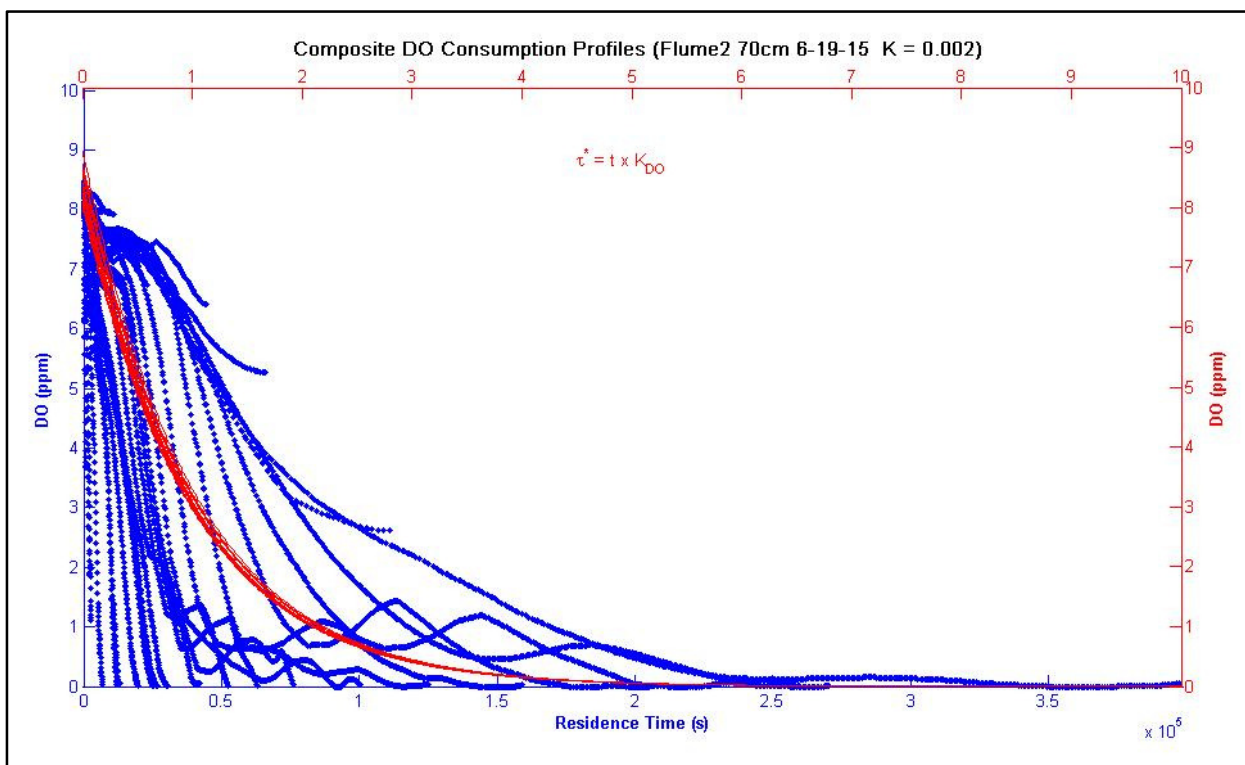
Figure 4-2. DO concentration versus residence time (τ) for each of the individual flowlines (blue traces) in a single dune. Note the range of slopes exhibited by the individual traces, indicating a significant range of DO consumption rates (KDO). When the residence times (τ) for each of the individual flowlines are multiplied by KDO for those flowlines, the DO consumption curves collapse to, essentially, a single trace (red lines).

The spatial and temporal responses of DO consumption are driven by different mechanisms. In addition, within the context of our experiment, the spatial variation in K_{DO} was significantly larger than the magnitude of temporal change in K_{DO} values. As such, the plurality of spatial responses (Figure 4-2) and the magnitude of the spatial variance (Figure 4-3) could easily mask temporal trends in DO consumption when it is being evaluated against

sparse measurements. Thus, to understand the spatial and temporal effects properly it is useful to separate them. In the companion paper [*Reeder et al.*, 2017a], we demonstrated that the spatial variation in K_{DO} is driven by the variability in the hyporheic flux and, from the perspective of the microbes, the rate at which DO is delivered to local populations. That variability is relatively fixed and changes only as flow hydraulics and/or bed morphology change. In contrast, for a system that is characterized by episodic carbon (nutrient) replenishment, the rate of DO consumption is expected to change continuously and progressively over time. Specifically, unless organic carbon is continuously replenished to the hyporheic environment, the rate of metabolic activity, as measured by DO consumption rate, will decrease as bioavailable carbon is depleted. This can be illustrated by isolating a single flowline and tracking its response over time as carbon is depleted. Additionally, by isolating and tracking a single flowline we eliminate any spatial variability from the DO consumption response, assuming that flow hydraulics and bed morphology have not changed significantly. For this experiment, we held the latter two factors constant. Figure 4-4 traces the DO consumption response of a typical flowline over two months of run time. This particular flowline entered the HZ in the middle of the stoss face of the 70 cm dune in Channel A and exited the lee face of the same dune. The red, left-most line shows the DO consumption profile at about 5 weeks into the experimental run. The aqua, right-most line shows the DO consumption profile approximately two months later. The green and blue lines are, progressively, intermediate profiles. Over time, the rate of DO consumption (K_{DO}) is decreasing as witnessed by the decreasing slope of the DO consumption profiles. Over this span in time and without carbon replenishment, the measured K_{DO} values ranged from 1.6×10^{-5} s^{-1} on 4/19/15 (Day 33) to 0.6×10^{-5} s^{-1} on 6/19/15 (Day 91), decreasing by a factor of 2.75. Additionally, as run time increases, the overall residence time needed for the flowline to reach a fully anoxic state ([DO] = 0) increases, further illustrating the diminishing rate of oxygen consumption.
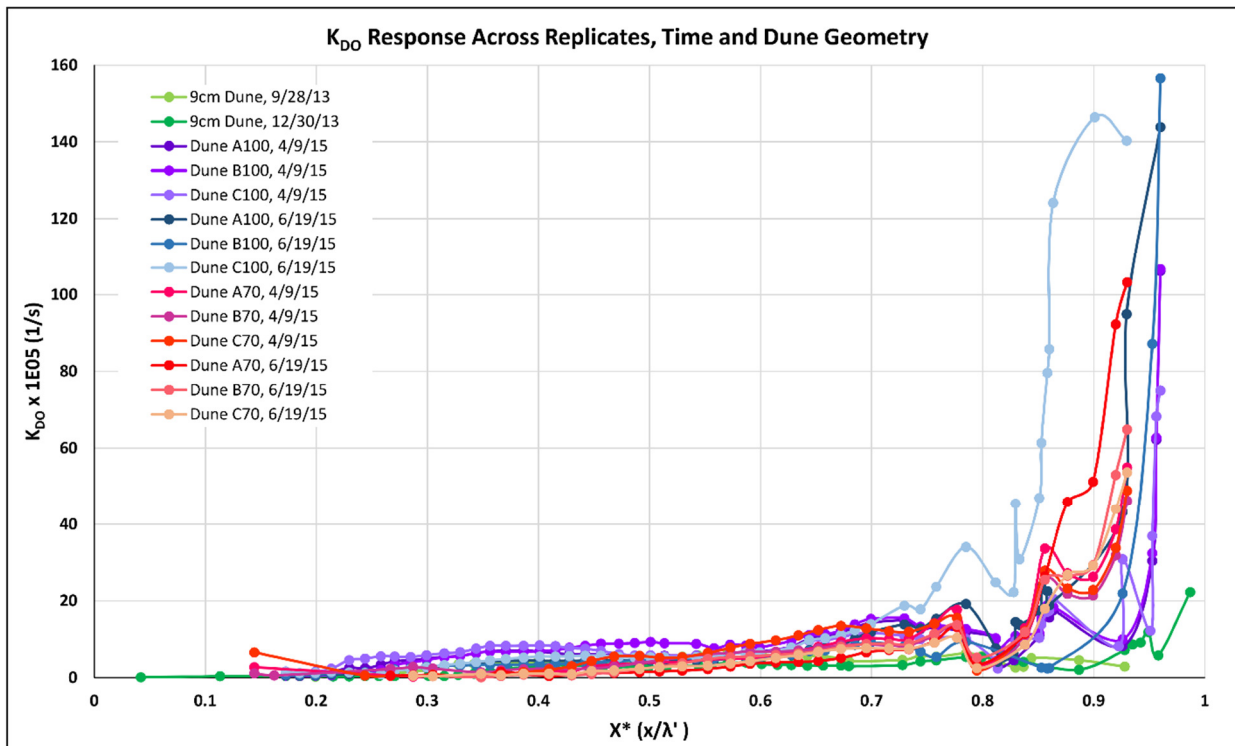
Figure 4-3. K_{DO} values calculated for individual flowlines (each dot representing one flowline) plotted at the entry position of the flowline along the dune surface. X^* is the position along the dune profile normalized by the downwelling length (λ'). $X^* = 0$ is at the trough of the leading edge of the dune and $X^* = 1.0$ is at the crest of all of the dunes. K_{DO} profiles are presented for all of the dunes considered in this experiment. Profiles are presented for each dune at the beginning and end of the experimental runs.
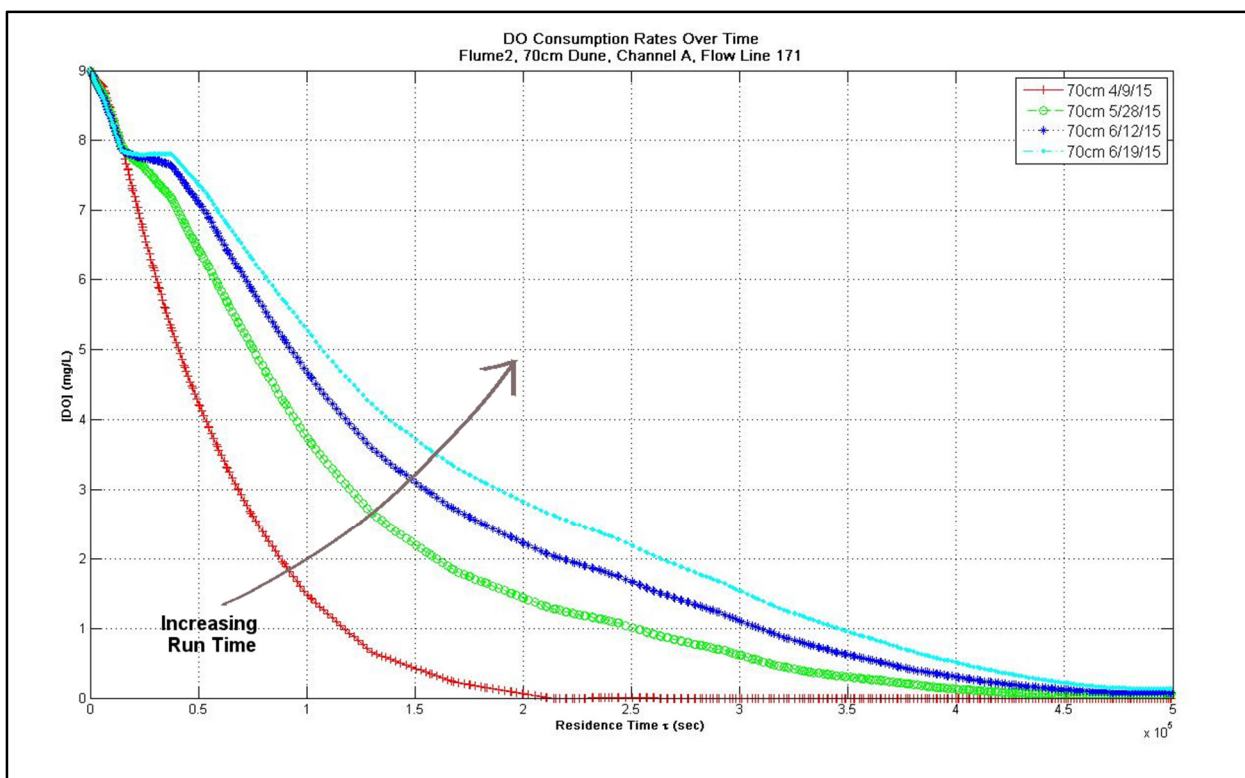
Figure 4-4. In a system that is characterized by episodic nutrient (carbon) replenishment, K_{DO} will decrease over time as labile carbon is depleted. This is illustrated by tracking a single flowline over two month's run time. On 4/9/15 (Day 33) the K_{DO} value for flowline 171 in the 70cm dune in Channel A was 1.6×10^{-5} s^{-1}. On 6/19/15 (Day 91) the K_{DO} value for the same flowline was 0.61×10^{-5} s^{-1}, decreasing by a factor of 2.75.

This trend of generally decreasing DO consumption rates can also be observed in the overall K_{DO} profiles for the individual dunes. Figure 4-5 shows the K_{DO} profiles at four different dates for the Channel C, 70 cm dune. Each dot on the profiles represents the calculated K_{DO} value for an individual flowline. The K_{DO} values are mapped to the x-location of the entry point of the flowline into the HZ. All of the profiles have the characteristic spatial profile in which K_{DO} rises slowly along the stoss face of the dune and then terminates in a sharp rise at the crest of the dune. Superimposed on this spatial profile is a temporally decreasing trend in DO consumption rates that is consistent and exhibited across the dune profile. It is particularly prominent in the middle of the stoss face of the dune in the center of the downwelling area. It is interesting to note that this transition is not so readily apparent in the crest region of the downwelling area. This is a bit counterintuitive. It would seem that this area should exhibit the largest delta in K_{DO} values since, due to the significantly higher

fluxes in that area, the rate of carbon depletion should be highest in that area. The crest had some slight bed turnover and sediment movement. It may be the case that there was some local carbon replenishment occurring due to particle transport and modest bed mobility at the crest [*Drummond et al.*, 2014; *J. W. Harvey et al.*, 2012].
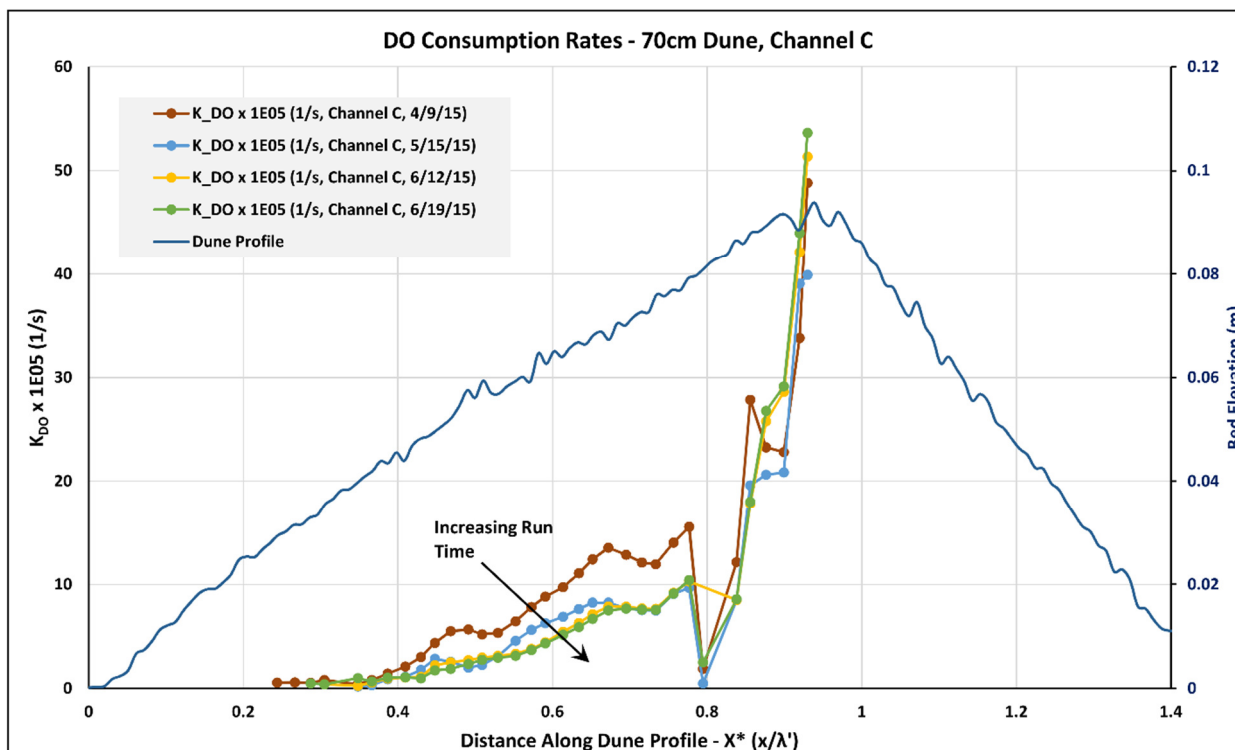
Figure 4-5. The temporal changes in flowline K_{DO} is manifest across the downwelling area. Here we see the steady and consistent decrease in K_{DO} values over a two month time period.

For the physical system in which we conducted our experiments, the supply of bioavailable carbon was fixed at the beginning of the run and not replenished at any point during the experimental run. The flow hydraulics and bed morphology were held as relatively fixed quantities for the duration of the experiments (~15 weeks) as was water temperature and chemistry. Thus, the observed decrease in K_{DO} must be linked to internal changes in the hyporheic environment as opposed to some external forcing. The only free variables here are carbon reactive concentration and the composition and quantities of the microbial communities. Barring some disruptive event, the microbial communities will adapt their numbers and activity to match availability of resources -in this case DO and organic carbon. Except for any lithoautotrophic activity, organic carbon reactivity/availability should

only decrease with time. Metabolic depletion of labile carbon would be first observed near the surface of the bedform and move progressively downward into the HZ. The net effects of decreasing carbon are the observed decrease in bioactivity (K_{DO}) and deeper penetration of DO into the HZ.   As a result of this progressive depletion of labile carbon, the extent of the DO plume expands over time (Figure 4-6). For this system, the volume of the DO plume increased linearly with time and, similarly, the K_{DO} values for the same dune decreased linearly with time (Figure 4-7). Given sufficient runtime and lacking nutrient replenishment, the volume of the oxic plume would be expected to occupy the entire volume encompassed by the hyporheic flow lines. Based upon the extent of the flowlines and the linear expansion rate described in Figure 4-7, the 70 cm dune analyzed in Figure 4-6 would take approximately 240 days to become fully oxic. Along with the expanding extent of the oxic volume is an associated decrease in the anoxic volume and with that a decrease in the residence time available for anaerobic processes.
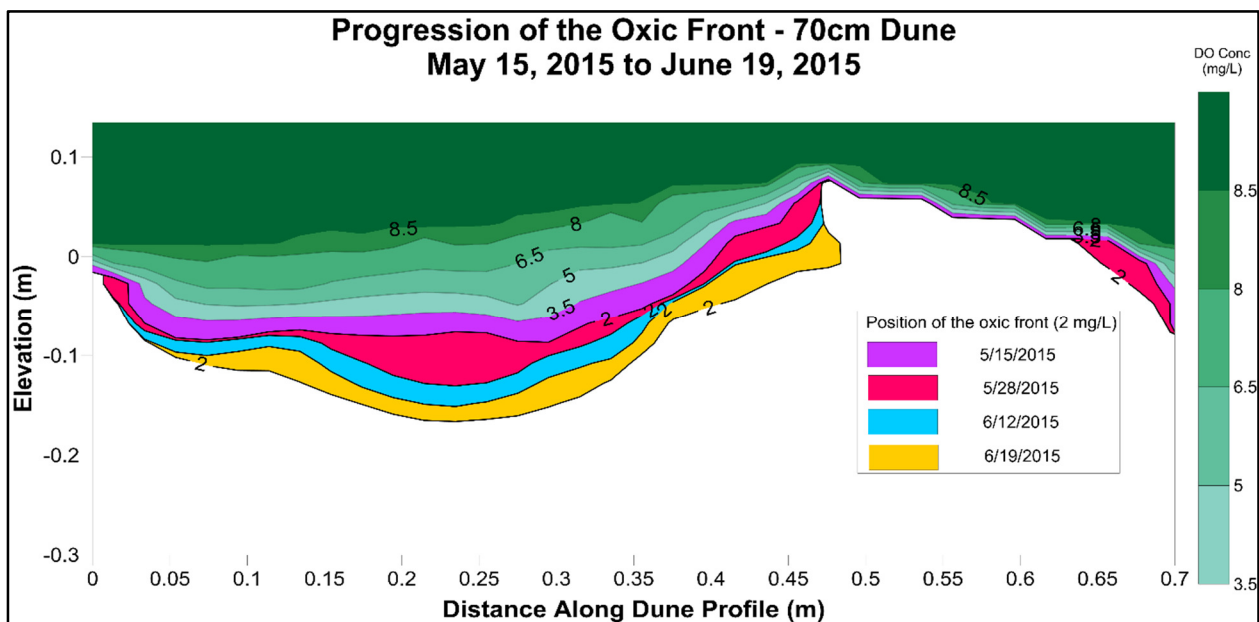
Figure 4-6. As the supply of labile carbon is depleted (first near the surface of the downwelling area), the DO consumption rate, K_{DO}, decreases causing the plume of DO to extend further into the HZ. The rate of expansion for the volume of the oxic plume is, over the time period of this experiment, linear (see inset). Given sufficient runtime and lacking nutrient replenishment, the volume of the oxic plume would be expected to occupy the entire volume encompassed by the hyporheic flow lines.

This shifting balance between the relative extents of the aerobic and anaerobic regions in the HZ becomes important when coupled aerobic/anaerobic processes are active. For instance, hyporheic metabolic processes are the primary mechanisms by which rivers and streams consume and potentially eliminate reactive nitrogen compounds (nitrate, ammonia, organic nitrogen) that enter streams as pollutant runoff from agricultural and industrial processes [*Böhlke et al.*, 2002; *Böhlke et al.*, 2009; *Kessler et al.*, 2012; *Lansdown et al.*, 2012; *Mulholland et al.*, 2008; *Ranalli and Macalady*, 2010]. These nitrogen-transforming processes are generally termed the nitrification/denitrification cycle. Nitrification, which occurs in the oxic portion of the HZ, is the metabolic oxidation of ammonia (NH_3) or ammonium (NH_4^+) to nitrate (NO_3^-). Denitrification, which is generally initiated once the local DO level falls below approximately 2 mg/L [*Beaulieu et al.*, 2008; *Chapelle*, 1993; *Tiedje*, 1988; *Wrage et al.*, 2001], is the sequential anaerobic reduction of $NO_3^- \rightarrow NO_2^- \rightarrow NO \rightarrow N_2O\uparrow \rightarrow N_2\uparrow$. The degree to which the denitrification sequence will be carried to completion is determined by the specific reaction rate along a flowline and the amount of residence time that remains on that flowline from the anaerobic initiation point to the point at which that flowline exits back into the stream water. If the residence times are long, relative to the denitrification reaction rate, then the predominate effluent will be nitrogen gas (N_2) the primary natural component of our atmosphere. Alternatively, if residence times are very short relative to the time scale of the denitrification sequence then the primary effluent is likely to be NO_3^-. Intermediate residence times are likely to produce an effluent mixture of N_2 and N_2O [*Bardini et al.*, 2012; *Cardenas et al.*, 2008; *A. Marzadri et al.*, 2012; *Quick et al.*, 2016]. Urban and rural rivers and streams have been recently identified as significant producers of N_2O emissions, with approximately 10% of anthropogenically sourced N_2O attributed to streams [*Beaulieu et al.*, 2008; *Ravishankara et al.*, 2009]. This is of concern since N_2O is a particularly potent greenhouse gas, which, on an equal mass basis, has approximately 300 times the atmospheric warming potential as compared to CO_2. Additionally, N_2O is very persistent with an observed half-life of about 50 years in the upper atmosphere [*IPCC*, 2007]. Thus, we can see that the ultimate outcome of coupled aerobic and anaerobic processes may likely be determined by the position of the oxic front in the HZ and how much of the HZ is apportioned between oxic and anoxic domains.
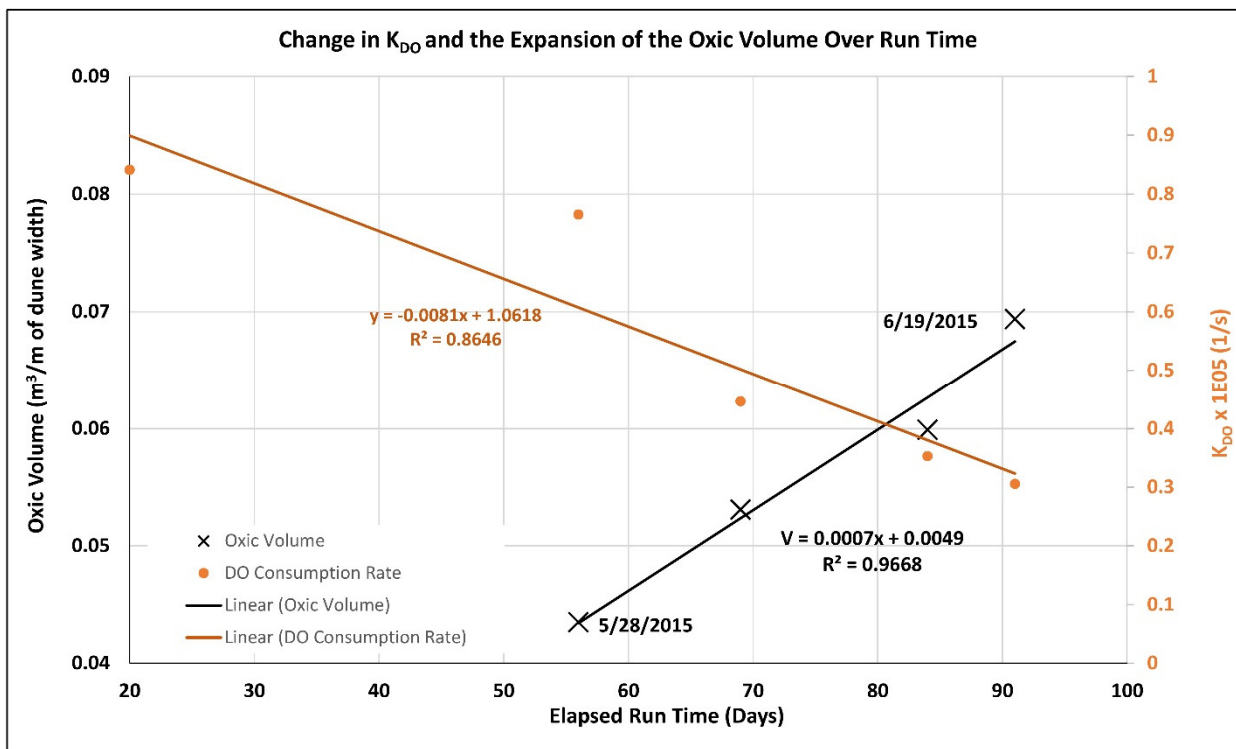
Figure 4-7. The volume of the oxic plume in the HZ (black Xs) increases linearly over time. Similarly, the rate of DO consumption (orange dots) decreases linearly with run time.

We have argued consistently throughout this discussion that the observed temporal decrease in bioactivity is tied primarily to the decrease in bioavailable organic carbon. To test this hypothesis we measured carbon content of the sediments only at the start and end of each experiment (Figure 4-8). The main reason for this was that a major objective in our experimental approach was to disturb the system as little as possible, thus the *in situ* DO measurements and pore water extraction ports. The technique available to us for carbon assessment involved the physical removal of sediments samples, which would have prohibitively disruptive to the larger objectives of the project. Nonetheless, these measurements demonstrate that substantial carbon was consumed and released as CO_2. It should be noted that carbon assessment samples collected at the end of the experiments were collected from the top 10 cm of the bed profile, the region of the highest rate of carbon consumption. Because of this bias in the carbon data, the decrease in carbon (>50%) shown in the graph likely overstates the carbon removed from the totality of the bedforms. This observation is consistent with first-order calculations of carbon consumption, which, based

upon mass flux rates of DO, the volume of aerobic zone, and the assumption that the carbon concentrations throughout the aerobic zone were uniformly depleted, suggest that Figure 4-8 overstates the carbon consumption by a factor of 2 to 3. If, however, we were able to properly define the carbon concentration gradients we would expect that those same calculations would align much more closely to the measurements.

To this point, we have focused upon internal changes in the system (carbon consumption) that drive changes in DO consumption rates. However, in a natural system, there are external forcing factors that could elicit temporal shifts in bioactivity levels. Human activities (agriculture, dam releases and stream maintenance) could enhance or restrict nutrient supplies. Animal migrations and mortality could have similar effects. Seasonal changes in litter or stream flow along with storm surges and recessions will cause changes to the downwelling velocity and fluxes. As we have demonstrated, bioactivity (K_{DO}) is linked to downwelling velocity and so changes to streamflow that drive changes in the downwelling flux will, in turn, cause changes to the reaction rates within the sediments. Depending on the interaction between flow and bed morphology, K_{DO} may increase with discharge or decrease as the flow stage recedes. Microbial communities will accelerate or decelerate their DO consumption during unsteady flow. For instance, K_{DO} will increase during strong downwelling flows, such as in a storm surge, and decrease as the surge recedes. This suggests that biogeochemical processes will likely be different during the rising and lowering limb of flood events. The degree of difference will depend on the relative rates at which downwelling fluxes change during the rising and falling limbs of the flow event, the history of nutrient consumption prior to the flow event and thus the hysteresis of DO concentration at a point.

It is clear that few if any natural systems will be as tightly constrained as our flume system. Nonetheless, many managed streams in which bed altering flows are controlled, deadfall is routinely removed and riparian vegetation is held back from the banks are likely to strongly exhibit elements of what has been presented here. In general, the spatial and temporal trends that have been presented in this and the companion paper suggest that researchers engaged in field studies need to be cognizant of the temporal and spatial nutrient regime of the study area as well as the hydraulic context and complexity of that area. Where

and when one takes measurements makes a difference. Biologic activity is not a fixed, bulk property of the system.
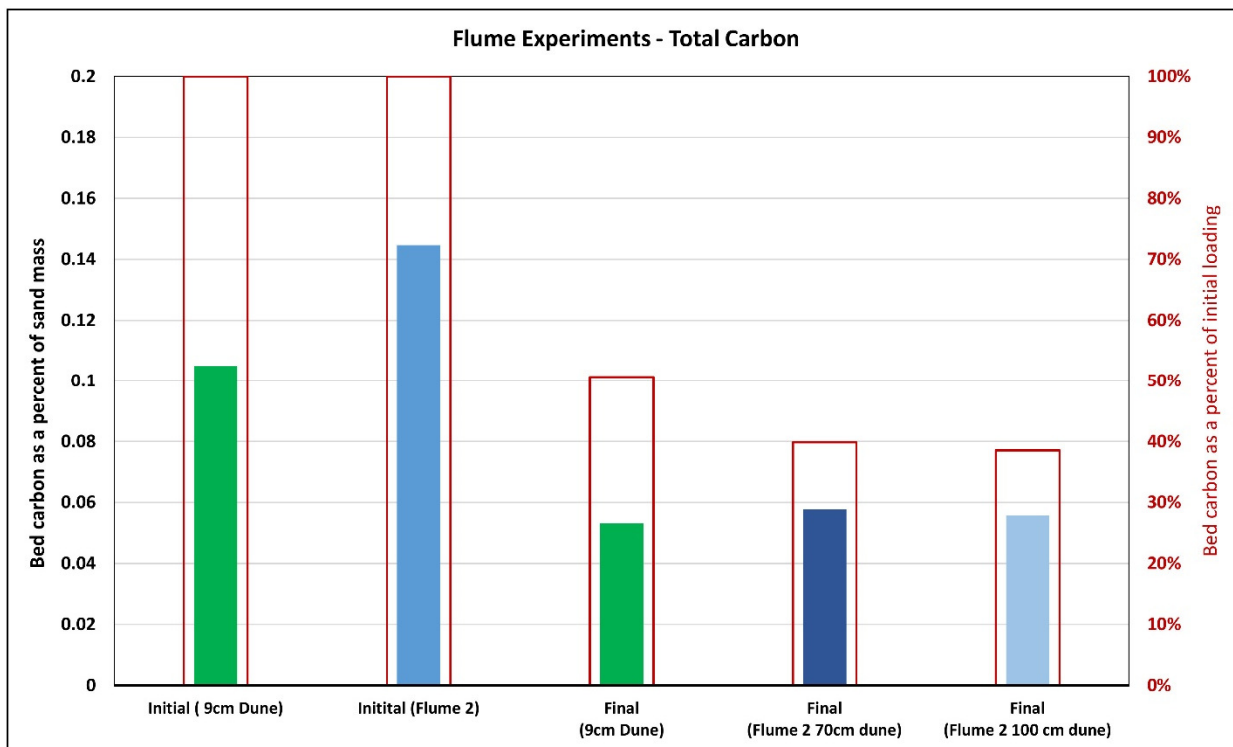
Figure 4-8. Total carbon, in the sand that was used to make up the beds, was measured at the beginning and end of the experiments. Carbon values for the beginning of the experiment are characteristic of the entire bed since the carbon (crushed leaves) was well mixed and homogeneously distributed through the whole bed. The carbon values reported for the end of the experiment represent only the approximately top 10cm of the bed (the only sand collected for carbon analysis was from the top of the bed). As such, the cabon values at the end of the experiment are biased towards the most carbon-depleted portion of the bed.

4.4 Conclusions

In a hyporheic system, which is relatively abundant in labile carbon and characterized by nutrient replenishment that is primarily episodic, the rate of DO consumption changes over time. Specifically, within the aerobic zone and once the microbial communities are established, the rate of DO consumption decreases over time. Within the constraints of the period in which the available carbon is above a minimum threshold, regardless of the time

since nutrient replenishment, the impact of the surface hydraulics will be seen in the K_{DO} distribution. However, as the most readily available organic carbon is consumed, (first near the bed surface/water interface) respiration rates, in that area, will drop and DO will be transported deeper into the HZ. Over time, and lacking either an external source of bioavailable carbon or an alternate electron donor substrate, microbial metabolic activity will slow substantially and the majority of the HZ will be rendered oxic. As the bioavailable carbon falls below a threshold, at which the microbial activity is truly carbon limited, it is expected that the K_{DO} profile will flatten and the stream hydraulics will exert less control over the biologic activity.

4.5 Acknowledgements

4.6 Funding Sources

4.7 Data

The data that was used in support of these findings will be made available at the time of publication through an open-access data repository.

4.8 References

Bardini, L., F. Boano, M. B. Cardenas, R. Revelli, and L. Ridolfi (2012), Nutrient cycling in bedform induced hyporheic zones, *Geochimica et Cosmochimica Acta*, *84*, 47-61.

Beaulieu, J. J., C. P. Arango, S. K. Hamilton, and J. L. Tank (2008), The production and emission of nitrous oxide from headwater streams in the Midwestern United States, *Global Change Biology*, *14*(4), 878-894.

Beaulieu, J. J., et al. (2011), Nitrous oxide emission from denitrification in stream and river networks, *Proceedings of the National Academy of Sciences*, *108*(1), 214-219.

Böhlke, J. K., R. Wanty, M. Tuttle, G. Delin, and M. Landon (2002), Denitrification in the recharge area and discharge area of a transient agricultural nitrate plume in a glacial outwash sand aquifer, Minnesota, Water Resources Research, 38(7), 10-11-10-26.

Böhlke, J. K., R. C. Antweiler, J. W. Harvey, A. E. Laursen, L. K. Smith, R. L. Smith, and M. A. Voytek (2009), Multi-scale measurements and modeling of denitrification in streams with varying flow and nitrate concentration in the upper Mississippi River basin, USA, *Biogeochemistry*, *93*(1-2), 117-141.

Budwig, R., and P. Goodwin (2012), The Center for Ecohydraulics Research Mountain StreamLab - a facility for collaborative research and education, in *Innovations 2012: world innovations in engineering education and research*, edited, iNeer, Potomac, Maryland, USA.

Cardenas, M. B., P. L. M. Cook, H. Jiang, and P. Traykovski (2008), Constraining denitrification in permeable wave-influenced marine sediment using linked hydrodynamic and biogeochemical modeling, *Earth and Planetary Science Letters*, *275*(1–2), 127-137.

Chapelle, F. H. (1993), *Ground-Water Microbiology and Geochemistry*, John Wiley & Sons, New York.

Drummond, J. D., R. J. Davies-Colley, R. Stott, J. P. Sukias, J. W. Nagels, A. Sharp, and A. I. Packman (2014), Retention and remobilization dynamics of fine particles and microorganisms in pastoral streams, *Water Research*, *66*, 459-472.

Elliott, A. H., and N. H. Brooks (1997), Transfer of nonsorbing solutes to a streambed with bed forms: Theory, *Water Resources Research*, *33*(1), 123-136.

Findlay, S. (1995), Importance of surface-subsurface exchange in stream ecosystems: The hyporheic zone, *Limnology and Oceanography*, *40*(1), 159-164.

Fischer, H., F. Kloep, S. Wilzcek, and M. T. Pusch (2005), A River's Liver: Microbial Processes within the Hyporheic Zone of a Large Lowland River, *Biogeochemistry*, *76*(2), 349-371.

Greig, S. M., D. A. Sear, and P. A. Carling (2007), A review of factors influencing the availability of dissolved oxygen to incubating salmonid embryos, *Hydrological Processes*, *21*(3), 323-334.

Harvey, J. W., J. K. Böhlke, M. A. Voytek, D. Scott, and C. R. Tobias (2013), Hyporheic zone denitrification: Controls on effective reaction depth and contribution to whole-stream mass balance, Water Resources Research, 49(10), 6298-6316.

Harvey, J. W., et al. (2012), Hydrogeomorphology of the hyporheic zone: Stream solute and fine particle interactions with a dynamic streambed, *Journal of Geophysical Research: Biogeosciences*, *117*(G4), n/a-n/a.

Hunter, K. S., Y. Wang, and P. Van Cappellen (1998), Kinetic modeling of microbially-driven redox chemistry of subsurface environments: coupling transport, microbial metabolism and geochemistry, *Journal of Hydrology*, *209*(1–4), 53-80.

IPCC (2007), Climate Change 2007: The Physical Science Basis. Contribution of Working Group 1 to the Fourth Assessment Report of the Intergovernmental Panel on Climate Change

Rep., 996 pp, Intergovernmental Panel on Climate Change, Cambridge, United Kingdom and New York, NY, USA.

Kessler, A. J., R. N. Glud, M. B. Cardenas, M. Larsen, M. F. Bourke, and P. L. M. Cook (2012), Quantifying denitrification in rippled permeable sands through combined flume experiments and modeling, *Limnology and Oceanography*, *57*(4), 1217-1232.

Krause, S., D. M. Hannah, J. H. Fleckenstein, C. M. Heppell, D. Kaeser, R. Pickup, G. Pinay, A. L. Robertson, and P. J. Wood (2011), Inter-disciplinary perspectives on processes in the hyporheic zone, *Ecohydrology*, *4*(4), 481-499.

Lansdown, K., M. Trimmer, C. M. Heppell, F. Sgouridis, S. Ullah, A. L. Heathwaite, A. Binley, and H. Zhang (2012), Characterization of the key pathways of dissimilatory nitrate reduction and their response to complex organic substrates in hyporheic sediments, *Limnology and Oceanography*, *57*(2), 387-400.

Marzadri, A., D. Tonina, and A. Bellin (2010), A semianalytical three-dimensional process-based model for hyporheic nitrogen dynamics in gravel bed rivers, *Water Resources Research*, *47*(11).

Marzadri, A., D. Tonina, and A. Bellin (2011), A semianalytical three-dimensional process-based model for hyporheic nitrogen dynamics in gravel bed rivers, *Water Resources Research*, *47*(11), n/a-n/a.

Marzadri, A., D. Tonina, and A. Bellin (2012), Morphodynamic controls on redox conditions and on nitrogen dynamics within the hyporheic zone: Application to gravel bed rivers with alternate-bar morphology, *Journal of Geophysical Research: Biogeosciences*, *117*(G3).

Marzadri, A., M. M. Dee, D. Tonina, A. Bellin, and J. L. Tank (2017), Role of surface and subsurface processes in scaling N2O emissions along riverine networks, *Proceedings of the National Academy of Sciences*.

Master, Y., U. Shavit, and A. Shaviv (2005), Modified Isotope Pairing Technique to Study N Transformations in Polluted Aquatic Systems: Theory, *Environmental Science & Technology*, *39*(6), 1749-1756.

Moreno-Vivián, C., P. Cabello, M. Martínez-Luque, R. Blasco, and F. Castillo (1999), Prokaryotic Nitrate Reduction: Molecular Properties and Functional Distinction among Bacterial Nitrate Reductases, *Journal of Bacteriology*, *181*(21), 6573-6584.

Mulholland, P. J., et al. (2008), Stream denitrification across biomes and its response to anthropogenic nitrate loading, *Nature*, *452*(7184), 202-205.

Packman, A. L., M. Salehin, and M. Zaramealla (2004), Hyporheic Exchange with Gravel Beds: Basic Hydrodynamic Interactions and Bedform-Induced Advective Flows, *Journal of Hydraulic Engineering*, *130*(7), 647-656.

Quick, A. M., W. J. Reeder, T. B. Farrell, D. Tonina, K. P. Feris, and S. G. Benner (2016), Controls on Nitrous Oxide Emissions from the Hyporheic Zones of Streams, *Environmental Science & Technology*, *50*(21), 11491-11500.

Ranalli, A. J., and D. L. Macalady (2010), The importance of the riparian zone and in-stream processes in nitrate attenuation in undisturbed and agricultural watersheds – A review of the scientific literature, *Journal of Hydrology*, *389*(3–4), 406-415.

Ravishankara, A. R., J. S. Daniel, and R. W. Portmann (2009), Nitrous Oxide (N2O): The Dominant Ozone-Depleting Substance Emitted in the 21st Century, *Science*, *326*(5949), 123-125.

Reeder, W. J., A. M. Quick, T. B. Farrell, S. G. Benner, K. P. Feris, and D. Tonina (2017a), Spatial dynamics of dissolved oxygen concentrations and bioactivity in the hyporheic zone, *in review with Water Resources Research*.

Reeder, W. J., A. M. Quick, T. B. Farrell, S. G. Benner, K. P. Feris, D. Tonina, W. J. R. Basham, and C. Huber (2017b), Dissolved oxygen concentration profiles in the hyporheic zone through the use of a high-density fiber optic measurement system, *In revision*.

Rutherford, J., J. Boyle, A. Elliott, T. Hatherell, and T. Chiu (1995), Modeling Benthic Oxygen Uptake by Pumping, *Journal of Environmental Engineering*, *121*(1), 84-95.

Sobczak, W. V., and S. Findlay (2002), VARIATION IN BIOAVAILABILITY OF DISSOLVED ORGANIC CARBON AMONG STREAM HYPORHEIC FLOWPATHS, *Ecology*, *83*(11), 3194-3209.

Tiedje, J. M. (1988), Ecology of denitrification and dissimilatory nitrate reduction to ammonium, John Wiley and Sons, New York.

Tonina, D., and J. M. Buffington (2007), Hyporheic exchange in gravel bed rivers with pool-riffle morphology: Laboratory experiments and three dimensional modeling, *Water Resources Research*, *43*, W01421.

Tonina, D., and J. M. Buffington (2009), Hyporheic exchange in mountain rivers I: Mechanics and environmental effects, *Geography Compass*, *3*(3), 1063-1086.

Tonina, D., A. Marzadri, and A. Bellin (2015), Benthic Uptake Rate due to Hyporheic Exchange: The Effects of Streambed Morphology for Constant and Sinusoidally Varying Nutrient Loads, *Water*, *7*(2), 398.

Triska, F. J., J. H. Duff, and R. J. Avanzino (1993), The role of water exchange between a stream channel and its hyporheic zone in nitrogen cycling at the terrestrial-aquatic interface, *Hydrobiologia*, *251*(1-3), 167-184.

Wrage, N., G. L. Velthof, M. L. van Beusichem, and O. Oenema (2001), Role of nitrifier denitrification in the production of nitrous oxide, *Soil Biology and Biochemistry*, *33*(12–13), 1723-1732.

Wriedt, G., and M. Rode (2006), Modelling nitrate transport and turnover in a lowland catchment system, *Journal of Hydrology*, *328*(1–2), 157-176.

Wuhrmann, K. (1972), Stream Purification, in *Water pollution microbiology*, edited by R. Mitchell, pp. 119-151, Wiley-Interscience, New York, NY.

Zarnetske, J. P., R. Haggerty, S. M. Wondzell, and M. A. Baker (2011a), Dynamics of nitrate production and removal as a function of residence time in the hyporheic zone, *Journal of Geophysical Research: Biogeosciences*, *116*(G1), G01025.

Zarnetske, J. P., R. Haggerty, S. M. Wondzell, and M. A. Baker (2011b), Labile dissolved organic carbon supply limits hyporheic denitrification, *Journal of Geophysical Research: Biogeosciences*, *116*(G4).

Zarnetske, J. P., R. Haggerty, S. M. Wondzell, V. A. Bokil, and R. González-Pinzón (2012), Coupled transport and reaction kinetics control the nitrate source-sink function of hyporheic zones, *Water Resources Research*, *48*(11).

Chapter 5

A Flowline-Scale, Predictive Model of Nitrous Oxide Emissions from the

Hyporheic Zone of Streams[4]

Nitrous oxide (N_2O) is a potent greenhouse gas with an estimated 10% of anthropogenic sourced N_2O chiefly coming from the hyporheic zone (HZ) of streams and rivers. However, we have been unable to identify or understand its emission processes at the bedform or flowline scale because of difficulty in making accurate fine-scale measurements in the field. Using a large-scale, replicated flume experiments that employed high-density chemical concentration measurements, we have been able to refine the current conceptualization of N_2O production, consumption and emission from the HZ. We present a predictive model based on a Damköhler-type transform ($\tilde{\tau}$) of the residence times (τ) along a flowline multiplied by the dissolved oxygen consumption rate. This model can identify which bedforms have the potential to produce and emit N_2O as well as the portion and location from which those emissions may occur. Our results indicate that that flowlines that that have $\tilde{\tau}_{up}$, the $\tilde{\tau}$ value at which a flowline exits back into the surface water, between 0.54 and 4.4 are

likely to produce and emit N_2O. N_2O production peaks approximately at $\tilde{\tau} = 1.8$ along a flow line. A PDF of $\tilde{\tau}_{up}$ values for all of the flowlines in a bedform (or multiple bedforms) can be used to estimate the portion of flowlines with the potential to emit N_2O.

5.1 Introduction

Nitrous oxide (N_2O) is a potent greenhouse gas that is of particular interest because of its role in the depletion of stratospheric ozone. Due to actions taken in response to *The Montreal Protocol on Substances that Deplete the Ozone Layer* (MP), the abundance of anthropogenically-generated, ozone depleting substances (ODS) that are controlled by the MP have been steadily decreasing over the past few decades. However, N_2O is not among the substances included in the Montreal Protocol and in the time since its implementation, N_2O concentrations in the upper atmosphere have been steadily increasing, raising the prominence of N_2O as a cause for ozone depletion and as a forcing agent for atmospheric warming [*Ravishankara et al.*, 2009; *World Meteorological Organization (WMO)*, 2014; *Wuebbles*, 2009]. Recent estimates indicate that N_2O is responsible for 9% of the current climate forcing [*Rosamond et al.*, 2012]. Streams and rivers have been identified as a significant source of N_2O emissions. An estimated 10% of all anthropogenically generated N_2O that is emitted into the atmosphere comes from streams and rivers [*Beaulieu et al.*, 2011]. These emissions are largely correlated to pollutant runoff from agricultural practices [*Davidson*, 2009] with excess nitrogen stimulating N_2O production in rivers impacted by fertilizer runoff [*McMahon and Dennehy*, 1999; *Park et al.*, 2012]. However, field observations indicate that not all impacted streams emit N_2O [*Beaulieu et al.*, 2011].

Our current understanding of these emissions comes almost exclusively from reach or watershed-scale field studies [*Beaulieu et al.*, 2008; *Beaulieu et al.*, 2011; *Laursen and Seitzinger*, 2004; *Zarnetske et al.*, 2011a; b] or from numerical studies [*Alessandra Marzadri et al.*, 2010; *A. Marzadri et al.*, 2014], based upon a Damköhler number treatment, conducted at similar scales. While these studies and models, which have been quite useful in quantifying the regional and global impact of N_2O emissions from streams, they have been unable to resolve the source points of emission at the flowline or even bedform scale. Having an

understanding of N_2O emissions at these scales becomes important if you are trying to define the mechanisms that lead to and control the processes that cause N_2O emissions from streams. This level of understanding could usefully supplement planning and assessment of remediation and restoration projects whose objectives include reducing N_2O emissions. Our goal, in this study, is to resolve the controls over N_2O production and emission and to create a model (Figure 5-1) that resolves N_2O production at the flowline scale that can be scaled up the bedform, reach or watershed scale.
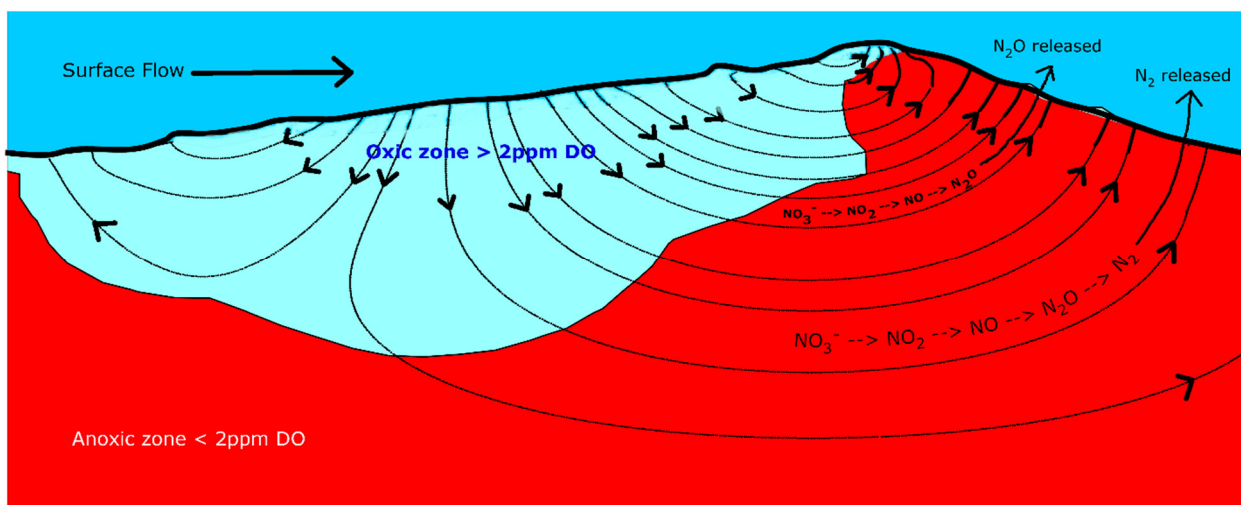
Figure 5-1. A conceptual model of reactive solute transport through the HZ. Due to pressure gradients along the bed surface, surface water flows into the bed sediments carrying with it DO and reactive nitrogen (Nr) compounds. Dissolved oxygen is consumed through aerobic respiration by microbes in the HZ. Some short flowlines return to the surface before all of the DO is consumed. For longer flowlines, DO is consumed to below 2 ppm and anaerobic respiration, in this case, denitrification is initiated. For very long flowlines, N_2 gas is the primary effluent. The effluent from medium-length flowlines is likely to include intermediate reaction products. The emission of N_2O is of particular concern and is illustrated here.

5.2 Methods and Materials

5.2.1 Experimental setup

The experimental setup and methodologies were described in detail in Quick et al [2016]. The key elements that are relevant to the current discussion are described below. We conducted two sets of experiments, in the large-scale flume (approximately 20 m x 2 m) at the Center for Ecohydraulics Research Stream Laboratory [*Budwig and Goodwin*, 2012] at the

University of Idaho, Boise, to test the impact of bed morphology, stream hydraulics and surface water chemistry (reactive nitrogen loading) on DO and nitrogen consumption dynamics and the impact of those processes on N_2O emissions from streams. The first flume experiment (Flume 1) ran continuously from August 2013 through December 2013 and the second (Flume 2) ran from February 2015 through June 2015. In both sets of experiments, the flume was divided into three stream channels (30 cm wide x 60 cm deep x 15 m long) which were separated by two access corridors. Triangular dunes of various sizes were constructed from 90% quarry sand (D_{50} ~1.5 mm) and 10% natural sand collected from the Boise River (Boise, ID, USA). The natural sand provided an inoculum, for the flume sand mix, to initiate bacterial communities, which were representative of those that typically reside in streambed sediments. To provide an organic carbon nutrient source, 0.15% by dry weight of finely divided (< 5 mm) cottonwood leaves were added to the sand mix. Water for surface flow over the dunes was pumped and recirculated from a 50,000-gallon catch basin into a headbox at the top of the flume and over individual sills into each of the three flume channels. For the present discussion, we will consider three different dune variants. From Flume 1, we will evaluate the response of a 9 cm tall by 1 m long dune, hereafter referred to as the "9 cm dune." The energy slope for the 9 cm dune was 0.002. From Flume 2, we will consider a 9 cm tall by 100 cm long dune and a 9 cm tall by 70 cm long dune, hereafter referenced as "100 cm dune" and "70 cm dune", respectively. The energy slope for the Flume 2 experiments was 0.003.

5.2.2 Pore water sampling

In-situ pore-water-extraction ports (rhizon soil-moisture samplers, Rhizosphere Research Products, Netherlands) were embedded through the sidewalls of the flume channels and into the bulk of the dunes allowing us to obtain high-density, repeatable pore water samples throughout the duration of the experimental runs. A typical placement of the *in situ* sampling ports is illustrated by the purple dots in Figure 5-2. The embedded portion of the rhizon sampling ports consisted of porous (0.45 µm) tubing (10 cm x 3 mm) that was supported by a stainless steel wire stiffener. The porous portion of the rhizon samplers was connected through the sidewall of the flume channel and into the access corridors by silicon

tubing that was terminated by a luer lock adapter and a cap. During sampling, the cap was replaced with a needle and, initially, the port was allowed to drip for a brief time to allow any stagnate water in the silicon tubing to be evacuated. For the actual pore water sample, a closed sampling method was used. The needle was inserted, under water, into the septa of an evacuated sample vial. Pore water was pulled, by the vacuum in the vial, through the rhizon sampling port and into the vial. The vial was held under water for the duration of the sample extraction. Approximately 10 ml of pore water was collected in 20 ml vial. To measure dissolved N_2O the samples were passed through a 0.45 µm filter into a headspace sampling vial and analyzed using an HP 7694 headspace autosampler and an Agilent 6890 gas chromatograph equipped with a GS_Carbon PLOT column (30 m x 0.53 mm) and a [63]Ni microelectron capture detector. Dissolved concentrations of N_2O were calculated using Henry's Law [*Hudson*, 2004].

5.2.3 Bed-surface pressure profiles and hyporheic flowlines

The dynamic pressure profile along dune-like bedform is the main pressure component driving hyporheic flow. Because of the relatively low flow velocities in the flume experiments (< 0.1 m/s), the dynamic pressures generated by the dunes are low, often substantially less than 5 Pa, which cause a manometer reading of approximately 0.5 mm, or less. This reduces the ability to measured pressure distribution with the accuracy and resolution needed to described the flow. Thus, we followed the approach described by Cardenas and Wilson [2007] and modeled the pressure profiles using ANSYS Fluent CFD (ANSYS Inc., Canonsburg, PA, USA). ANSYS CFD provides a numerical solution to the Reynolds-Averaged, Navier Stokes surface flow equations. Our models, which were meshed with between 65,000 and 95,000 triangular elements, used a k-ω turbulence closure with a Low-Reynolds-Number correction. The measured bed surface and water surface profiles provided the physical boundary of the numerical domain. We surveyed the bed surface and water surface profiles every 2cm along the centerline of each dune with a laser scanning and an ultrasonic sensor (Omega Engineering, Inc., CT, USA; Model LVU30), respectively; both with 1mm vertical resolution. The inlets and outlets of the surface flow models were treated as periodic boundaries with the periodic pressure gradient defined by the energy slope of the

water surface, which we measured along with the discharge. The water surface was modeled as a symmetry boundary and the bed surface as a no-slip wall boundary. Residual error for continuity, x-velocity, y-velocity, k and ω was set to less than 1x10-6 for convergence. The overall CFD modeling approach was validated against the pressure measurements provided by Fehlman [1985]. Excellent agreement between the simulated and measured bed-pressures, over a broad range of discharges and energy head, gave us a high degree of confidence that our modeling approach was robust, accurate and not overly sensitive to the applied boundary conditions.

The modeled pressure profiles were used as upper boundary condition for the hyporheic model of Marzadri [*Alessandra Marzadri et al.*, 2010] and GMS ModFlow (Aquaveo, LLC, Provo, Utah), which we used to quantify hyporheic flowlines and the associated residence times (τ) (red and green lines, Figure 5-2). Calculated residence times were calibrated with measured from a salt pulse injection with electrical conductivity (EC) sensors placed at a subset of the sampling ports (purple dots, Figure 5-2) Salt solution was constantly added into the head box of the flume for approximately 30 minutes. Residence times were then measured with EC sensors at 9 locations in a 70 cm dune and 20 locations in a 100 cm dune of Flume 2.
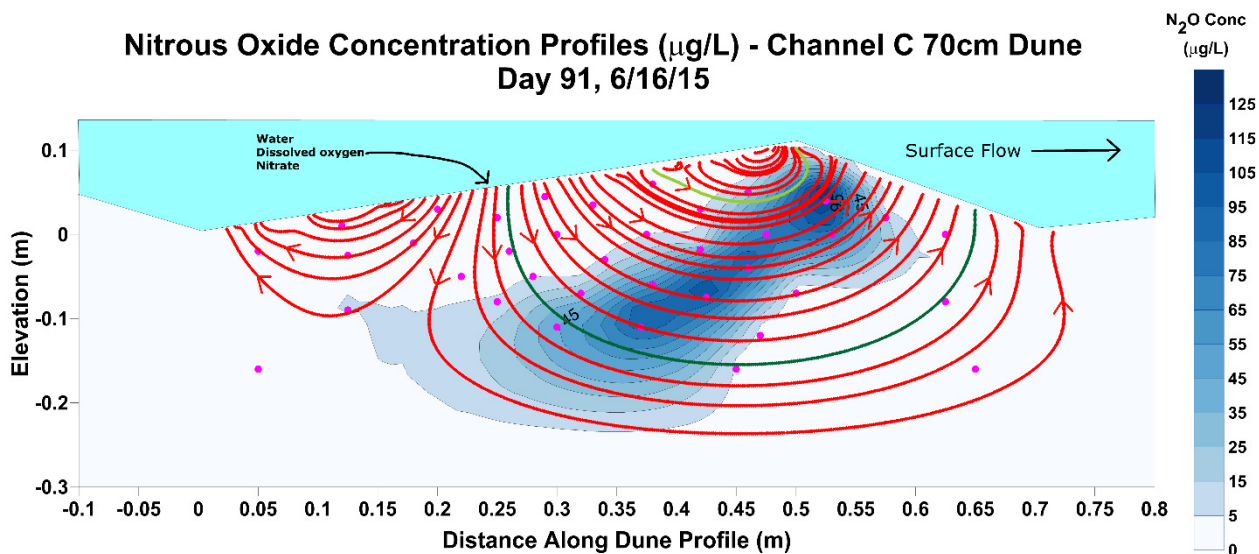
Figure 5-2. The measured N_2O concentration profiles and the calculated flowlines (red and green traces) for the Channel C, 70 cm Dune on Day 91 of the Flume 2 experiment. The green traces mark the flowlines for the N_2O vs τ profiles in (Figure 5-3).

5.2.4 Flowlines and chemical concentration profiles

The measured N_2O concentration data were krigged and gridded (Surfer ® Version 10, Golden Software, Inc., Golden CO) to create N_2O concentration maps for each dune. The concentration profile for the Channel C, 70 cm dune on Day 91 of the Flume 2 experiment is shown in Figure 5-2. The kriging operation creates a regular grid of X-Y locations and assigns an N_2O concentration, that is interpolated from the measured values, to each location. The interpolation is constrained such that the measured values are not altered. That is, at the measurement points (purple dots, Figure 5-2), the krigged profile is the measured value. For each of the dunes, flowlines (red and green traces, Figure 5-2) were calculated from the pressure profile for that particular dune. Those flowlines were mapped onto the associated N_2O concentration profile. In a similar manner to the krigged concentration profiles, the flowlines traces consist of a series of X-Y locations with a residence time at each location. For each flowline, from these co-mapped data sets, we extracted a data string of paired residence time and the N_2O concentration (τ, [N_2O]). The two profiles in Figure 5-3 are exemplary examples of individual-flowline N_2O concentration profiles presented as a function of residence time. With these data, we can parse the chemical activity in the HZ to a very fine

level. For instance, we can locate the residence time and position of the peak production of N_2O along the flowline as well as the N_2O concentration and residence time at flowline exit. Additionally, by calculating an exponential fit to the rising and falling limbs of the $[N_2O]$ versus τ profiles we can calculate the apparent (it is likely that production and consumption are happening simultaneously) first-order reaction kinetics for N_2O production and consumption, respectively. Dissolved oxygen and other chemical constituents can be treated in a similar manner. In fact, we used the same procedure, with τ versus [DO] data streams, to calculate the rate of metabolic DO consumption K_{DO} for all of the flowlines.
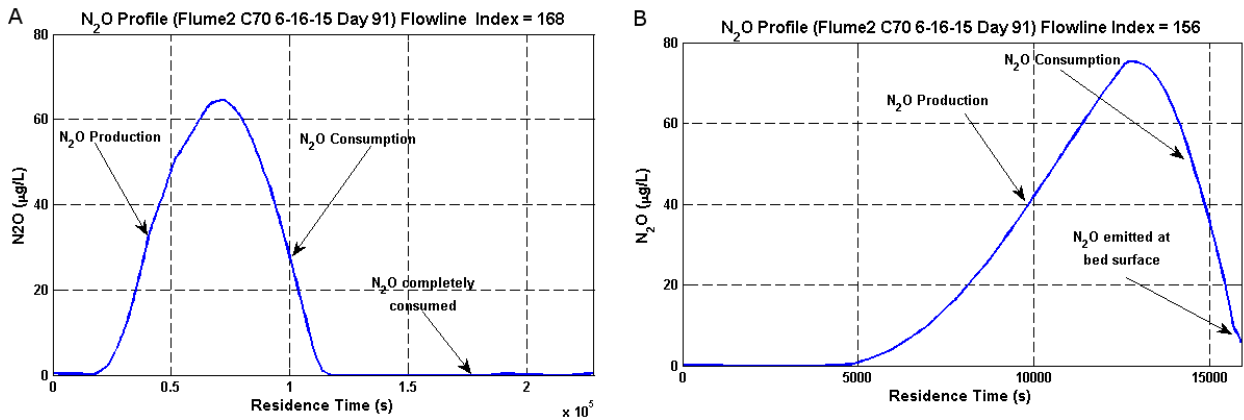
Figure 5-3. N_2O concentration versus τ profiles for two different flowlines from the Channel C, 70 cm Dune on Day 91 of the Flume 2 experiment. Panel A illustrates a long flowline (dark green trace, Figure 5-2) in which N_2O is consumed to below the surface water concentration. This flowline performs as a sink for N_2O. Panel B illustrates an intermediate length flowline (light green trace, Figure 5-2) whose exit concentration is above the surface water concentration. This flowline is a source of N_2O.

5.2.5 Calculation methodologies

We define a Damköhler-type transform that scales the residence times (τ) along each of the individual flowlines by a characteristic reaction rate for each of the flowlines. In this study we used K_{DO}, the rate constant for the metabolic consumption of dissolved oxygen. The transformed residence times are designated as $\tilde{\tau}$ and the transform is calculated by:

$$\tilde{\tau}_i = \tau_i \, x \, K_{DOi} \tag{5.1}$$

Where $\tilde{\tau}_i$ is the collection of transformed residence times (τ) from flowline (i) and K_{DOi} is the DO consumption rate along flowline (i). The $\tilde{\tau}$ transform is calculated for all of the

flowlines using individual K_{DO} values that have been calculated for each of the flowlines. In Reeder et al. [2017a] we showed that, for dune-like bedforms, K_{DO} values are log-normally distributed and that flowline K_{DO} values can be calculated from the mean K_{DO} and the standard deviation, which can be estimated.

$$f(X^*|\mu, \sigma) \; \frac{1}{X^*\sigma\sqrt{2\pi}} e^{\left\{ \frac{-(\ln x - \mu)^2}{2\sigma^2} \right\}} ; \; X^* > 0 \tag{5.2}$$

More simply, the flowline K_{DO} values can be calculated in Excel or Matlab using the expression

$$K_{DOi} = \exp(norminv(X^*, \ln(\overline{K_{DO}}), \ln(StdDev)) \tag{5.3}$$

X^* is the non-dimensional, horizontal distance along the downwelling face of the bedform.

$$X^* = x \cdot \lambda' \tag{5.4}$$

Where λ' is the horizontal length of the downwelling face of the bedform. In a triangular dune, λ' is simply the streamwise distance from the trough to the crest of the dune.

Alternatively, the $\tilde{\tau}$ transform can be calculated using the mean K_{DO} of a particular bedform for all of the flowlines in that bedform. This is less precise than the distributed transform but it may be useful in some situations. For this approach, the transform takes the form

$$\tilde{\tau}_i = \tau_i \; x \; \overline{K_{DO}} \tag{5.5}$$

N_2O flux was calculated as

$$f_i = \begin{cases} 0, & \tilde{\tau}_{up(i)} < 0.54 \\ v_{dw(i)} \; x \; A_{dw(i)} \; x \; [N_2O]_{up}, & 0.54 \leq \tilde{\tau}_{up(i)} \leq 4.4 \\ v_{dw(i)} \; x \; A_{dw(i)} \; x \; ([N_2O]_{surf} - [N_2O]_{min}), & \tilde{\tau}_{up(i)} > 4.4 \end{cases} \tag{5.6}$$

Where f_i is the flux from flowline (i), $V_{dw\,(i)}$ is the downwelling velocity into flowline (i), $A_{dw\,(i)}$ is the bed surface area associated with flowline (i), $[N_2O]_{up}$ is the N_2O concentration as flowline (i) exits the HZ, $[N_2O]_{surf}$ is the N_2O concentration of the surface

water and $[N_2O]_{min}$ is the minimum N_2O concentration along flowline (i). Total flux from a bedform is calculated by summing the fluxes from all of the flowlines.

5.3 Results

The blue, shaded profiles in Figure 5-2 show the krigged N_2O concentrations for the Channel C, 70 cm dune on Day 91 of the Flume 2 experiment. The C70 concentration profile is generally typical of the profiles for all of the dunes in the two experiments, though, because the C70 dune had the highest level of activity, its profile map is somewhat more extensive and continuous than for the other dunes. Nonetheless, the morphology, extent and location of the N_2O plumes for all of the dunes is quite similar to the C70 profile. We created N_2O concentration profiles (τ, $[N_2O]$) for all of the flowlines that intersected the various N_2O plumes. Two exemplary examples are shown in Figure 5-3. The concentration profile in Panel A is from a very long flowline (dark green flowline, Figure 5-2). The rising limb of the profile represents production of N_2O and the falling limb is consumption. The N_2O concentration at the entry point of the flowline was 0.55 µg/L, N_2O production peaked at about 65 µg/L and all of the N_2O was consumed before the flowline exited the HZ. This flowline functions as a sink of N_2O. First-order reaction kinetics can be calculated for both production and consumption by fitting an exponential function to the either the rising or falling limb, respectively. It should be noted, though, that the calculated rate constants should be viewed as "apparent" rates because it is quite likely that production and consumption are occurring simultaneously over a substantial portion of the profile. The concentration profile in Panel B is for an intermediate length flowline. As with the long flowline (Panel A), both production and consumption are occurring along this flowline. However, this flowline exits the bed before all of the N_2O is consumed. This flowline, at least on this measurement date, was acting as a source of N_2O to the surface flow. The N_2O concentration profiles for of the flowlines in dune C70, Day 91 are shown in Figure 5-4. Within this single dune, there is a wide range of production and consumption responses. From flowline to flowline, the

initiation of production and peak production occurs at different points in (residence) time. The magnitude of the peak and terminal concentrations varies by flowline.
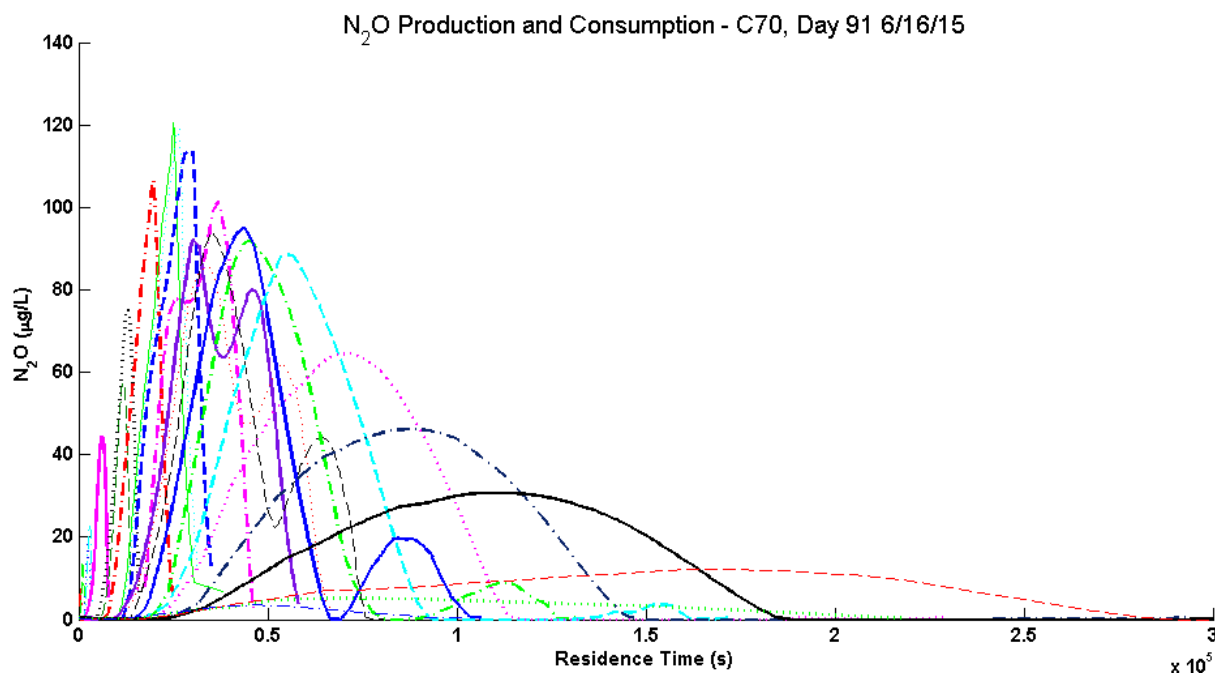
Figure 5-4. N_2O concentration profiles for all of the flowlines that produce and/or consume N_2O for the C70 on Day 91. The rate and magnitude of N_2O production is highly variable from flowline to flowline as is the timing of the production and consumption events.

The N_2O concentration profiles for all of the flowlines from all of the dunes included in this experiment are shown in Figure 5-5. The apparently tight grouping of the profiles in this chart is somewhat deceptive. The large number of data points (> 100,000) and the inherent similarity between the experiments tends to obscure the broad diversity of responses. When the flowlines are evaluated against the tendency to emit N_2O, it is difficult, if not impossible, to identify a concise range of residence times (τ) that identify, specifically, flowlines that have a high probability to emit N_2O. As such, while it gives a good overview of the broad range of responses that are exhibited by the various dunes and flowlines, the concentration data in this format is not particularly useful as a predictive too. Most of the variability among the concentration profiles in Figure 5-5 comes from variability between flowlines as opposed to variability between dunes. We know from previous work [*Reeder et al.*, 2017a] that, when evaluated at the flowline level, metabolic DO consumption expressed

as the reaction rate K_{DO} is a linear function of the of the downwelling velocity along a flowline. The flowline downwelling velocities for a bedform are lognormally distributed and, thus, so too are the values expressed by K_{DO}. Stated succinctly, bioactivity level within a dune are likely to be lognormally distributed.
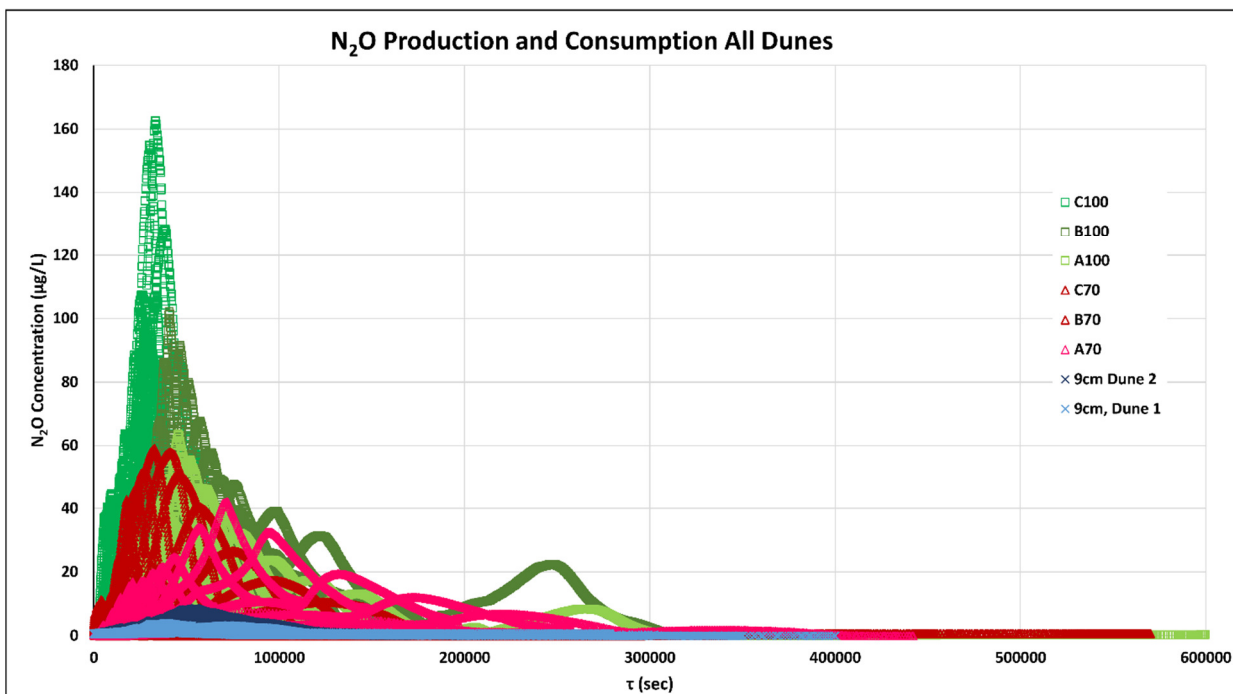
Figure 5-5. N$_2$O concentration profiles for all of the flowlines and all of the dunes considered in this experiment (A70, B70, C70, A100, B100, C100, 9cm Dune 1 and 9cm Dune 2). The 9 cm dune data is from Day 112 of the Flume 1 experiment. All of the other data is from Day 91 of the Flume 2 experiment. The apparently tight grouping of the profiles is somewhat deceptive. The large number of data points (> 100,000) and the inherent similarity between the experiments tends to obscure the natural diversity of the responses. The data presented in this format is not particularly useful as a predictive tool.

Based upon the above observations, it seemed a reasonable possibility that scaling the residence times (τ) by a characteristic reaction rate would yield a non-dimensional residence time that would tend to group similar events together. To test this idea, we multiplied the flowline residence times (τ (s)) by the DO consumption rate (K_{DO} (1/s)) for each flowline. K_{DO} values were calculated from the lognormal distribution of K_{DO} values for the dune in which a particular flowline resided. We designate the transformed, non-dimensional residence times as $\tilde{\tau}$. The results of the $\tilde{\tau}$ transform are shown in Figure 5-6. The grouping of

the transformed profiles is significantly more useful than that of the ungrouped (Figure 5-5) profiles. N_2O production for the majority of the profiles initiates within relatively small range of $\tilde{\tau}$ values (~0.5 to 1). The N_2O concentration peaks are reasonably well aligned as are the falling limbs (consumption) of the profiles. Collectively, these profiles potentially define a concise range of $\tilde{\tau}$ values that encompass N_2O production and consumption for a broad range of bedforms. The mean profile for all of the flowlines was calculated using two approaches. In the first approach, the N_2O values were binned by $\tilde{\tau}$ with each bin having a width of 0.1 (number of observations in each bin was ~ 1,000). All of the N_2O values in each bin were averaged and plotted to the mid-point of the bin (orange line, Figure 5-7). In the second approach, the amplitude of all of the flowlines were normalized to the maximum values of each of the individual flowlines. Thus transformed, all of the transformed flowlines exhibited values that ranged from 0 to 1. The transformed values were binned, averaged and plotted in the same manner as used in the first approach (blue line, Figure 5-7). The two approaches were used to test whether or not the different amplitudes from different experiments, dunes and flowlines would bias the location of the population mean and the value of the standard deviation. We calculated the mean and standard deviation of the untransformed and transformed data sets using the expressions:

$$\bar{\bar{\tau}} = \frac{1}{\sum c_i}\sum_1^n c_i \cdot \tilde{\tau}_i \tag{5.7}$$

for the mean and

$$\sigma^2 = \frac{1}{\sum c_i}\sum_1^n c_i \cdot (\tilde{\tau}_i - \bar{\bar{\tau}})^2 \tag{5.8}$$

for the variance. The mean and standard deviation (square root of the variance) for the untransformed data was 1.82 and 0.64, respectively. For the transformed data, the mean and standard deviation were 1.65 and 0.91. For both approaches, the mean and standard deviation were quite similar, suggesting that differing amplitudes among the flowlines was not overly biasing to the final result. Using the untransformed data, we define lower and upper boundaries for N_2O production and consumption. The lower boundary for production is defined as the mean (1.82) minus two standard deviations giving a lower limit of N_2O production at $\tilde{\tau} = 0.54$ (gray vertical line, Figure 5-6 and Figure 5-7). The upper limit of consumption is defined as the mean (1.82) plus four standard deviations giving an upper limit

of production at $\tilde{\tau} = 4.4$ (black vertical line, Figure 5-6 and Figure 5-7). The reason for unbalanced use of standard deviations is the relatively long tail on the consumption side of the profile. This unbalanced approach creates limits that match well to a threshold line (black, horizontal, dashed line, Figure 5-7) set at $[N_2O] = 0.65\ \mu g/L$, just above surface water equilibrium concentration. The meaning of these limits is that, on average, for any particular flowline N_2O production will be initiated at $\tilde{\tau} \approx 0.54$, the N_2O concentration will peak at $\tilde{\tau} \approx 1.8$ and, if the flowline is long enough, all of the N_2O will be consumed by $\tilde{\tau} \approx 4.4$. $\tilde{\tau}_{up}$ is the transformed residence time at the point where a flowline exits the bed and reenters the surface water. If a flowline has a $\tilde{\tau}_{up}$ between $\tilde{\tau} \approx 0.54$ and $\tilde{\tau} \approx 4.4$, it has the potential to emit N_2O.
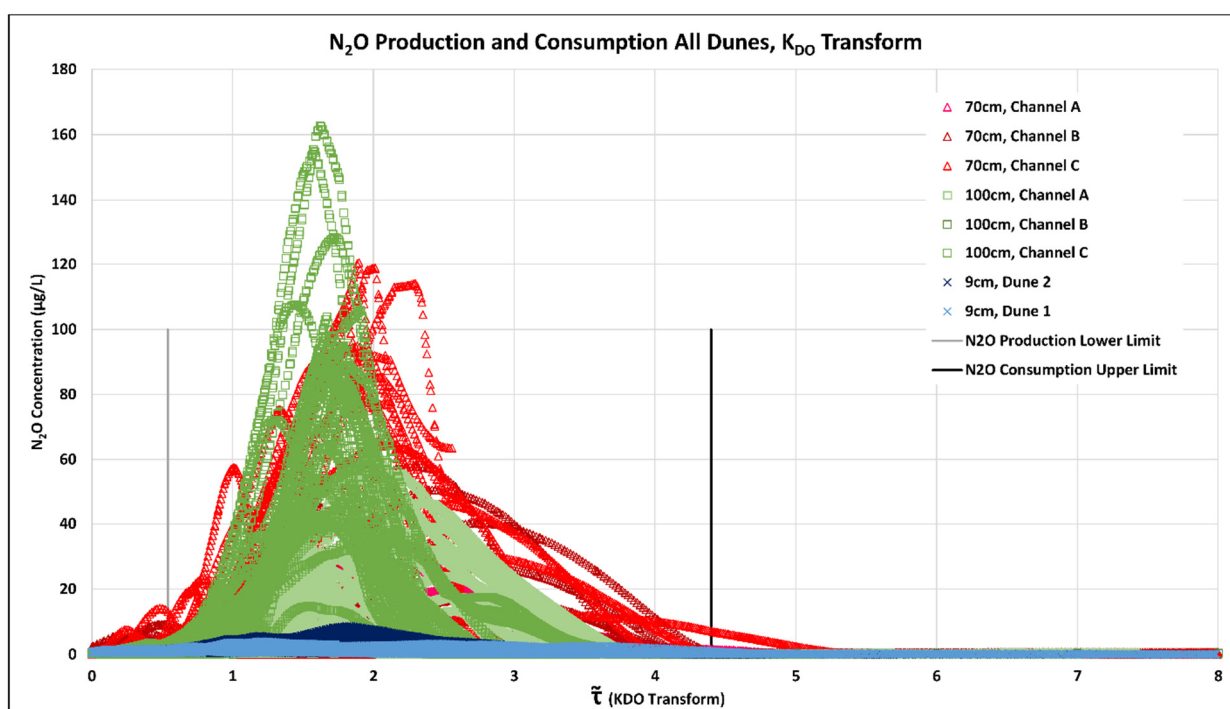
Figure 5-6. N20 concentration profiles for all of the flowlines and all of the dunes plotted against the non-dimensional residence time, $\tilde{\tau}$. In this case, the tight grouping of the concentration profiles is a result of the $\tilde{\tau}$ transform. This provides a useful tool for predicting N_2O production and consumption. For this chart, each flowline was transformed using the K_{DO} value calculated for that specific flowline.

It is also possible transform the residence time (τ) values for a bedform single value of K_{DO}. This might be single measured value for a particular bedform or the mean of a few measured values. An example of this approach is shown in Figure 5-8. The profiles in this figure were created by multiplying all of the residence times for each of the eight dunes, by

the mean value of K_{DO} for the individual dune. For example, all of the residence times for dune C70, were multiplied by the mean K_{DO} value for dune C70. This transform approach is less precise and, strictly speaking, if a reasonable of value of the mean of K_{DO} is known, using the less precise transform is unnecessary. The standard deviation can be estimated from the mean (see [*Reeder et al.*, 2017a] for details) and the lognormal K_{DO} distribution can be computed with relative ease. Nonetheless, this simplified transform may be used to good effect in some situations.
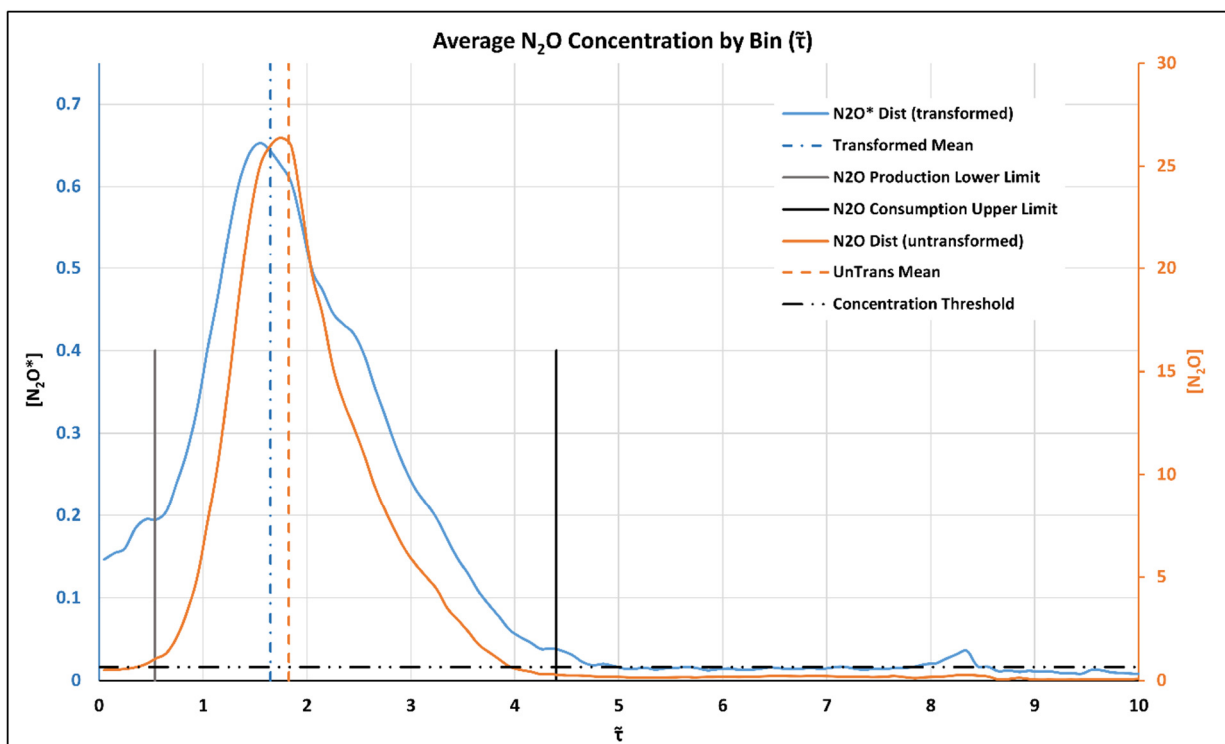
Figure 5-7. Mean N_2O concentration profiles (for all of the dunes) by two different approaches. In both approaches, N_2O concentration values were binned by $\tilde{\tau}$ with each bin having a width of 0.1. All of the N_2O values in each bin were averaged and plotted to the mid-point of the bin. In Approach 1 (orange line), averages were calculated against the raw (un-normalized data). In Approach 2 (blue line), the N_2O values for all of the flowlines were normalized by the peak N_2O value for each of the flowlines.

5.4 Discussion

Potentially, the $\tilde{\tau}$ transform allows us to extend our findings virtually any bedform. More experimental work needs to be done to clearly define just how widely these results can be interpreted. However, the consistency and repeatability of the responses across bedform

geometries, bedform replicates and the two experiments suggest that, for a broad range of bed morphologies, if the residence times within the HZ are known for a particular bedform or for a collection of bedforms the $\tilde{\tau}_{up}$ values for each of the flowlines can be used to evaluate the potential of that bedform(s) to produce and emit N_2O. Flowlines that have a $\tilde{\tau}_{up}$ value of less than 0.54 are too short to produce N_2O. These flowlines will likely remain relatively oxic and are unlikely to have a significant impact on the overall nitrogen chemistry of the stream or HZ. Flowlines that have a $\tilde{\tau}_{up}$ value that is greater than 4.4 will produce N_2O but, for the most part, all of the N_2O will have been consumed before the flowline exits the bed. These flowlines have the potential to act as a sink of N_2O by consuming it to concentrations below that of the surface water. Flowlines that have a $\tilde{\tau}_{up}$ between those two limits have a significant potential to produce and emit N_2O. The above classifications all assume that the concentration of nitrate and/or ammonium in the surface water and the sediments is sufficient to produce significant levels of nitrification and denitrification. It is also assumed that the bed sediments contain sufficient levels of bioavailable carbon to support the anaerobic metabolic activities that drive the denitrification reaction sequence.
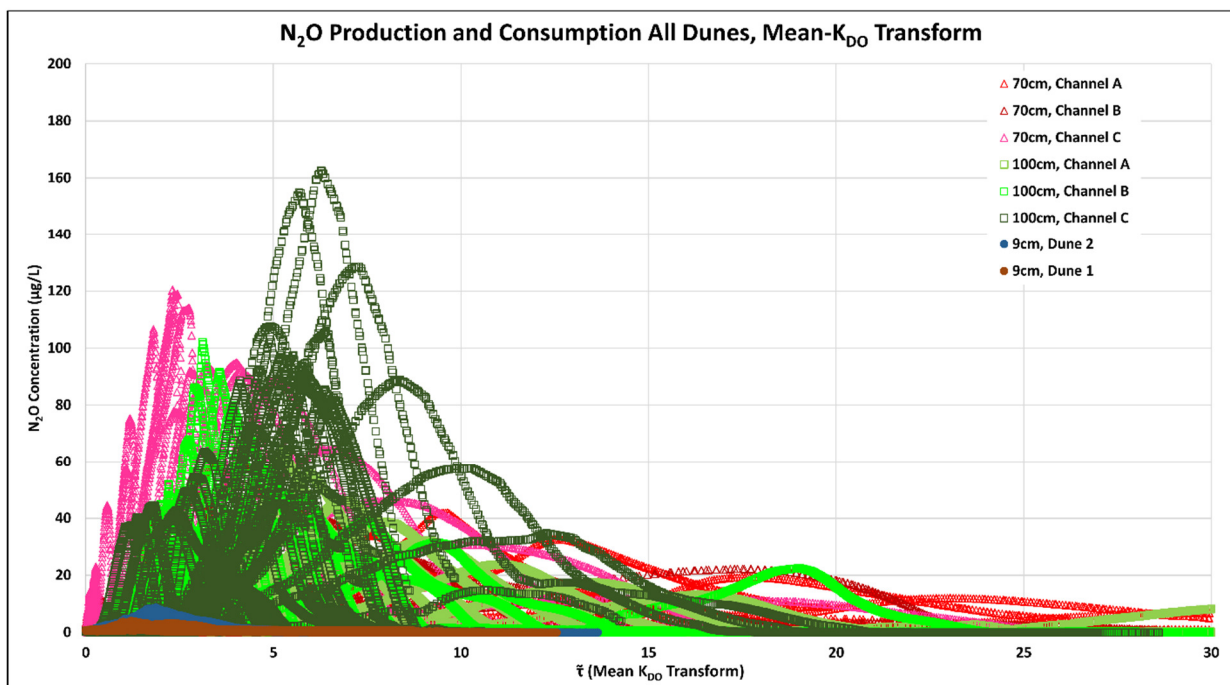
Figure 5-8. N_2O concentration profiles for all flowlines from all dunes plotted against a non-dimensional RT. In this case, the K_{DO} transform was done using the mean K_{DO} for each bedform – for any particular dune; τ was transformed using the same value of K_{DO} for all flowlines. The grouping is significantly wider than the grouping where each flowline is transformed via its individual, associated K_{DO} value (Figure 5-6).

This classification approach is illustrated in Figure 5-9. The green lines in this figure are flowlines that have been identified and being too short ($\tilde{\tau}_{up} < 0.54$) to produce and emit N_2O. The black lines are flowlines that are identified as being too long ($\tilde{\tau}_{up} > 4.4$). The red lines are the flowlines that have the potential to emit N_2O. The two panels compare the flowline classifications using the distributed and mean K_{DO} transform techniques. In Panel A, the $\tilde{\tau}_{up}$ values and flowline classifications are derived from the distributed K_{DO} transform – all flowlines are transformed by a K_{DO} value that is specific to that flowline. In Panel B, all of the flowlines were transformed using the mean K_{DO} value for that dune. The same limits were applied to the flowlines from both transforms and it is interesting to note, at least for this bedform, that the two classifications are remarkably similar. This is a bit of a surprise given the broad dispersion of the mean K_{DO} transform, relative to the distributed K_{DO} transform. The mean K_{DO}, because of its broad dispersion, classifies fewer flowlines as potential emitters, but, nonetheless, gives a useful estimation of which flowlines have the potential to emit. The idea of "potential to emit" needs to be stressed. Not all of the red flowlines, from either classification scheme, are certain to emit N_2O. Our model defines an upper limit on what is possible based upon the ambient chemistry and the stream hydraulics. We know, for instance, that the flowlines on the left side of the dune near the upstream trough (between x = 0 and 0.2, Figure 5-9), which have been classified as potential emitters, actually do not emit N_2O. On the date captured by this figure, that area was oxic [*Reeder et al.*, 2017b] and, thus, anaerobic respiration and denitrification processes were not active. The power of this approach is twofold. First, it can be used in natural streams in which the hydraulics and hyporheic residence times are known to connect measured N_2O emissions to the source locations. Second, if the analysis is done prior to restoration or experimental work, it can be used to improve the effectiveness of those efforts.
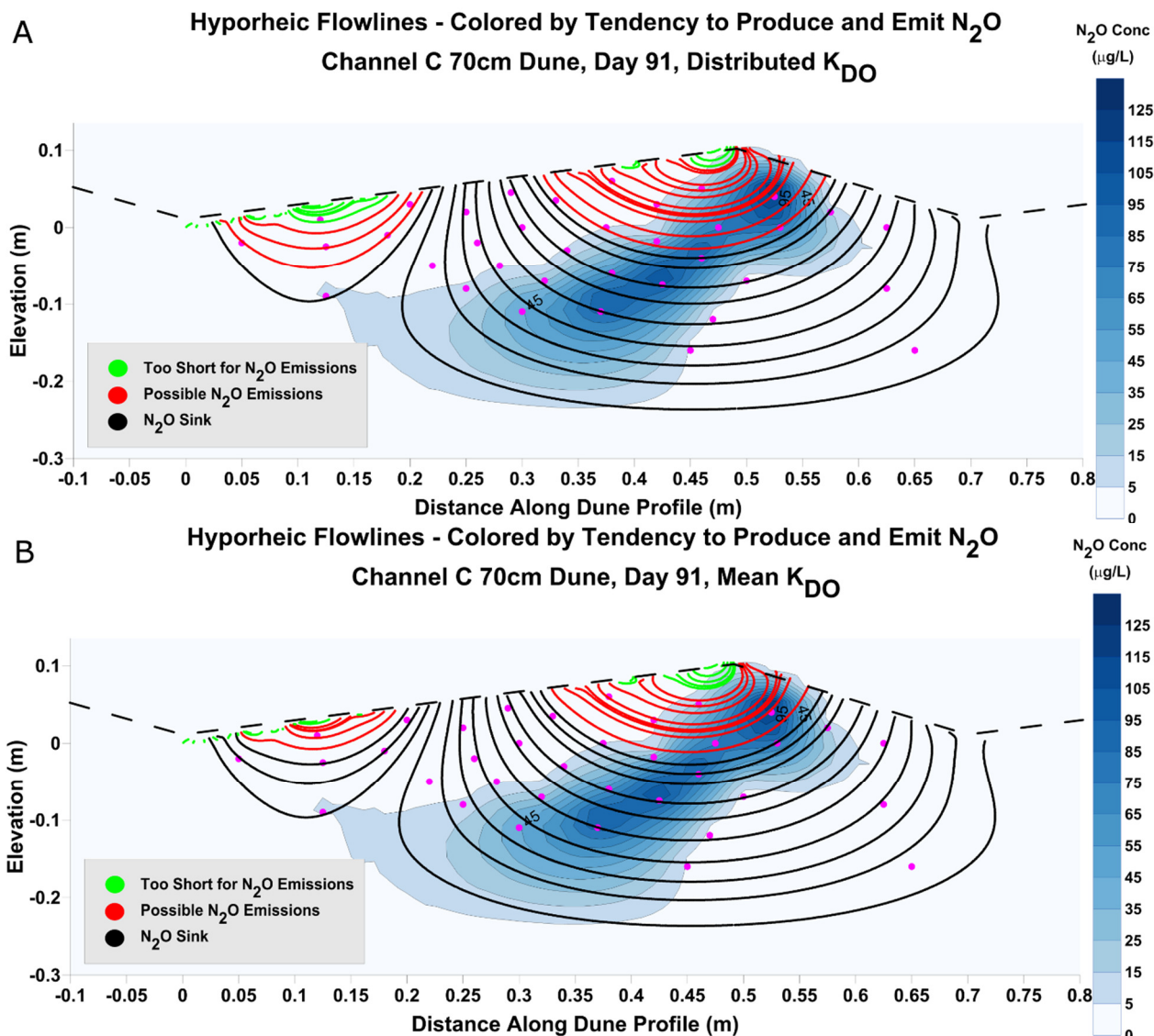
Figure 5-9. Flowlines are colored by their tendency to produce and emit N_2O. Green lines ($\tilde{\tau}_{up} < 0.54$) are too short to produce or emit. Black lines ($\tilde{\tau}_{up} > 4.4$) are too long to emit N_2O and may act as a sink. Red lines ($0.54 < \tilde{\tau}_{up} < 4.4$) have the potential to produce and emit N_2O. In Panel A, the $\tilde{\tau}$ values were calculated using the individual K_{DO} values for each flowline. In Panel B, the $\tilde{\tau}$ values were calculated using the mean K_{DO} value for the dune – one K_{DO} value was used for all of the flowlines.

If it is only desired to estimate the portion of the flowlines from a bedform or collection of bedforms that have the potential to emit N_2O, then a somewhat simpler procedure than mapping the flowlines can be used. A probability density function (PDF) of the $\tilde{\tau}_{up}$ values can be constructed (Figure 5-10). The portion of the PDF that falls between the lower and upper limits for N_2O production and consumption will be the portion of the

flowlines that have the potential of emit N_2O. The two PDFs presented in Figure 5-10 are from the same dune (C70, Day 91) as illustrated in the mapping profiles in Figure 5-9. Consistent with the flowline classifications in Figure 5-9, the PDF for the distributed K_{DO} transform classifies approximately 34% of the flowlines as potential emitters, while the PDF for the mean K_{DO} transform nominates only 26% as potential emitters. This approach does not identify which flowlines or bedforms have the potential to emit.
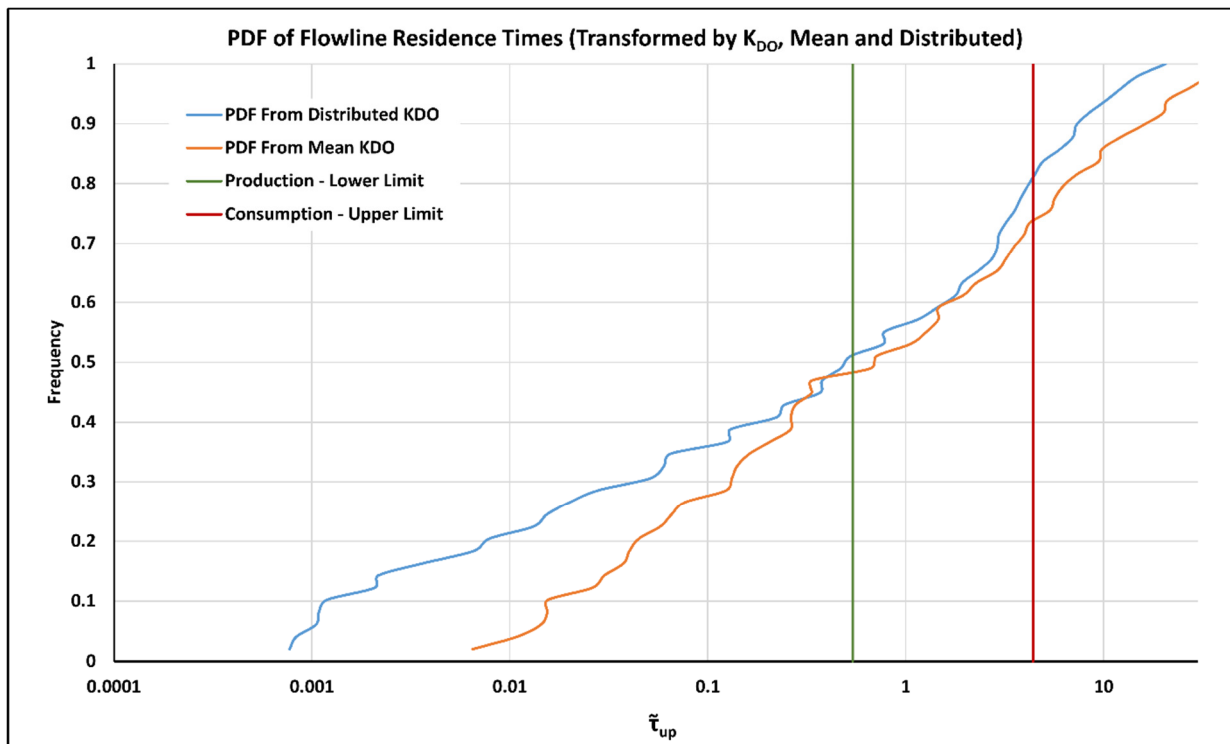

Figure 5-10. PDFs of the $\tilde{\tau}_{up}$ values for the flowlines in the Channel C, 70 cm Dune on Day 91. The blue line is the PDF for $\tilde{\tau}$ values calculated using the distributed (individual) K_{DO} values and the orange line is the PDF of $\tilde{\tau}$ values calculated using the mean K_{DO}.

In cases where the N_2O concentration profiles and flowline residence times are known or can be modeled, the $\tilde{\tau}$ can be used to refine estimations of N_2O emissions. This can be easily accomplished by coding Equation 6 into a program such as Matlab ® and summing the fluxes from the individual flowlines. Using this procedure and the classifications from the distributed K_{DO} transform, the net fluxes were calculated for all of dunes examined in this experiment. The results are presented in Figure 5-11. The blue bars represent the flux estimations with all of the individual, flowline flux calculations base strictly upon the $\tilde{\tau}_{up}$

classifications in Equation 6. However, as previously noted, not all flowlines in the "possible emissions" class will emit N_2O. In our data sets, it was observed that some of the flowlines included in that class did not exhibit a significant level of $[N_2O]$ production. For "possible emissions" flowlines whose peak N_2O concentrations did not exceed the surface concentration by at least 5% the effluent flux was set to zero. The result of the effort is shown by the orange bars in Figure 5-11. For the 70 cm dunes the difference between the adjusted and unadjusted fluxes was negligible. For the 100 cm dune and the 9 cm dunes the difference was slightly more than that of the 70 cm dunes but still quite modest. All-in-all, the upper and lower $\tilde{\tau}$ limits seem to be correctly placed and the potential error in the model is small. One small side note about Figure 5-11; the high flux value (and high N_2O concentrations) for dune C70 are not explained by any specific observation that we can offer at this time. However, the behavior is real. The concentrations are not anomalous - they were observed on multiple dates. For reasons that are unknown, this dune exhibited a higher level of activity than the others.
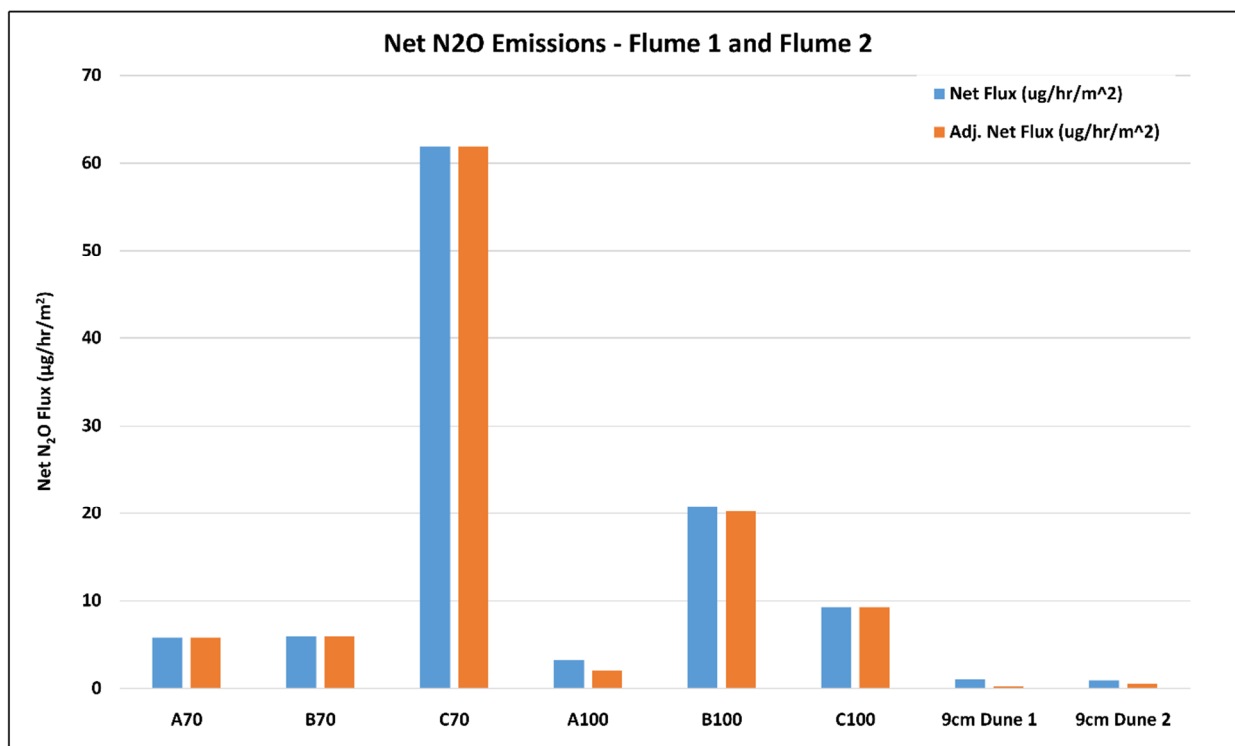

Figure 5-11. Net N_2O flux from each dune. All calculations are base upon the distributed K_{DO} transform. Adjust flux values are based upon the observation that some of the flowlines that were included in the "Possible Emissions" bin exhibited no N_2O concentrations that exceeded the surface concentration by at least 5%. For these flowlines, the net flux has been set to zero.

The spatial distribution of biochemical activity, with respect to N_2O emissions from the HZ has not been previously described. The actual behavior may be a bit counterintuitive. Figure 5-12 shows the spatial distribution of N_2O production and emission for all of the dunes considered in this study. A bit of explanation about the organization of this figure may be warranted. The brown line at the bottom represents a simplified dune-surface profile. So that we could plot both the 70 cm long dunes and the 100 cm long dunes over the same profile, the horizontal distances along the dune profiles were normalized by the length of the dune from trough to crest. Thus $X^* = X/\lambda'$. Where X^* is the normalized horizontal distance along the dune profile (X) and λ' is the length from trough to crest (0.49 m for the 70 cm dune and 0.7 m for the 100 cm dune). For this diagram, emissions were assigned to the entry point of that particular flowline into the bed. This was done to highlight which flowlines and portions of the bedform are responsible for specific outcomes. Actual emissions occur downstream of the crest (blue arrow, Figure 5-12). N_2O sinking occurs mostly along the flowlines that enter the bed between $X^* = 0.2$ and $X^* = 0.55$. Most N_2O sourcing occurs between $X^* = 0.55$ and $X^* = 1$ (the dune crest). There is a generally rising trend in N_2O emissions from flowlines that enter at $X^* = 0.55$ to those that enter at $X^* = 1$, with the strongest emissions coming from flowlines that enter between $X^* = 0.8$ and $X^* = 0.9$. It is not intuitively obvious that the maximum emissions should come from flowlines that enter the bed near the crest of the dune. This is not where the highest N_2O concentrations are observed. However, N_2O emissions are the product of the velocity along the flowline and the N_2O concentration at flowline exit. Concentrations vary by a factor of three or four, whereas downwelling velocities vary by an order of magnitude [*Reeder et al.*, 2017a]. Thus, peak production is a result of the synergy between strong flowline flux and N_2O concentration.
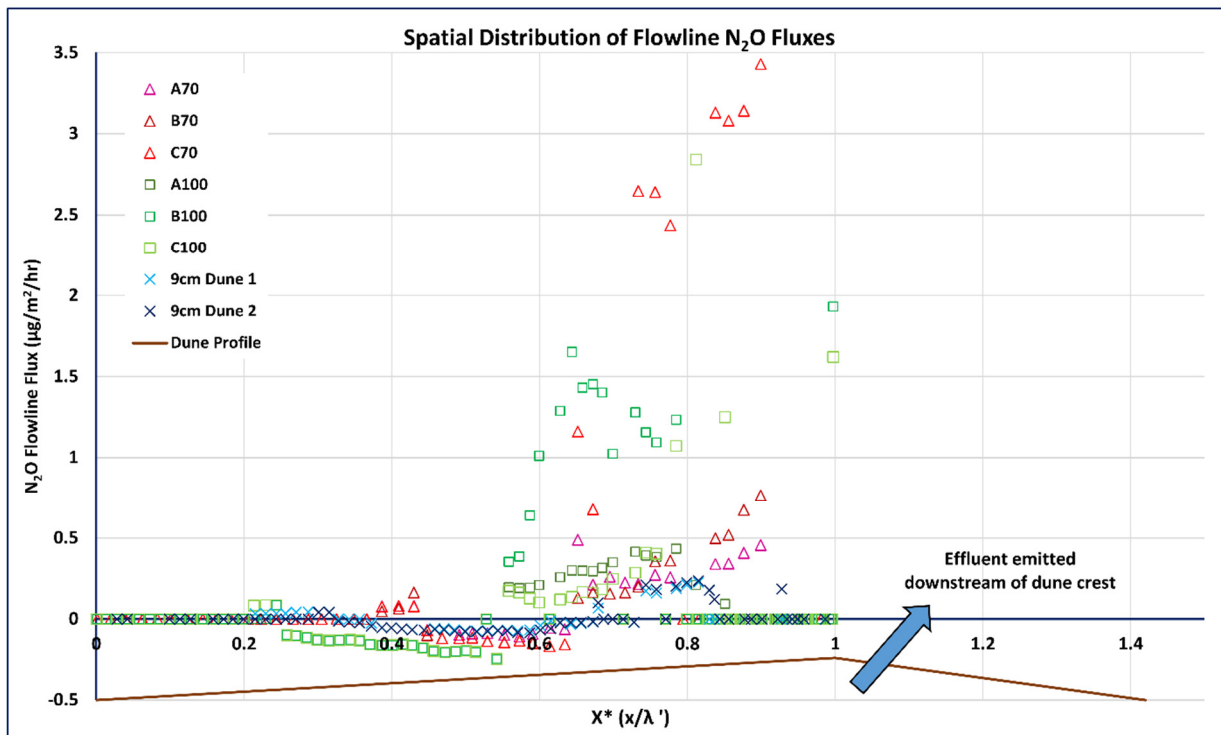
Figure 5-12. Spatial distribution of N_2O flux values from all of the dunes in the two experiments. The brown line at the bottom of the chart represents a generalized dune surface profile. Note that the horizontal distance along the dune has been transformed to a non-dimensional distance, X^* ($X^* = x \cdot \lambda'$). Where x is the untransformed horizontal distance along the dune profile and λ' is the length of the dune from trough to crest. The fluxes are assigned to the entry point of the flowline – the actual emissions occur downstream of the dune crest (blue arrow). N_2O sinking occurs mainly between $X^* = 0.2$ and $X^* = 0.55$. Most N_2O sourcing occurs between $X^* = 0.55$ and $X^* = 1.0$ (dune crest). There is a generally rising trend in flowline flux from $X^* = 0.55$ to $X^* = 1.0$, with the strongest emissions between 0.8 and 0.9.

5.5 Conclusions

Our results show that only a portion of the flowlines through the HZ can emit N_2O, with most of the emissions occurring from flowlines that exit the bed just downstream of the crest of a bedform. The primary factors that determine whether or not a particular flowline will emit N_2O are the residence time and biological activity level along that flowline. Very short or very long flowlines are unlikely to emit N_2O. Very short flowlines may have not started denitrification thus will not produce N_2O. For very long flowlines, the denitrification reaction sequence will likely be carried to completion and the primary effluent from those

flowlines will be nitrogen gas. Long flowlines may act as a sink by consuming N_2O to below the concentration of the surface water that entered the HZ. Because reaction rates (DO consumption, N_2O production and N_2O consumption) are variable from flowline to flowline, residence time, by itself, is not an adequate predictor of N_2O emissions. However, as a general predictor of N_2O emissions for most bedforms, we propose to transform the residence times (τ (s)), for the individual flowlines, to a non-dimensional, Damköhler number, $\tilde{\tau}$, by multiplying the τ values by a characteristic reaction rate for that flowline, in this case K_{DO} (1/s) ($\tilde{\tau} = \tau \cdot K_{DO}$). Through the $\tilde{\tau}$ transform, we can predict the locations and portions of a bedform that will act as source or sink for N_2O. Our results suggest that the initiation of denitrification occurs at values of $\tilde{\tau} > 0.54$. Peak N_2O production occurs at $\tilde{\tau} \cong 1.8$. N_2O consumption is complete at values of $\tilde{\tau} > 4.4$. Flowlines whose $\tilde{\tau}_{up}$, the $\tilde{\tau}$ residence time at which a flowline exits back into the surface water, is between 0.54 and 4.4 will produce and potentially emit N_2O. An adequate estimation of $\tilde{\tau}$ can be calculated by multiplying the τ values for all of the flowlines in a bedform by the mean K_{DO} value for that bedform. However, if the mean K_{DO} value and standard deviation is known, or can be estimated, individual K_{DO} values can be calculated for each flowline refining the predictive power of the $\tilde{\tau}$ transform. Previous work showed that K_{DO} distribution is associated with hyporheic downwelling flows, which have a lognormal distribution and thus K_{DO} for dune-like bedform. In either case, mean K_{DO} or distributed K_{DO}, a PDF of the $\tilde{\tau}_{up}$ values for all of the flowlines in a bedform (or multiple bedforms) can be constructed and the portion between 0.54 and 4.4 is a direct estimate of flowlines that have the potential of emitting N_2O.

5.6 Acknowledgements

5.7 Funding Sources

5.8 References

Beaulieu, J. J., C. P. Arango, S. K. Hamilton, and J. L. Tank (2008), The production and emission of nitrous oxide from headwater streams in the Midwestern United States, Global Change Biology, 14(4), 878-894, doi:10.1111/j.1365-2486.2007.01485.x.

Beaulieu, J. J., et al. (2011), Nitrous oxide emission from denitrification in stream and river networks, Proceedings of the National Academy of Sciences, 108(1), 214-219, doi:10.1073/pnas.1011464108.

Budwig, R., and P. Goodwin (2012), The Center for Ecohydraulics Research Mountain StreamLab - a facility for collaborative research and education, in Innovations 2012: world innovations in engineering education and research, edited, iNeer, Potomac, Maryland, USA.

Cardenas, M. B., and J. L. Wilson (2007), Exchange across a sediment–water interface with ambient groundwater discharge, Journal of Hydrology, 346(3–4), 69-80, doi:http://dx.doi.org/10.1016/j.jhydrol.2007.08.019.

Davidson, E. A. (2009), The contribution of manure and fertilizer nitrogen to atmospheric nitrous oxide since 1860, Nature Geosci, 2(9), 659-662, doi:http://www.nature.com/ngeo/journal/v2/n9/suppinfo/ngeo608_S1.html.

Fehlman, H. M. (1985), Resistance components and velocity distributions of open channel flows over bedforms, 169 pp, Colorado State University, Fort Collins, CO.

Hudson, F. (2004), Sample Preparation and Calculations for Dissolved Gas Analysis in Water Samples Using a GC Headspace Equilibration Technique, edited, pp. 1-14, Ground Water and Ecosystems Restoration Division of the U.S. Environmental Protection Agency.

Laursen, A. E., and S. P. Seitzinger (2004), Diurnal patterns of denitrification, oxygen consumption and nitrous oxide production in rivers measured at the whole-reach scale, Freshwater Biology, 49(11), 1448-1458, doi:10.1111/j.1365-2427.2004.01280.x.

Marzadri, A., D. Tonina, and A. Bellin (2010), A semianalytical three-dimensional process-based model for hyporheic nitrogen dynamics in gravel bed rivers, Water Resources Research, 47(11), doi:10.1029/2011WR010583.

Marzadri, A., D. Tonina, A. Bellin, and J. L. Tank (2014), A hydrologic model demonstrates nitrous oxide emissions depend on streambed morphology, Geophysical Research Letters, 41(15), 5484-5491, doi:10.1002/2014GL060732.

McMahon, P. B., and K. F. Dennehy (1999), N2O Emissions from a Nitrogen-Enriched River, Environmental Science & Technology, 33(1), 21-25, doi:10.1021/es980645n.

Park, S., et al. (2012), Trends and seasonal cycles in the isotopic composition of nitrous oxide since 1940, Nature Geosci, 5(4), 261-265, doi:http://www.nature.com/ngeo/journal/v5/n4/abs/ngeo1421.html#supplementary-information.

Quick, A. M., W. J. Reeder, T. B. Farrell, D. Tonina, K. P. Feris, and S. G. Benner (2016), Controls on Nitrous Oxide Emissions from the Hyporheic Zones of Streams, Environmental Science & Technology, 50(21), 11491-11500, doi:10.1021/acs.est.6b02680.

Ravishankara, A. R., J. S. Daniel, and R. W. Portmann (2009), Nitrous Oxide (N2O): The Dominant Ozone-Depleting Substance Emitted in the 21st Century, Science, 326(5949), 123-125, doi:10.1126/science.1176985.

Reeder, W. J., A. M. Quick, T. B. Farrell, S. G. Benner, K. P. Feris, and D. Tonina (2017a), Spatial dynamics of dissolved oxygen concentrations and bioactivity in the hyporheic zone, in review with Water Resources Research.

Reeder, W. J., A. M. Quick, T. B. Farrell, S. G. Benner, K. P. Feris, and D. Tonina (2017b), Temporal dynamics of dissolved oxygen concentrations and bioactivity in the hyporheic zone, in review with Water Resources Research.

Rosamond, M. S., S. J. Thuss, and S. L. Schiff (2012), Dependence of riverine nitrous oxide emissions on dissolved oxygen levels, Nature Geosci, 5(10), 715-718, doi:http://www.nature.com/ngeo/journal/v5/n10/abs/ngeo1556.html#supplementary-information.

World Meteorological Organization (WMO) (2014), Scientific Assessment of Ozone Depletion: 2014, World Meteorological Organization, Global Ozone Research and Monitoring Project—Report No. 55Rep., 416 pp, Geneva, Switzerland.

Wuebbles, D. J. (2009), Nitrous Oxide: No Laughing Matter, Science, 326(5949), 56-57, doi:10.1126/science.1179571.

Zarnetske, J. P., R. Haggerty, S. M. Wondzell, and M. A. Baker (2011a), Dynamics of nitrate production and removal as a function of residence time in the hyporheic zone, Journal of Geophysical Research: Biogeosciences, 116(G1), G01025, doi:10.1029/2010jg001356.

Zarnetske, J. P., R. Haggerty, S. M. Wondzell, and M. A. Baker (2011b), Labile dissolved organic carbon supply limits hyporheic denitrification, Journal of Geophysical Research: Biogeosciences, 116(G4), n/a-n/a, doi:10.1029/2011JG001730.